

POLITECNICO DI TORINO

College of Chemical and Materials Engineering

Master's Degree Course in Chemical Engineering and Sustainable Processes

Master's Degree Thesis

Technical-economic analysis of the electrosynthesis of ammonia



Supervisors:

prof. Alessandro Monteverde
prof. Raffaele Pirone

Candidate:

Joaquín Barrera Gajardo
Student ID: 275880

March 2021

Index

1. Riassunto	1
2. Abstract	11
3. Introduction	13
4. Description of the Main Feedstocks and Product	15
4.1. Nitrogen	15
4.1.1. Main Characteristics and Description	15
4.1.2. Applications	15
4.1.3. Physical Properties	15
4.1.4. Sources	16
4.1.5. Safety Aspects and Procedures	17
4.2. Hydrogen	17
4.2.1. Main Characteristics and Description	17
4.2.2. Physical Properties	17
4.2.3. Hydrogen as an Energy Carrier	18
4.2.4. Applications	19
4.2.5. Hydrogen as A Green Fuel	20
4.2.6. Sources	20
4.2.7. Safety Aspects and Procedures	22
4.3. Ammonia	23
4.3.1. Main Characteristics and Description	23
4.3.2. Physical Properties	23
4.3.3. Main Chemical Reactions Involving Ammonia	23
4.3.4. Applications	24
4.3.5. Ammonia as a green fuel	24
4.3.6. Sources	25
4.3.7. Safety Aspects and Procedures	26
4.4. Water	27
4.4.1. Main Characteristics and Description	27
4.4.2. Physical Properties	27
4.4.3. Sources	27
4.4.4. Safety Aspects and Procedures	29
5. Main Processes for the Production of Green Ammonia	31
5.1. Haber-Bosch Process	31
5.1.1. Haber-Bosch History and Schemes	31
5.1.2. Ammonia production kinetics	32
5.1.3. Reaction Rate and Equilibrium	34
5.1.4. Environmental Concerns and Energy Use of the Haber-Bosch process	35
5.2. Air Separation Process	36
5.2.1. Air Separation Unit (ASU) for Cryogenic Distillation: Cryogenic Air Separation	36
5.2.2. Air Separation using Adsorption	39

5.2.3.	Air Separation using Membrane Technology	40
5.3.	Steam Methane Reforming	41
5.3.1.	Carbon Capture and Storage (CCS)	43
5.4.	Electrolyser	46
5.4.1.	Cell Types: Gap cells, Zero-gap Cells and Solid Polymer Electrolyte (SPE) cells	47
5.4.2.	Membranes	48
5.4.3.	Basic principles of Water Electrolysis	48
5.4.4.	Alkaline Water Electrolysis (AWE)	50
5.4.5.	Proton Exchange Membrane Electrolyser (PEM)	50
5.5.	Ammonia Separation Process	52
6.	Chile's Geographical Context and Saltpetre History	55
6.1.	Chile's Geography and Economy	55
6.2.	Chile's Renewable Energy Potential	55
6.3.	Chile's Saltpetre History	56
7.	Market Research and Availability	61
7.1.	Ammonia Worldwide Production	61
7.2.	Green Ammonia Plants	63
7.3.	Conventional Ammonia Plants	64
8.	Main Reasons to Conduct This Thesis	67
9.	Process Simulation of the Base Case	71
9.1.	First Simulation to Determine Required Nitrogen and Hydrogen Inputs	71
9.1.1.	Optimization of the Haber-Bosch Reactor's Temperature and Pressure	73
9.1.2.	Ammonia Recovery Calculation	74
9.2.	Alkaline Electrolyser	75
9.2.1.	Calculation of the Real Cell Voltage and the Amount of Water Required	76
9.2.2.	Aspen Plus AWE Simulation	80
9.2.3.	Aspen Plus AWE: Voltage calculation	81
9.2.4.	Aspen Plus AWE: Amount of Water Feed Required	82
9.2.5.	Aspen Plus AWE: Electricity Input Requirement	83
9.3.	Air Separation Unit	83
9.3.1.	Aspen Plus ASU Model	83
9.4.	Haber-Bosch Process	86
9.4.1.	Optimization of the Reactor's Dimension	86
9.5.	Ammonia Separation Process by Condensation	88
10.	Improvements of the Base Case	89
10.1.	PEM Electrolyser	89
10.1.1.	Calculation of the Real Cell Voltage and the Amount of Water Required	89
10.1.2.	Aspen Plus Electrolyser Simulation PEM	94
10.1.3.	Aspen Plus Electrolyser PEM: Voltage Calculation	95

10.1.4. Aspen Plus Electrolyser PEM: Amount of Water Required Calculation	96
10.1.5. Aspen Plus Electrolyser PEM: Electricity Input Requirement . . .	97
10.2. ASU with 2 Distillation Columns	97
10.3. Multi-bed Reactor System With Intercooling	102
10.3.1. Description of the process	104
10.3.2. Optimization of the multi reactor system with inter-cooling using Aspen Plus	105
10.4. Addition of a Recycle Loop	109
10.4.1. Optimization of the multi reactor system with inter-cooling and addition of a recycle stream using Aspen Plus	110
11. Results and Discussion	115
11.1. Feasibility of each case	115
11.2. Amount of ammonia produced and conversion of each reactor comparison between both cases	119
11.3. Comparison of the Energy Requirements between Both Plants	120
11.4. Economic Analysis of the Green Ammonia Plant	127
11.4.1. Capital Costs	127
12. Conclusions and Recommendations	139
13. Nomenclature	141
13.1. Abbreviations	141
13.2. List of main Symbols	142
13.3. Greek Symbols	143
14. Bibliography	145
15. Annexes	151
15.1. Guthrie Method for Estimating Equipment Installation Costs	151
15.1.1. Shell-and-Tube Heat Exchangers	151
15.1.2. Gas Compressors	152
15.1.3. Distillation Columns, Reactors and Flash Units	152
15.2. Aspen Plus diagram of the final case process simulated	154
16. Acknowledgments	155

Table Index

1.1.	Costi dell'elettrolizzatore simulato senza scale-up per gli anni 2020 e 2030	8
1.2.	Costi degli elettrolizzatori simulati con scale-up per gli anni 2020 e 2030	8
4.1.	Air composition in the Earth's atmosphere [25]	16
4.2.	Comparison of ammonia with other fuels including hydrogen [32]	25
4.3.	Further comparison of ammonia with other fuels including hydrogen [32]	25
5.1.	Different types of air separation processes, adapted from [25]	39
5.2.	Different techniques for H ₂ purification [16]	42
5.3.	Comparison of main water electrolysis technologies [18]	52
7.1.	Principal Ammonia Production Countries, adapted from [9]	61
7.2.	EU statistics on plant size, 2013 [50]	65
9.1.	Coefficients considered for the electrochemical model of an alkaline water electrolysis cell	79
9.2.	AWE base case conditions used in the paper	80
9.3.	Inputs for AWE Electrolyser simulation in Aspen Plus	81
9.4.	Optimization of the Haber-Bosch reactor's dimension	88
10.1.	PEM Electrolyser Parameters [52]	91
10.2.	Inputs for PEM Electrolyser simulation in Aspen Plus	94
10.3.	Compression ratio for each compressor	99
10.4.	Outlet temperatures of the air after each intercooling	99
10.5.	Cryogenic distillation column parameters	99
10.6.	Heat subtracted from each air outlet stream after compression	99
10.7.	Amount of water needed in each heat exchanger	100
10.8.	Stream outlet temperature after compression and cooling water temperature after intercooling	100
10.9.	Design specification for both distillation columns	101
10.10.	Parameters for distillation columns COL-101 and COL-102	101
10.11.	Desired output specifications for both multi-heat exchangers	101
10.12.	Energy requirements for each equipment in the ASU	102
10.13.	Parameters established for multi stage compression with interrefrigeration system for feeding stream entering the multi stage reactor system	105
10.14.	Input parameters for multi reactor system configuration	106
10.15.	Outputs obtained with the optimization conducted in Aspen Plus for the first two steps	107
10.16.	Outputs obtained with the optimization conducted in Aspen Plus for steps three and four	108
10.17.	Conversion and amount of ammonia exiting each reactor	109
10.18.	Amount of ammonia exiting the liquid stream within the flash along with its recovery	109
10.19.	Input parameters for multi reactor system configuration with addition of a recycle loop	111
10.20.	Outputs obtained with the optimization conducted in Aspen Plus for the first two steps for the configuration with a recycle stream	111
10.21.	Outputs obtained with the optimization conducted in Aspen Plus for steps three and four with the addition of a recycle stream	112
10.22.	Volume of each reactor of the final case	113
10.23.	Length, diameter and volume of each reactor after the optimization	113

10.24.	Conversion and amount of ammonia exiting each reactor in the configuration with recycle stream	113
10.25.	Amount of ammonia exiting the liquid stream within the flash along with its recovery in the configuration with recycle stream	113
11.1.	Comparison of the amount of ammonia at each reactor outlet, amount of ammonia after the recovery and nitrogen conversion of each reactor between both cases	119
11.2.	Energy requirements for every equipment in the base case simulated	120
11.3.	Energy requirements for each block unit in the base case simulated	120
11.4.	Energy requirements for the sum of all equal equipments in the base case simulated	121
11.5.	Energy requirements for every equipment in the final case simulated	122
11.6.	Energy requirements for every equipment in the final case simulated: part 2	123
11.7.	Energy requirements for each process unit for the final case	123
11.8.	Energy requirements for the sum of all equal equipments in the final case simulated	123
11.9.	Electrolyser costs without scale-up, adapted from [73]	127
11.10.	Electrolyser costs with scale-up, adapted from [73]	127
11.11.	Costs of the electrolyser simulated without scale-up for years 2020 and 2030	128
11.12.	Costs of the electrolyzers simulated with scale-up for years 2020 and 2030 .	128
11.13.	Type of compressor used in the final case simulated in Aspen Plus	129
11.14.	Type of heat exchanger used in the final case simulated in Aspen Plus . . .	129
11.15.	Type of distillation column used in the final case simulated in Aspen Plus .	130
11.16.	Type of distillation column tray used in the final case simulated in Aspen Plus	130
11.17.	Type of reactor used in the final case simulated in Aspen Plus	130
11.18.	Type of flash used in the final case simulated in Aspen Plus	130
11.19.	Heat coefficients of the heat exchangers simulated in the final case	131
11.20.	Installation costs of each heat exchanger in the final simulation	131
11.21.	Installation costs of each compressor in the final simulation	132
11.22.	Installation costs of each distillation column in the final simulation	132
11.23.	Installation costs of each reactor in the final simulation	132
11.24.	Installation cost of the flash unit in the final simulation	133
11.25.	Installation costs of the sum of all equipment units in the final simulation .	133
11.26.	Price for the utilities required in the green ammonia plant	134
11.27.	Total salaries paid each year	135
11.28.	Electricity paid each year to run out the plant	135
11.29.	Sales Revenue and additional operational costs to conduct the plant	136
15.1.	CEPCI Index for years 1969 and 2019, adapted from [84]	151
15.2.	Factor value in function of the equipment material	151
15.3.	Factor value in function of the heat exchanger design type	152
15.4.	Factor value in function of the heat exchanger design pressure	152
15.5.	Factor value in function of the compressor type	152
15.6.	Factor value in function of the distillation column, reactor or flash unit design pressure	153
15.7.	Values of the different factors in function of the tray spacing, type and material of the distillation column	153

Figure Index

1.1.	Modello di elettrolizzatore PEM/alcalino in Aspen Plus	2
1.2.	Modello Aspen Plus della compressione multistadio dell'aria con intercooling	2
1.3.	Modello Aspen Plus di un sistema criogenico a doppia colonna di distillazione con integrazione energetica	2
1.4.	Modello Aspen Plus della miscelazione di idrogeno e azoto come materie prime per il reattore Haber-Bosch: Parte 1	3
1.5.	Modello Aspen Plus della miscelazione di idrogeno e azoto come materie prime per il reattore Haber-Bosch: Parte 2	3
1.6.	Modello Aspen Plus il sistema di compressione multistadio con intercooling per l'alimentazione che entra nel processo Haber-Bosch	4
1.7.	Modello Aspen Plus del sistema multi reattore con intercooling, seguito dal processo di condensazione e recupero dell'ammoniaca	4
1.8.	Modello Aspen Plus del ciclo di riciclo aggiunto alla simulazione	5
1.9.	Temperatura del flusso di uscita di ogni compressore nel caso base	5
1.10.	Temperatura del flusso di uscita di ogni reattore nel caso finale	6
1.11.	Confronto del fabbisogno energetico delle unità di blocco tra i due casi	6
1.12.	Confronto dei requisiti energetici delle unità di blocco tra il caso finale e il caso modificato	7
1.13.	Valori calcolati per le diverse spese operative (CaPeX)	7
1.14.	Valori calcolati per le diverse spese operative (OpEx)	9
1.15.	Prezzo dell'ammoniaca in cui le spese operative sono uguali alle entrate delle vendite: Confronto dei casi	9
3.1.	Components and flow chart of a P2A system integrated with renewable energy resources and nuclear energy is shown [1]	14
4.1.	Nitrogen cycle in nature [11]	17
4.2.	Comparison of different volumetric and gravimetric energy densities of several metal hydrides and other hydrogen storage media [33]	20
4.3.	Main Hydrogen sources [12]	22
4.4.	World's Water Availability by country, 1950 and 1995, adapted from [37]	28
4.5.	World's expected Water Availability by country, 2025, adapted from [37]	28
5.1.	Methane fed Haber-Bosch process scheme [15]	31
5.2.	Electrically driven Haber-Bosch process scheme [15]	32
5.3.	Improvement in the efficiency of ammonia production over the last decades [15]	36
5.4.	Scheme of the double distillation column [27]	38
5.5.	General Structure of an ASU [25]	38
5.6.	Scheme of an adsorption-based air separation process [27]	39
5.7.	Scheme of an air separation process by membrane [27]	40
5.8.	Competitive ranges of the various nitrogen production methods [27]	41
5.9.	Scheme of a conventional SMR process [16]	41
5.10.	Schematic of an SMR process showing heat and materials integration [62]	43
5.11.	Typical processing steps in SMR with CO ₂ capture [39]	43
5.12.	Hydrogen Output System [38]	44
5.13.	Electric-Output System Configuration [38]	44
5.14.	Small-Scale steam methane-reforming with CCS by using adsorbents [39]	45

5.15.	Mechanism of CO ₂ capture into MEA solution [41]	46
5.16.	Two dimensional schematic diagrams of (a) gap-cell, (b) zero-gap cell and (c) SPE cell [17]	47
5.17.	Energy Requirements for water splitting as function of operating temperature [4]	49
5.18.	PEM Electrolysis Cell [20]	51
5.19.	Conventional ammonia separation versus absorption based ammonia separation [63]	53
6.1.	Potential Capacity factors for solar and wind energy in the North of Chile. Maps on the right side take into account the land restrictions such as high altitude, vicinity to national parks, etc. [36]	56
6.2.	Saltpetre Office Jaspampa, Tarapaca. 1889 [34]	58
6.3.	<i>Santa Laura</i> saltpetre office [35]	59
7.1.	Main Ammonia Production Countries, adapted from [9]	62
7.2.	Main Chilean ammonia importers [42]	63
7.3.	Main Chilean ammonia exporters [42]	63
8.1.	Global levelised cost of electricity from utility-scale renewable power generation technologies, 2010-2017 [51]	68
8.2.	Learning curves for the global weighted average levelised cost of electricity from CSP, solar PV and onshore and offshore wind, 2010-2020 [51]	69
8.3.	GHG cycle [12]	70
8.4.	World Primary energy substitution in terms of the fraction F of total resources by the identified source [12]	70
9.1.	Parameters for first kinetic equation	71
9.2.	Coefficients and exponents for first kinetic equation	72
9.3.	Parameters for second kinetic equation	72
9.4.	Coefficients and exponents for second kinetic equation	72
9.5.	First tentative simulation in Aspen Plus to obtain the required nitrogen and hydrogen inputs	73
9.6.	Sensitivity analysis conducted in Aspen Plus	74
9.7.	Stream table corresponding to the simulation carried out to obtain the required nitrogen and hydrogen inputs	75
9.8.	Alkaline water electrolyser model in Aspen Plus	81
9.9.	Aspen Plus Air Separation Unit model	85
9.10.	Aspen Plus Haber-Bosch process model	86
9.11.	Sensitivity analysis conducted in Aspen Plus to optimize the Haber-Bosch reactor dimensions	87
9.12.	Conversion versus reactor length	87
9.13.	Ammonia separation section modelled in Aspen Plus	88
10.1.	PEM electrolyser model in Aspen Plus	95
10.2.	Aspen Plus model of the multistage compression of air with inter-cooling	98
10.3.	Aspen Plus model of a cryogenic double distillation column system with energy integration	98
10.4.	Aspen Plus model of the mixing of hydrogen and nitrogen as feedstocks for the Haber-Bosch reactor: Part 1	103
10.5.	Aspen Plus model of the mixing of hydrogen and nitrogen as feedstocks for the Haber-Bosch reactor: Part 2	103

10.6.	Aspen Plus model the multi stage compression system with inter cooling for the feed entering the Haber-Bosch reactor	104
10.7.	Aspen Plus model of the multi reactor system with intercooling, followed by the ammonia condensing and recovery process	104
10.8.	Aspen Plus model of the recycle loop added to the simulation	110
11.1.	Outlet stream temperature of each compressor in the base case	115
11.2.	Outlet stream temperature of the reactor in the base case	116
11.3.	Outlet stream temperature of each compressor in the final case	116
11.4.	Outlet stream temperature of each reactor in the final case	116
11.5.	Outlet stream temperature of the cooling water exiting each heat exchanger in the final case	117
11.6.	Comparison of the energy requirements of the block units between both cases	124
11.7.	Comparison of the energy requirements of the equipment between both cases	125
11.8.	Comparison of the energy requirements of the block units between the final case and the modified case	125
11.9.	Comparison of the energy requirements of the equipment between the final case and the modified case	126
11.10.	Price of ammonia where the operational expenditures are equal to the sales revenue: Cases comparison	136
11.11.	Calculated values for the different operational expenditures	137
11.12.	Calculated values for the different operational expenditures, % of the total	137
11.13.	CAPEX values for each equipment in the final case	138
15.1.	Final case simulated in Aspen Plus	154

1. Riassunto

Per quanto riguarda l'elevato aumento delle emissioni di CO₂ negli ultimi anni, l'Unione Europea (UE) si è posta l'obiettivo di ridurre le emissioni di gas serra (GHG) dell'80-95 % entro il 2050. Per raggiungere questo obiettivo, l'uso delle energie rinnovabili è necessario. A tal proposito, l'energia solare ed eolica sono diventate tecnologie accessibili per la produzione di energia, anche se sono ostacolate da variabilità, stagionalità e incertezza.

Dal 1970 al 2004, le emissioni annuali di biossido di carbonio (CO₂) derivanti dall'attività umana sono aumentate del 70 %. Oggi raggiungono oltre i 32 miliardi di tonnellate/anno e si prevede il raggiungimento di almeno 50 miliardi di tonnellate/anno entro il 2050. Attualmente, solo 110 milioni di tonnellate di CO₂/anno dei 32 miliardi di tonnellate che vengono prodotte, sono utilizzate e di queste la maggior parte sono impiegate per produrre altri composti chimici. Pertanto, è indispensabile diminuire al più presto possibile le emissioni di CO₂.

Grazie all'utilizzo dell'energia solare ed eolica, si prevede che in futuro l'idrogeno sarà uno dei migliori candidati tra i carburanti senza carbonio, in quanto è un combustibile pulito e la sua combustione non causa emissioni nocive. Tuttavia, il costo di produzione, stoccaggio e compressione è ancora molto alto. L'ammoniaca sembra essere una potenziale soluzione per lo stoccaggio dell'idrogeno, essendo una delle sostanze chimiche inorganiche più importanti e prodotte nel mondo, usata principalmente per produrre fertilizzanti. La produzione globale di ammoniaca è in costante crescita; nel 2019 in tutto il mondo si sono raggiunte i 150 milioni di tonnellate.

In questa tesi verrà presentato un processo dettagliato di produzione di ammoniaca verde, considerando un impianto situato in Cile. Il processo in oggetto consisterà principalmente in un elettrolizzatore ad acqua per produrre H₂ come materia prima per un processo Haber-Bosch finalizzato all'ottenimento di ammoniaca, oltre a tutti i necessari processi intermedi. L'elettrolizzatore funzionerà con elettricità prodotta mediante risorse energetiche rinnovabili. L'uso di Aspen Plus accoppiato a blocchi di calcolo Excel sarà utilizzato per simulare l'operazione di produzione di ammoniaca.

La tesi consiste principalmente nella simulazione di due impianti di produzione di ammoniaca: un primo caso base semplificato di un impianto di produzione accoppiato con un elettrolizzatore e un caso finale, ottenuto partendo dal caso base e prevedendo l'integrazione di alcuni elementi. Nello specifico, è stata prevista l'integrazione energetica utilizzando due colonne di distillazione invece di una, la multi compressione per l'ASU e il processo Haber-Bosch, i multi reattori che utilizzano il quenching e uno scambiatore di calore per diminuire le richieste di energia dalle utility. Infine, è stato aggiunto un flusso di riciclo accoppiato con un altro scambiatore di calore, al fine di aumentare la produzione di ammoniaca nei tre reattori Haber-Bosch.

L'obiettivo principale è quello di confrontare il caso base con il caso finale in termini di requisiti energetici, produzione e conversione di ammoniaca in ogni reattore, fattibilità, ecc. Inoltre, è stata fatta un'analisi economica del caso finale, al fine di determinare il CaPeX e l'OpEx dell'impianto, insieme ai fattori più determinanti che influenzano questi due parametri.

Nelle Figure 1.1, 1.2, 1.3, 1.4, 1.5, 1.6, 1.7 e 1.8 viene mostrato il processo di simulazione condotto in Aspen Plus del caso finale.

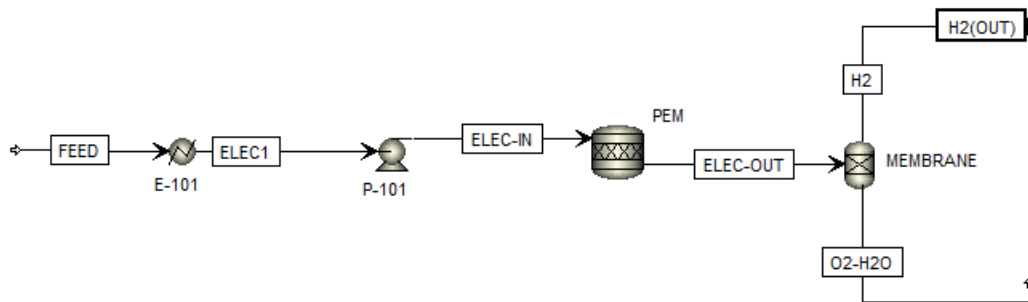


Figure 1.1: Modello di elettrolizzatore PEM/alcalino in Aspen Plus

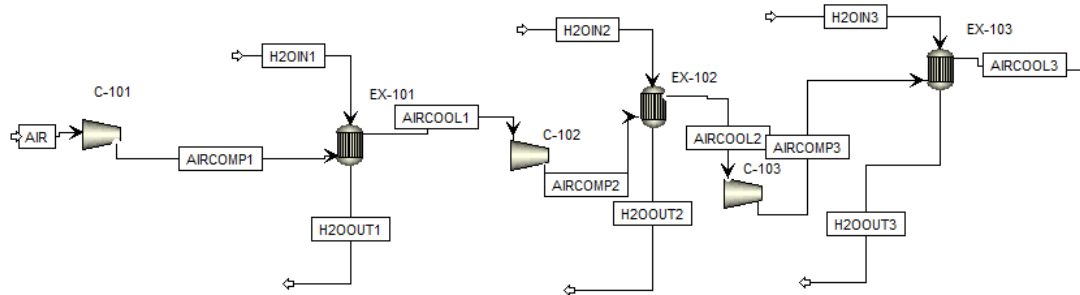


Figure 1.2: Modello Aspen Plus della compressione multistadio dell'aria con intercooling

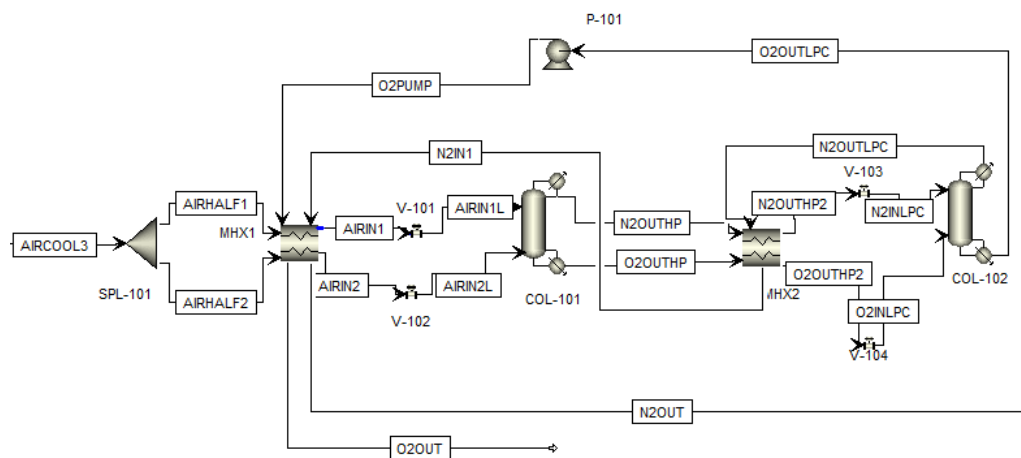


Figure 1.3: Modello Aspen Plus di un sistema criogenico a doppia colonna di distillazione con integrazione energetica

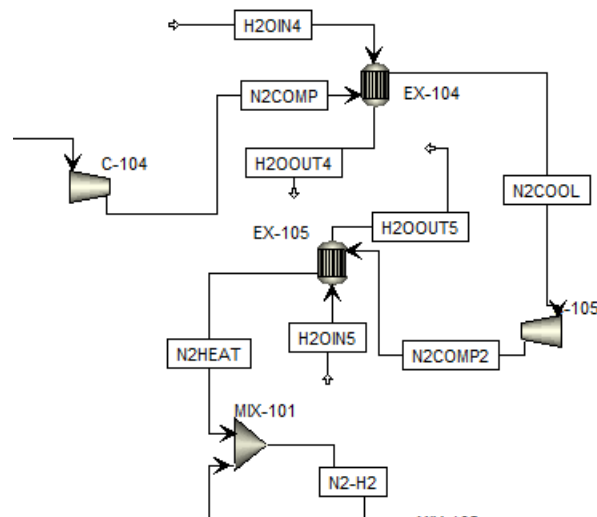


Figure 1.4: Modello Aspen Plus della miscelazione di idrogeno e azoto come materie prime per il reattore Haber-Bosch: Parte 1

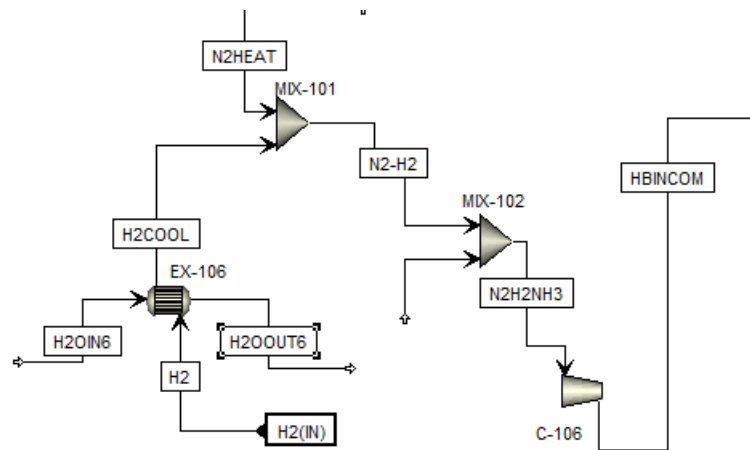


Figure 1.5: Modello Aspen Plus della miscelazione di idrogeno e azoto come materie prime per il reattore Haber-Bosch: Parte 2

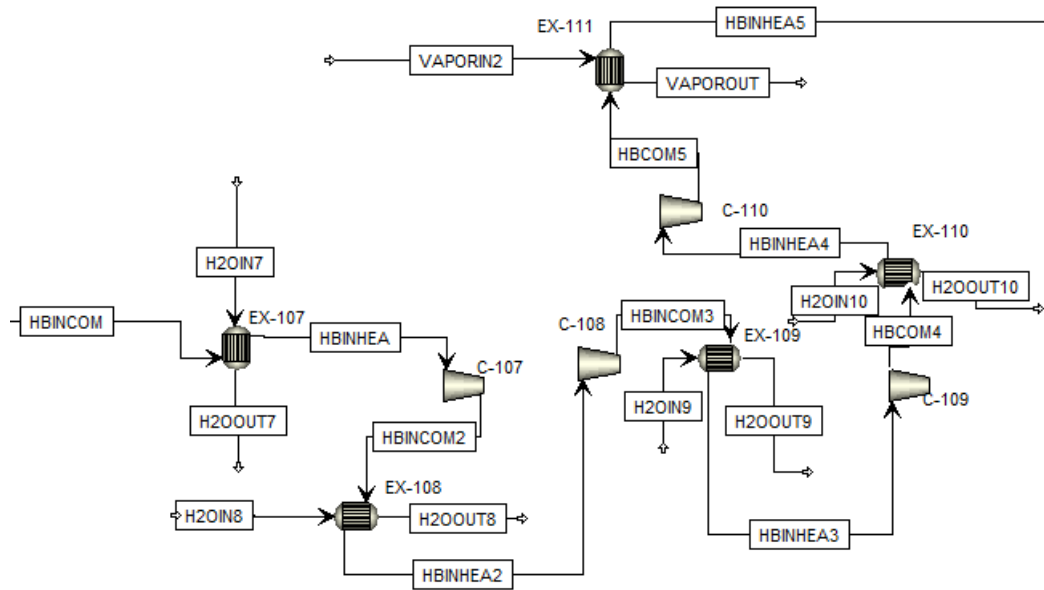


Figure 1.6: Modello Aspen Plus il sistema di compressione multistadio con intercooling per l'alimentazione che entra nel processo Haber-Bosch

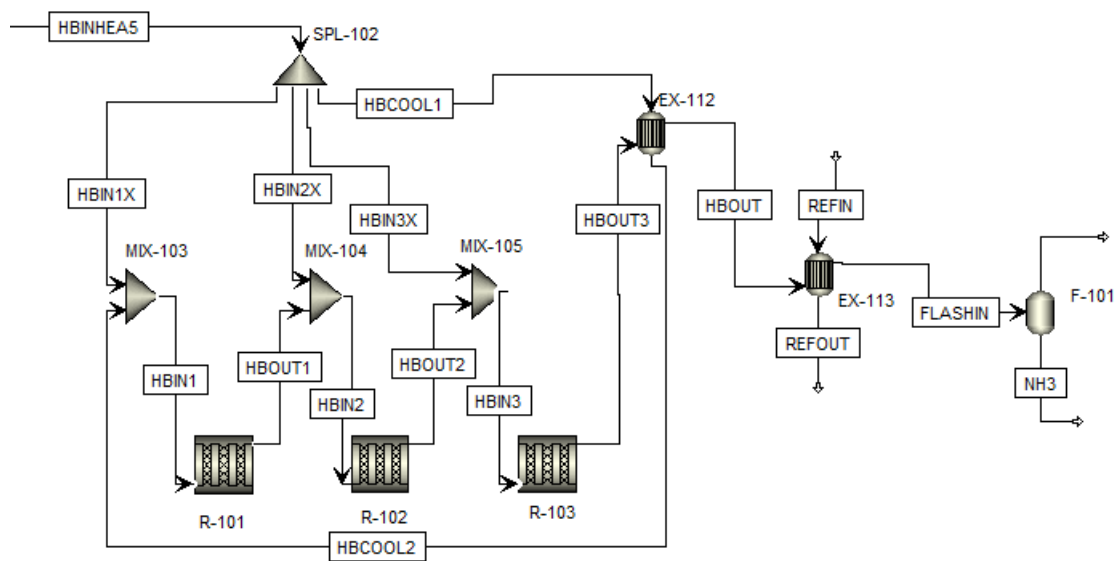


Figure 1.7: Modello Aspen Plus del sistema multi reattore con intercooling, seguito dal processo di condensazione e recupero dell'ammoniaca

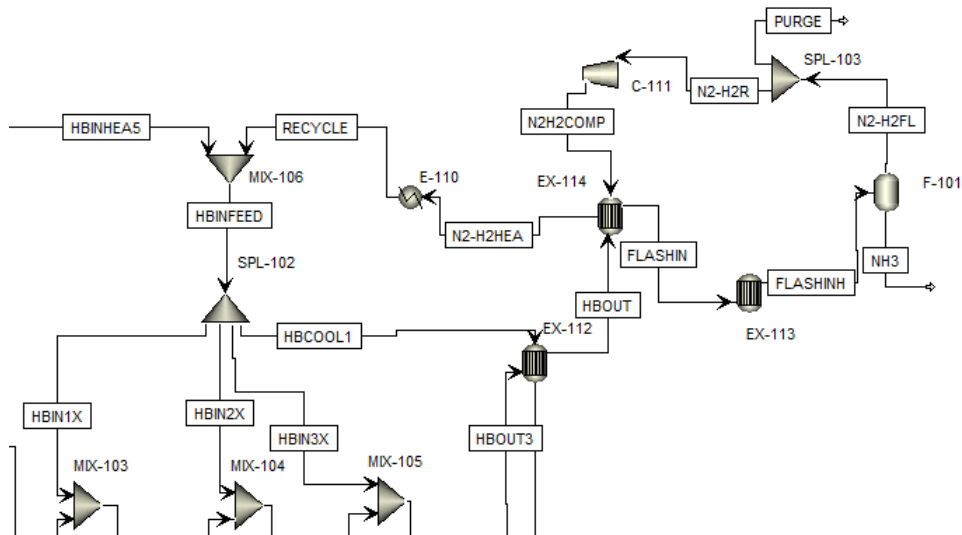


Figure 1.8: Modello Aspen Plus del ciclo di riciclo aggiunto alla simulazione

Risultati e discussione

In quanto riguarda le Figure 1.9 e 1.10, se può vedere che nel caso base la temperatura del flusso uscente di ogni compressori è maggiore che la temperatura massima fissata per non avere dei problemi nel funzionamento del compressore, mentre nel caso finale la temperatura del flusso uscente di ogni compressore è minore a la temperatura massima fissata. Questo indica che il caso finale è più fattibile rispetto al caso base.

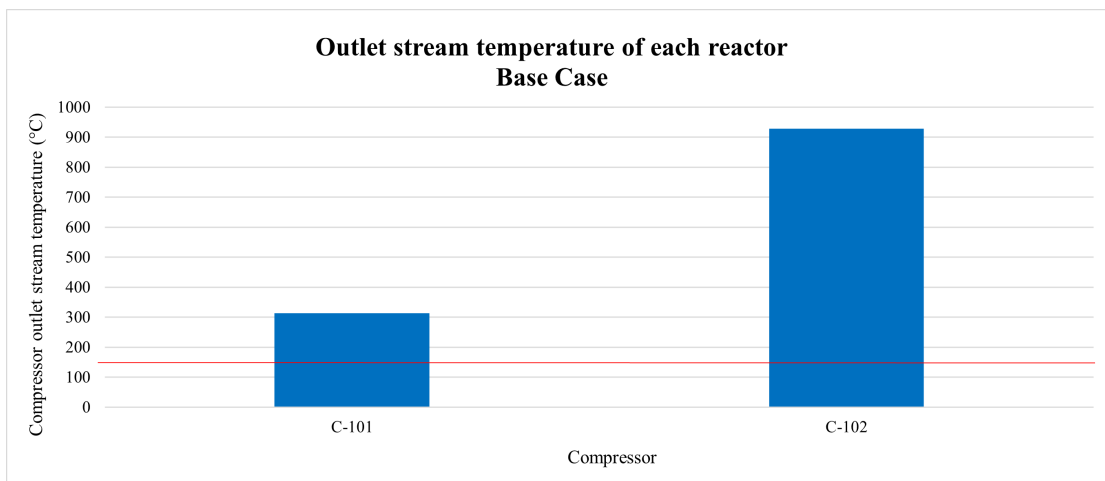


Figure 1.9: Temperatura del flusso di uscita di ogni compressore nel caso base

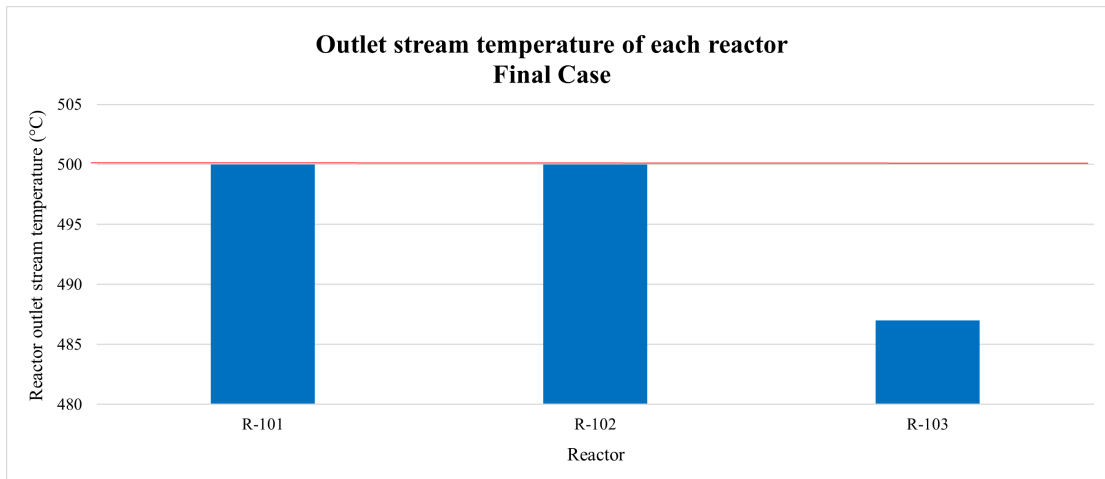


Figure 1.10: Temperatura del flusso di uscita di ogni reattore nel caso finale

Ogni figura rappresenta una parte diversa del processo simulato in Aspen Plus, che sarebbe la parte elettrolizzatore, la separazione dell'aria, il processo Haber-Bosch e la separazione dell'ammoniaca.

Nella figura 1.11 vengono messi a confronto i requisiti energetici dei due processi (i due casi diversi)

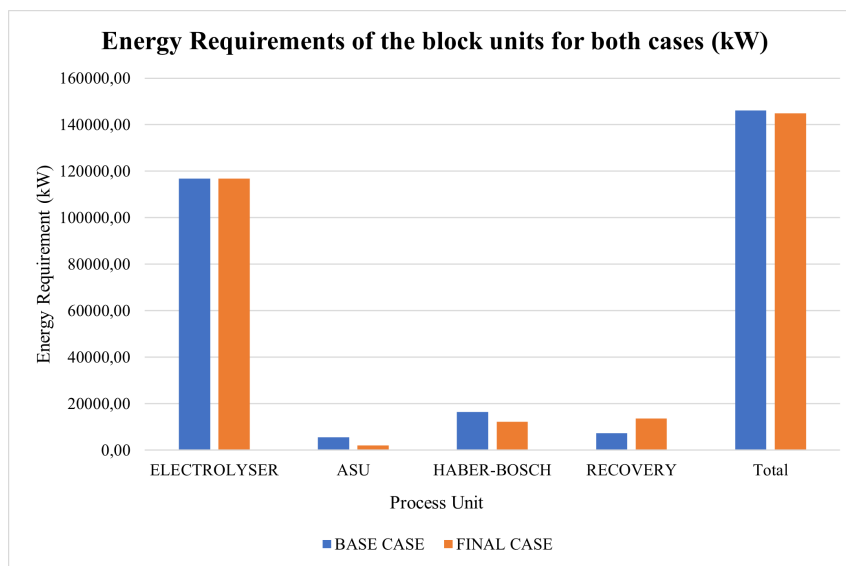


Figure 1.11: Confronto del fabbisogno energetico delle unità di blocco tra i due casi

Nonostante il fatto che la quantità di ammoniaca prodotta nel caso finale sia 4,58 volte superiore, le richieste di energia sono inferiori al caso base. Questo è legato principalmente all'integrazione di calore condotta nell'unità di separazione dell'aria e nel sistema multi-reattore. In aggiunta, lo scambiatore di calore che integra il flusso di uscita del reattore finale e il flusso di ingresso del riciclo, dà la possibilità di utilizzare meno utenze per condensare l'ammoniaca alla fine del processo. Questo può essere spiegato dalla presenza dei tre reattori, i quali nonostante un vincolo di T massima all'uscita di ognuno pari a T =

500 °C, permettono il raggiungimento di un tasso di riciclo totale del 95 %. Di conseguenza, la quantità di azoto e idrogeno che reagiscono è molto più alta.

In Figura 1.12 il confronto dei requisiti energetici in ogni step di processo è mostrato per il caso base modificato e per il caso finale. Il caso modificato corrisponde al caso in cui la produzione di ammoniaca è uguale a quella del caso finale. Come se può vedere, i fabbisogni energetici del caso base sono più alti rispetto al caso finale.

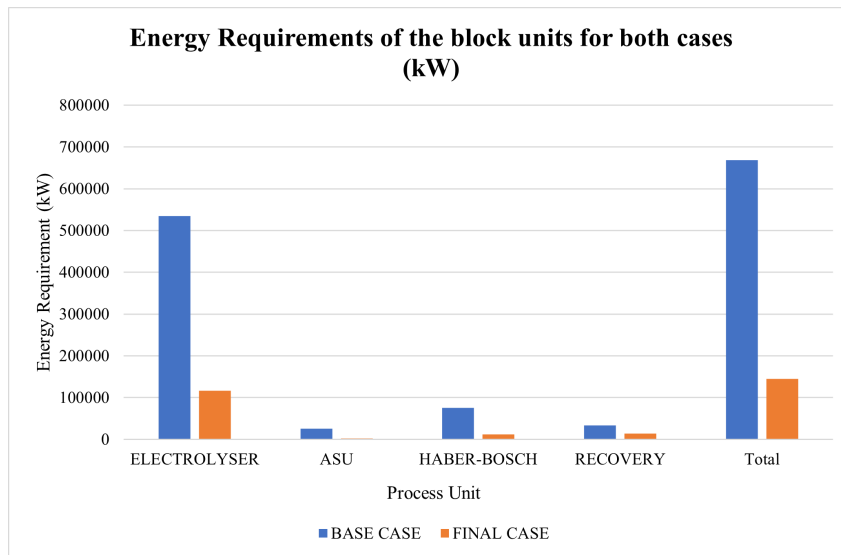


Figure 1.12: Confronto dei requisiti energetici delle unità di blocco tra il caso finale e il caso modificato

Come si evince nella figura 1.13, i due fattori determinanti per il CaPeX sono il costo dell'elettrolizzatore e compressori. Tale condizione è determinata dal fatto che l'elettrolizzatore, sia esso un AWE o un PEM, non è ad oggi una tecnologia molto matura, specialmente l'ultima tipologia. Pertanto, i suoi prezzi sono ancora molto alti.

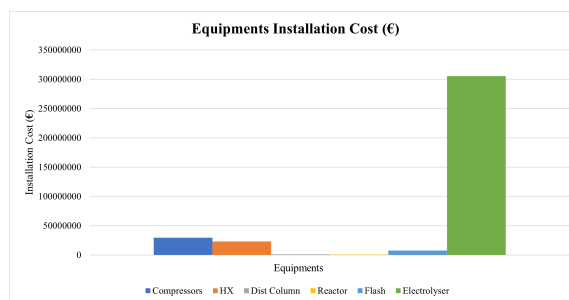


Figure 1.13: Valori calcolati per le diverse spese operative (CaPeX)

Tuttavia, come si vede nelle tabelle 1.1 e 1.2 se nel 2030 la produzione degli elettrolizzatori subisse uno scale-up il costo finale dell'unità elettrolizzatore diminuirebbe.

Table 1.1: Costi dell'elettrolizzatore simulato senza scale-up per gli anni 2020 e 2030

Type of electrolyser	Without scale-up			
	Year reference 2020		Year reference 2030	
	Cost (€)	Cost (€)	Cost (€)	Cost (€)
AEW	59.497.224	118.994.448	59.497.224	84.996.034
PEM	63.392.169	174.328.465	55.468.148	160.065.227

Table 1.2: Costi degli elettrolizzatori simulati con scale-up per gli anni 2020 e 2030

Type of electrolyser	With scale-up			
	Year reference 2020		Year reference 2030	
	Cost (€)	Cost (€)	Cost (€)	Cost (€)
AEW	48.787.723	97.575.447	43.432.973	62.047.105
PEM	52.615.500	144.692.626	42.710.474	120.809.626

Per quanto riguarda gli compressori, gli alti costi di CaPeX possono essere spiegati principalmente a causa del sistema di multi compressori con intercooling previo ad entrare nel processo Haber-Bosch, usato per portare il flusso entrante a 250 bar.

Prendendo in considerazione l'OpEx, il principale fattore che contribuisce al valore finale è l'alto costo dell'elettricità e i costi operazionali riguardanti il costo di installazione di tutte le apparecchiature, come si può vedere nella figura 1.14.

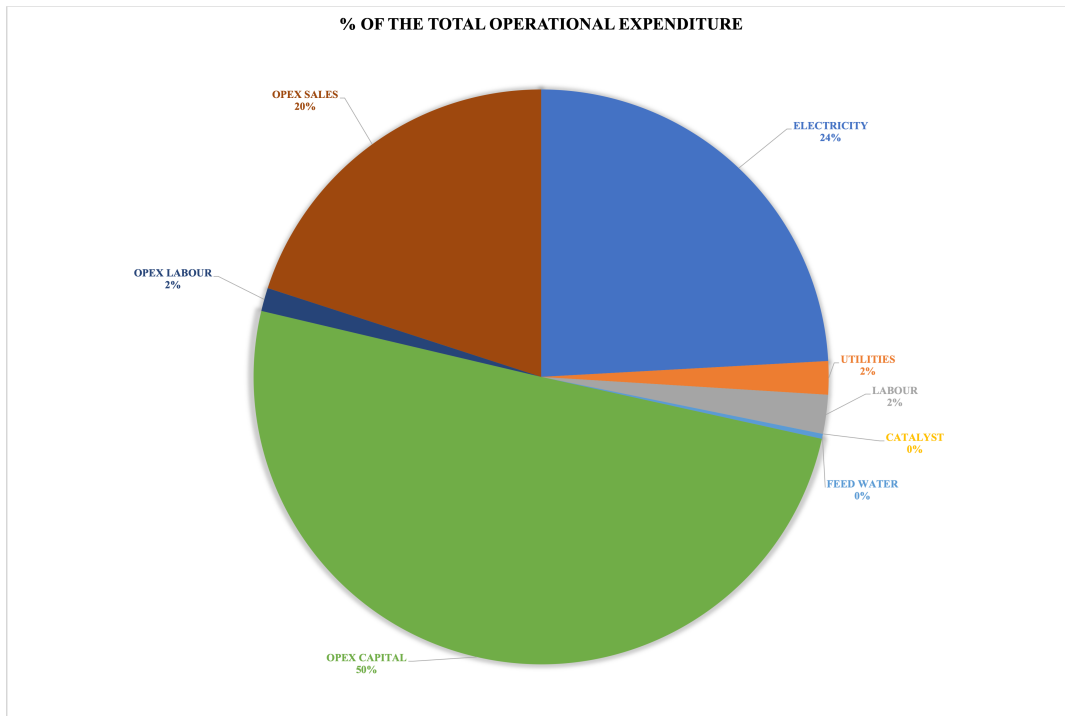


Figure 1.14: Valori calcolati per le diverse spese operative (OpEx)

Nello specifico, il costo dell'elettricità rappresenta un 24% di tutti i costi OpEx. Finalmente, nella figura 1.15, se può vedere il costo di vendita di ammoniaca che fa uguale l'OPEX con i guadagni annuali.

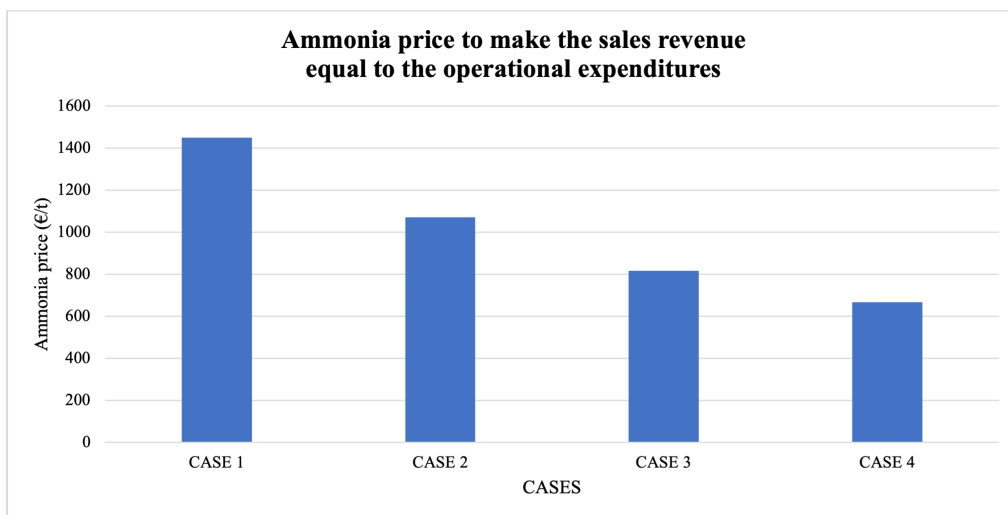


Figure 1.15: Prezzo dell'ammoniaca in cui le spese operative sono uguali alle entrate delle vendite: Confronto dei casi

Conclusioni e raccomandazioni:

È stata condotta un'analisi tecnico-economica di un processo di produzione di ammoniaca verde utilizzando il processo Haber-Bosch accoppiato con un elettrolizzatore per produrre idrogeno. I fattori più rilevanti emersi dell'analisi in oggetto sono stati i costi

dell'elettrolizzatore e dell'elettricità. Pertanto, è opportuno che in futuro vengano incrementati i finanziamenti a supporto di attività di R&D sugli elettrolizzatori PEM insieme a una riduzione dei prezzi dell'elettricità.

Sebbene i costi finali e requisiti energetici calcolati siano molto alti, è importante mantenere la T in uscita di ogni compressore inferiore ai 150 °C e la T in uscita di ogni reattore pari a 500°C. Tali misure permettono di assicurare la sicurezza del personale che lavora nell'impianto e nelle aree circostanti. Il metodo Guthrie utilizzato per calcolare i costi di installazione delle attrezzature e l'analisi di regressione lineare usata per determinare i costi dell'elettrolizzatore (cit.) hanno sempre un \pm % di errore nei loro calcoli. Pertanto, dovrebbero essere usati come analisi preliminare, per valutare la possibilità di costruire o meno un impianto.

In conclusione, nonostante i costi più elevati rispetto ad un processo Haber-Bosch convenzionale, è necessario convertire gli attuali impianti, in quanto il processo di produzione di ammoniaca verde mostrato in questa tesi non produce quasi CO₂. Tale condizione è assolutamente necessaria al giorno d'oggi per ridurre i gas serra e prevenire il riscaldamento globale.

2. Abstract

Hydrogen is becoming each day more attractive as an energy carrier. R&D are being carried out for producing high amounts of hydrogen by using AWE or PEM units, mainly to be used for fuel cells to produce electricity and as a feedstock for other process. However, the cost to store and compress hydrogen is very high, due to its low energy density. Therefore, ammonia appears as a potential substitute for hydrogen. Its combustion produces no harmful effects, apart that it can be used as hydrogen storage. A green ammonia plant located in the North of Chile was simulated in Aspen Plus. The main results showed that the energy requirements decrease highly when energy integration using two distillation columns and a multi reactor system with inter-cooling by using quenching and heat exchangers with a recycle stream was used. Regarding the economic analysis, the most conditioning factors were the high costs of the installation of the electrolyser and the electricity price. Consequently, it is mandatory to increase the funding in R&D and scale-up of electrolysers, along with reducing the electricity costs to make this process attractive in the future. More improvements, optimizations and analysis can always be carried out to make more efficient and feasible this process.

3. Introduction

Regarding the high increase in CO₂ emissions over the last years, the European Union (EU) has set itself the goal of reducing greenhouse gases (GHG) emissions by 80-95 % by 2050 in comparison to 1990. Hence, the use of renewable energies is mandatory in order to achieve this goal. Solar and wind power have become affordable technologies for energy production, although they are hindered by variability, seasonality and uncertainty [1].

The immense utilization of fossil fuels in the past decade has affected the environmental sustainability adversely. In order to avoid this problem, it is essential to move our energy matrix towards a sustainable and renewable energy matrix [2]. Problems such as pollution, GHG emissions and climate change, along with availability, are challenges that one must overcome nowadays in order to achieve the EU long-term goal [3].

From 1970 to 2004, annual carbon dioxide (CO₂) emissions originating from human activity have raised by 70 %. Nowadays, it reaches over 32 billion tonnes/year, while at least 50 billion tonnes/year are expected by 2050 [4]. Currently, we only use 110 million tonnes of CO₂/year from the 32 billion tonnes that we produce, mainly to produce other chemicals. Therefore, it is mandatory to decrease the CO₂ emissions as soon as possible.

With the use of solar and wind power, hydrogen is anticipated to be one of the best candidates for carbon-free fuels. It is a clean fuel and its burning causes no harmful emissions. However, the cost to produce, storage and compress it is very high [5].

Ammonia appears to be a potential solution as a hydrogen storage [6], being one of the most important and widely produced inorganic chemicals in the world, which is mainly used to produce fertilizers. [7]. In Chile, for example, ammonia is mainly used to produce explosives for the mining industry [8].

Global Ammonia production has been constantly growing, reaching 150.000 thousand tonnes worldwide in 2019 [9]. Consequently, it is mandatory to move to an ammonia green production process in order to prevent the global warming from rising even more the earth's temperature.

A detailed process of green ammonia production will be provided in this thesis by simulating two different cases, focusing in the case of Chile. One will be a simply base case, while the other one will be an optimization and improvement of the base case, called final case. They will consist mainly in a water electrolyser to produce H₂ as a feedstock for a Haber-Bosch process to produce ammonia, apart from all the necessary intermediate processes. The electrolyser will operate with electricity produced from renewable energy resources. This process is called Power-to-ammonia (P2A) [1].

The compounds properties and uses, unit operations, calculation and economic analysis will be done with didactic purposes. The use of Aspen Plus coupled with Excel calculator blocks will be used to simulate the ammonia production operation. Aspen Plus is a chemical engineering software designed for simulating processes, which provides all the chemical properties, mass and energy balances required for this process design.

4. Description of the Main Feedstocks and Product

In the following chapter, a description of the main raw materials and the main product will be done. Concepts, applications, sources and principal properties will be reported, many of which will be useful for the simulation section. References [8], [10],[11] , [14], [21], [22], [23], [33] and [37] were the main sources of information used in order to conduct this chapter.

4.1. Nitrogen

4.1.1. Main Characteristics and Description

Nitrogen is an element with atomic symbol N, atomic number 7 and atomic weight of 14,01. It appears as a colorless and odorless gas.

4.1.2. Applications

The importance of nitrogen to life is that it constitutes (with carbon, hydrogen and oxygen) the major part of proteins of all living materials. Most of living beings cannot use N_2 as a source of nitrogen and need different forms of fixed nitrogen as a supply for their requirement of protein synthesis (NO_3 and NH_4 for plants) [11]. Its main applications are:

- Food processing.
- Air purge.
- Air conditioning.
- Refrigeration systems.
- Pressurizing of aircraft tires.

4.1.3. Physical Properties

- Molecular Weight: 28,014 g/mol.
 - Boiling Point: $-195,79^{\circ}C$ (77,36K) at 1 bar.
 - Melting Point: $-210,01^{\circ}C$ (63,14K) at 1 bar.
 - Water Solubility: $1,81 \cdot 10^4$ mg/L at $21^{\circ}C$ (294,15K).
 - Critical Temperature: $-147,1^{\circ}C$ (126,05K).
 - Critical Pressure: 33,5 atm.
 - Heat of Vaporization: 5,57 kJ/mol at $-195.79^{\circ}C$ (77,36K).
 - Gas density: 1.251 g/L at $0^{\circ}C$ (273,15K) and 1 atm.
-

4.1.4. Sources

Nitrogen in its elemental form is the major component of the air with an equivalent of five billion tonnes presented in the atmosphere. It constitutes about 78% of the gases in the air, as shown in Table 4.1:

Table 4.1: Air composition in the Earth's atmosphere [25]

Component	Volume Fraction
Nitrogen	78,08 vol. %
Oxygen	20,95 vol. %
Argon	0,93 vol. %
Carbon Dioxide	400 vppm ^a
Neon	180 vppm
Helium	5 vppm
Methane	1,8 vppm
Krypton	1,1 vppm
Hydrogen	0,5 vppm
Nitrous Oxide	0,3 vppm
Carbon monoxide	0,2 vppm
Xenon	0,09 vppm

^a vppm: volume parts per million

The elemental form of nitrogen (N_2) is very unreactive and difficult to extract from the environment. Therefore, complex processes must be operated in order to extract it from the air. Nitrogen is nowadays separated from other compounds by using Pressure Swing Adsorption (PSA) systems or cryogenic distillation. There are also different nitrogen gaseous compounds that exist in the atmosphere including NH_3 , NO and N_2O .

Nitrogen exists naturally in our environment and is constantly being converted from organic to an inorganic form and vice versa. Naturally occurring and anthropogenic production make up the whole nitrogen cycle today.

The significant increase in human population along the past 100 years increased the demand for food which lead to mass production of synthetic nitrogen fertilizers for agricultural activities. These activities, summed up to energy generation, transport and use of fossil fuels, alter the nitrogen cycle.

Figure 4.1 shows a resume of the nitrogen cycle. This cycle is very important, since it shows how N_2 is returned back to the atmosphere (feedstock for our process) and how plants use nitrogen fixation in order to grow.

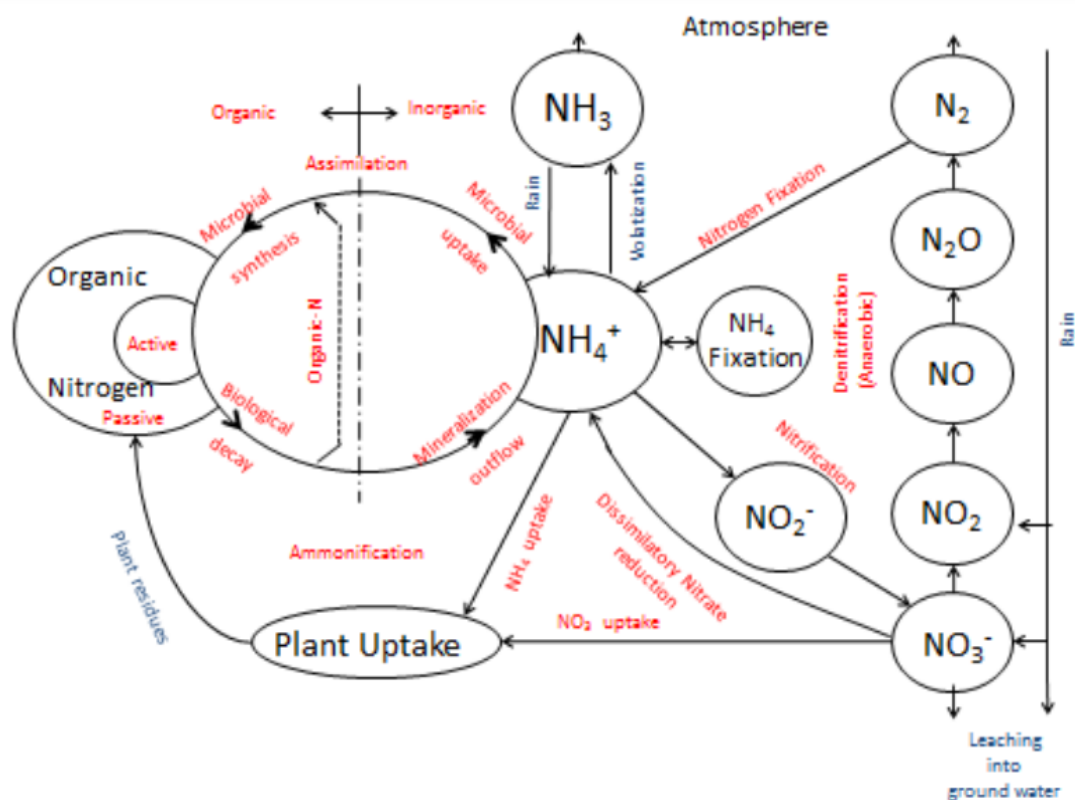


Figure 4.1: Nitrogen cycle in nature [11]

4.1.5. Safety Aspects and Procedures

Globally Harmonized System of Classification and Labelling of Chemicals (GHS) Hazard Statements H280 (100%): In case of container with N_2 under pressure, may explode if under prolonged exposure to fire and rocket. In high concentrations it may cause asphyxiation by displacement of air.

4.2. Hydrogen

4.2.1. Main Characteristics and Description

Hydrogen is an element with atomic symbol H, atomic number 1 and atomic weight of 2,016 g/mol. It appears as a colorless and odorless gas. It can be easily ignited, and its ignition can be seen with a pale blue, almost invisible flame. Dihydrogen is the molecule obtained when two atoms of hydrogen join by a single bond.

4.2.2. Physical Properties

- Molecular Weight: 2,016 g/mol.
- Boiling Point: $-253\text{ }^\circ\text{C}$ (20,15K) at 1 atm.
- Melting Point: $-259,2^\circ\text{C}$ (13,95K).
- Water Solubility: $1,62 \cdot 10^4$ mg/L at 21°C (294,15K).

- Critical Temperature: -240,15 C (33K).
- Critical Pressure: 12,4 atm.
- Heat of Vaporization: 0,9 kJ/mol at -252,87°C (20,28K).
- Heat of Combustion: -285,8 kJ/mol.
- Gas Density: 0,082 g/L at 0°C (273,15K) and 1 atm.

4.2.3. Hydrogen as an Energy Carrier

Hydrogen is not an energy source, as it cannot be found in the Earth. Therefore, it can only be obtained from other compounds with H₂ composition on them, making it an energy carrier like electricity.

It can be stored and transported, and it can be used as a fuel or converted to electrical energy in devices such as fuel cells. Hydrogen can be benign environmentally depending on the energy source from which it is derived.

The main advantages of hydrogen as an energy carrier are [12]:

- **Producible:** Can be manufactured from hydrocarbon and non hydrocarbon sources such as water.
- **Utilizable:** Can be used as a chemical fuel and as a chemical feedstock in many industrial processes.
- **Storable:** Unlike electricity, it can be stored in large quantities and in various forms (ammonia for example). Some ways to store hydrogen are:
 - As compressed in liquid tanks.
 - As a cryogenic liquid (20,3K) in well insulated tanks.
 - As a mixed phase, called hydrogen slush.
 - As a gas in underground reservoirs and caverns (similar to how natural gas is stored).
 - In chemical bonds with other materials such as metal hydrides.
 - By adsorption of H₂ molecules by a porous material.
- **Recyclable:** Hydrogen is recyclable as an energy carrier; it oxidizes to water and water can be separated to generate hydrogen.
- **Transportable:** It can be easily transported through various means of transport such as road, rail, ship, among others. Besides, it is transportable over long distances using conventional pipeline technology with losses lower than those associated with electrical lines.

Hydrogen as an energy carrier has some disadvantages too, such as:

- Hydrogen storages have energy storage densities that are less than those for gasoline storages on both mass and volume bases. For example, on a mass basis, the highest hydrogen energy storage density is attained using a liquid hydrogen storage, which energy storage density is approximately 80 % that of a gasoline storage. This is an issue in hydrogen fuel applications. Moreover, it is important to consider that up to 20 % of the energy content of hydrogen is required to compress the gas, and up to 40 % to liquefy it.
- It is more expensive to produce hydrogen compared to fossil fuels at present.
- Hydrogen can cause materials problems, such as embrittlement on alloys or vessel leaking.

4.2.4. Applications

The main applications of hydrogen are [13]:

- As an antioxidant.
 - As an electron donor.
 - As a human metabolite.
 - As a food packaging gas.
 - As a coolant in electric generators.
 - As a reactant:
 - To synthesize ammonia (most of the H_2 produced is used to synthesize ammonia).
 - Hydrocarbon cracking and hydroprocessing. In the hydrocracking processes, cracking and hydrogenation of hydrocarbons takes place simultaneously to produce refined fuels with smaller molecules and higher H/C ratios.
 - Petrochemical production such as methanol.
 - In the reduction stage of producing nickel.
 - As an oxygen scavenger:
 - To chemically remove trace amounts of O_2 to prevent oxidation and corrosion.
 - Hydrogen mixed with nitrogen is used for heat treating applications to remove O_2 as O_2 scavenger. O_2 reacts with H_2 to produce H_2O , which oxidation potential is much lower than O_2 .
 - As a fuel:
 - The primary application as a fuel is in the Aerospace Industry. A mixture of liquid H_2 and O_2 has been found to release the highest amount of energy per unit weight of propellant.
 - In fuel cells that use H_2 to produce electricity.
 - In a future prospective as fuel in cars.
-

4.2.5. Hydrogen as A Green Fuel

In a combustion reaction ($\text{CH}_4 + 2\text{O}_2 \rightarrow \text{CO}_2 + 2\text{H}_2\text{O}$), the energy contribution from hydrogen (H) is 120 kJ/g, while the contribution from carbon (C) is only 33 kJ/g. Apart from this, the hydrocarbon reaction produces CO_2 , which is one of the main GHG we want to avoid to produce.

Hydrogen reacts with oxygen in a combustion reaction to produce water and energy ($2\text{H}_2 + \text{O}_2 \rightarrow 2\text{H}_2\text{O}$), with a lower heating value (LHV) of 120 kJ/g. Since hydrogen has got no carbon, it has the highest possible energy density of any hydrogen-based fuel. Moreover, the water produced from hydrogen combustion can be used again to create more hydrogen to provide a sustainable cycle.

The problem is, since H_2 has a very low energy density, more than 3500 gallons of H_2 gas are necessary to replace just one gallon of gasoline at standard temperature and pressure (STP). A solution to this is to store it in metal hydrides, which gives a higher volumetric and gravimetric energy density, as it is shown in the Figure 4.2.

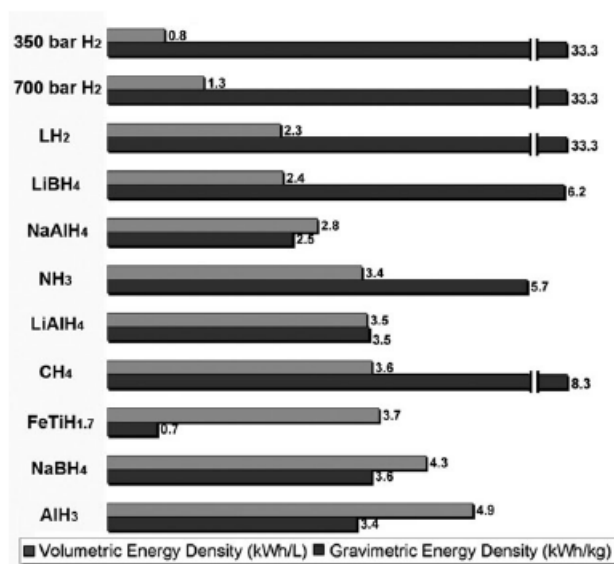


Figure 4.2: Comparison of different volumetric and gravimetric energy densities of several metal hydrides and other hydrogen storage media [33]

4.2.6. Sources

Hydrogen is not an energy source, is an energy carrier, since it does not occur in nature in its elemental or molecular form, as mentioned before. Consequently, it must be obtained from other compounds.

Currently, 96 % of H_2 is produced directly from fossil fuels and about 4 % is produced indirectly by using electricity generated through fossil fuels. This accounts for coal gasification, partial oxidation of hydrocarbons such as biomass and steam methane reforming (SMR), which nowadays is the dominant hydrogen production process. [5]. However, these

fuels have a limited supply, and in addition, they release GHG during the production of hydrogen.

Hydrogen can also be produced by catalytic decomposition of natural gas, partial oxidation of heavy oil, coal gasification, thermal water decomposition, photochemical, electrochemical and biological processes, and water electrolysis.

Steam reforming is the less polluting option among using fossil fuels, and its efficiency ranges from 70 to 80 %. The technology for hydrogen production from both of these feedstocks is well advanced, and significant experience exists in the operation of these type of plants.

Hydrogen can be produced from various feedstocks, although the most used are natural gas and coal. Natural gas, a fossil fuel, is in general found near areas with large oil or coal reserves. Coal is also a fossil fuel formed millions of years ago from prehistoric vegetation. This vegetation accumulated in swamps and peat bogs where it was buried due to the movement of the earth's crust and the build-up of sediment.

As the supply of fossil fuel decreases, alternatives to hydrogen production must be developed for both environmental and economic reasons. The cost of fossil fuels is rapidly increasing while many alternative sources of energy are decreasing in cost as technologies improve and economies of scale are achieved.

The most common alternative way to obtain H₂ is from water. The two main procedures are either by using electricity via electrolysis or using heat with a thermochemical process such as thermal cracking. Both of these processes break water down into its hydrogen and oxygen components.

In order to drive a green hydrogen production process, the electricity to supply the electrolyser must be obtained via renewable energy, such as wind, solar, hydroelectric, geothermal, etc.

In Figure 4.3 a schematic representation of the principal hydrogen production methods is shown:

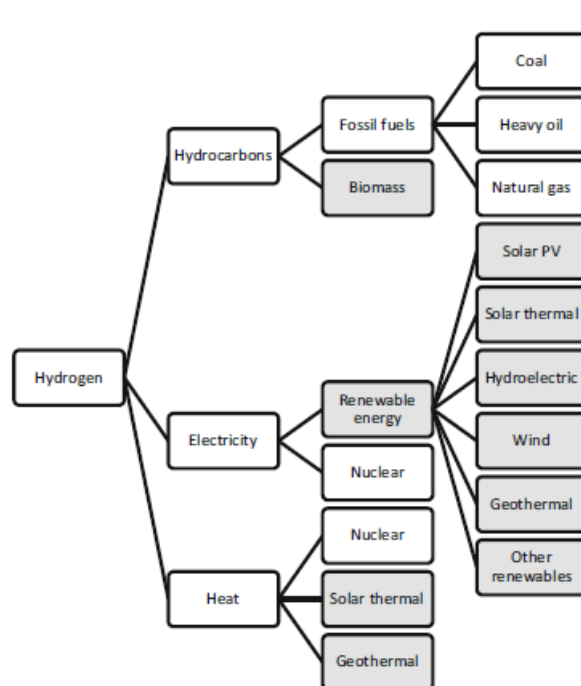


Figure 4.3: Main Hydrogen sources [12]

4.2.7. Safety Aspects and Procedures

Vapors may cause dizziness or asphyxiation without warning, while contact with gas or liquefied gas may cause burns, severe injury and/or frostbite.

It is flammable over a wide range of vapor/air concentrations (has a Lower Flammability Limit (LFL) of 4 and an Upper Flammability Limit (UFL) of 75% respect to air volume). Moreover, under prolonged exposure to fire or intense heat the containers may rupture violently and rocket.

In case of fire it is recommended to shut off the supply. In case it is not possible and there is no risk to surroundings, let the fire burn itself out. In other case the fire must be extinguished by using water spray or carbon dioxide.

GHS Hazard Statements H220: It is an extremely flammable gas with highly dangerous fire and severe explosion hazard when exposed to heat, flame, or oxidizers.

NFPA Statements for hydrogen:

- NFPA Health Rating 0: Under emergency conditions it will not offer hazard beyond that of ordinary combustible materials.
- NFPA Fire Rating 4: Has a rapidly or completely vaporization at atmospheric pressure and normal ambient temperature.
- NFPA Instability Rating 0: Is stable under fire conditions.

4.3. Ammonia

4.3.1. Main Characteristics and Description

Ammonia is an inorganic compound composed of a single nitrogen atom covalently bonded to three hydrogen atoms. It appears as a colorless gas or as a compressed liquid with a pungent odor. Its molecular formula is NH_3 , and has an atomic weight of 17,031 g/mol. Dissolved in water is called liqueous or aqueous ammonia.

4.3.2. Physical Properties

- Molecular Weight: 17,031 g/mol.
- Boiling Point: $-33,35^\circ\text{C}$ (239,8K) at 1 atm.
- Melting Point: $-77,7^\circ\text{C}$ (195,45) at 1 atm.
- Water Solubility: $4,82 \cdot 10^5$ mg/L at 24°C .
- Critical Temperature: $132,4^\circ\text{C}$ (405,55K).
- Critical Pressure: 111,5 atm.
- Heat of Vaporization: 5,581 kcal/mol.
- Gas Density: 0,082 g/L at 0°C and 1 atm.

4.3.3. Main Chemical Reactions Involving Ammonia

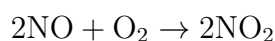
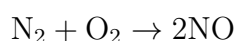
Ammonia can self ionize following the next reaction:



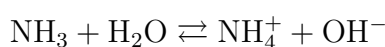
Also, ammonia can be combusted, although its combustion proceeds with difficulty but yields nitrogen gas and water, which are not categorized as GHG.



Ammonia can react with oxygen too to produce nitric oxide, and oxidize again to form nitrogen dioxide, compound used in the industrial synthesis of nitric acid, precursor of Trinitrotoluene (TNT) and nitroglycerin.



In addition, ammonia dissolves in water with the liberation of heat.



4.3.4. Applications

Ammonia is mainly used as a precursor for fertilizers. The main compounds containing ammonia used as fertilizers are:

- Ammonium nitrate (NH_4NO_3).
- Ammonium sulfate ($(\text{NH}_4)_2\text{SO}_4$).
- Ammonium phosphates.
- Urea ($(\text{H}_2\text{N})_2\text{CO}$) (the most utilized worldwide).

Ammonia is also used in the mining industry as explosives, where TNT and nitroglycerin are the most employed.

In the textile industry, ammonia is utilized in the manufacture of synthetic fibres, such as nylon and rayon.

Further applications of ammonia are mainly to develop catalysts in different reactions, the metallurgical industry and as a fuel.

4.3.5. Ammonia as a green fuel

Ammonia has been used occasionally in the past as a fuel for internal combustion engines (ICE) and fuel cells. Ammonia has a high content of hydrogen atoms per unit of volume and a density 4 times higher compared to the most advanced storage methods of H_2 in metal hydrides. As a fuel, ammonia has the following advantages compared to hydrogen and methanol:

- Has an octane rate of 110-130, which makes it an excellent fuel for ICE, although it cannot be used in regular ICE engines due to its low flame speed. Even though, by partially decomposing NH_3 into H_2 and N_2 , the three compounds mixture can feed a normal ICE.
- It can be thermally cracked into hydrogen and nitrogen using low energy (12 % from the Higher Heating Value (HHV) of ammonia to produce hydrogen for fuel-cells).
- It is safer respect to some fuels and H_2 because:
 - If escapes into the atmosphere it dissipates rapidly because its density is lighter than air.
 - It is self alarming: Any leakage can be detected by nose in concentrations as low as 5 ppm.
 - Has a narrow flammability range (LFL of 14,8% and UFL of 33,5% concentration of ammonia by volume in air).

In the case of ammonia combustion in internal combustion engines (ICE), some amounts of NO_x will result due to the excess of nitrogen in the combustion chamber. Although, this amounts can be minimized by adjusting the air-fuel ratio: at excess air over 3 the NO emission is almost 0 and at excess air over 5 the NO_2 emission is below 50 ppm.

It is also important to account that NH_3 serves as a reduction agent for NO_x emissions. NO_x gases contribute to air pollution and smog, therefore its production should be avoided as maximum as possible. The reaction of NO_x with ammonia produces only steam and nitrogen. An average car needs only 30 ml of ammonia per 100 to neutralize all NO_x emissions, which is an insignificant amount compared to the amount presented in a car fuel tank.

In Tables 4.2 and 4.3, a comparison of ammonia with other fuels is shown. It can be seen that ammonia has a higher HHV/ m^3 compared to hydrogen, methanol and compressed natural gas (CNG). Also, the cost per kmol of carried hydrogen is lower for ammonia compared to other fuels.

Table 4.2: Comparison of ammonia with other fuels including hydrogen [32]

Comparison of ammonia with other fuels including hydrogen							
Fuel/Storage	P [bar]	Density [kg/ m^3]	HHV [MJ/kg]	HHV' [GJ/ m^3]	c [CN\$/kg]	C [CN/ m^3]	C/HHV' [CN\$/GJ]
Gasoline, C_8H_{18} /liquid	1	736	46,7	34,4	1,36	1000	29,1
CNG, CH_4 /integrated storage	250	188	42,5	10,4	1,20	226	28,2
LPG, C_3H_8 /pressurised tank	14	388	48,9	19,0	1,41	548	28,8
Methanol, CH_3OH /liquid	1	786	14,3	11,2	0,54	421	37,5
Hydrogen, H_2 /metal hydrides	14	25	142,0	3,60	4,00	100	28,2
Ammonia, NH_3 /pressurised tank	10	603	22,5	13,6	0,30	181	13,3

HHV: Higher Heating Value per kg, HHV': Higher Heating Value per m^3 , c: cost per kg, c': cost per m^3

Table 4.3: Further comparison of ammonia with other fuels including hydrogen [32]

Further comparison of ammonia with other fuels including hydrogen			
Fuel/Storage	Hydrogen Content [kmol/ m^3]	Hydrogen Content [kmol/kg]	C ¹ [CN\$/kmol]
Gasoline, C_8H_{18} /liquid	116,2	0,16	8,5
CNG, CH_4 /integrated storage	47	0,25	4,8
LPG, C_3H_8 /pressurised tank	70,5	0,18	7,8
Methanol, CH_3OH /liquid	98,3	0,13	4,2
Ammonia, NH_3 /pressurised tank	106,4	0,18	1,7

C¹: Cost per kmol of carried hydrogen regarding the fuel as hydrogen carrier.

4.3.6. Sources

Ammonia can be manufactured either by using the Haber-Bosch process employing nitrogen and hydrogen as feedstocks (almost all ammonia comes from this process), produced naturally from bacterial processes (bacteria in the intestine) or from the breakdown of organic matter (human activity).

Worldwide, two thirds of the ammonia production is obtained from natural gas-derived hydrogen, and in China 97% of ammonia is produced from natural gas and coke-derived hydrogen.

An innovative way to produce ammonia from a cyclic process by using electrolysis is studied in [28]. This process can be run at Standard Temperature and Pressure (STP) conditions, and requires no H_2 . Moreover, it can be powered sustainably by using solar or wind powered energy.

This process is done in three steps:

1. LiOH electrolysis:
 - Total Cell : $6\text{LiOH} \rightarrow 6\text{Li} + 3\text{H}_2\text{O} + 3/2\text{O}_{2(\text{g})}$
 - Cathode : $6\text{Li}^+ + 6\text{e}^- \rightarrow 6\text{Li}$
 - Anode : $6\text{OH} \rightarrow 3\text{H}_2\text{O} + 3/2\text{O}_{2(\text{g})} + 6\text{e}^-$
2. Direct reaction of metallic Li with N_2 to form Li_3N :
 - $6\text{Li} + \text{N}_{2(\text{g})} \rightarrow 2\text{Li}_3\text{N}_{(\text{s})}$
3. Release of NH_3 by reaction with H_2O :
 - $2\text{Li}_3\text{N}_{(\text{s})} + 6\text{H}_2\text{O} \rightarrow 6\text{LiOH} + 2\text{NH}_3$

The demonstrated process has an initial overall current efficiency of 88,5% to ammonia, based on the individually determined efficiencies of each step. Furthermore, techno-economic electricity cost analysis and energy input considerations for this process reveal promise for suitable markets.

4.3.7. Safety Aspects and Procedures

In one hand, gas ammonia is generally regarded as nonflammable, but does burn within certain vapor concentration limits and with strong ignition. Moreover, fire hazard increases in the presence of oil or other combustible materials. Additionally, prolonged exposure of ammonia containers to fire or heat may cause violent rupturing and rocketing. On the other hand, liquid ammonia is very safe, as it quickly turns into a gas when exposed to air.

In terms of toxicity, long-term inhalation of low concentrations of the vapors or short-term inhalation of high concentrations has adverse health effects.

GHS Hazard Statements:

- H221: Flammable gas.
- H314: Causes severe skin burns and eye damage.
- H331: Toxic if inhaled.
- H400: Very toxic to aquatic life.

NFPA Statements:

- NFPA Health Rating 3: Under emergency conditions can cause serious or permanent injury.
- NFPA Fire Rating 1: Must be considerably preheated under all ambient conditions before ignition can occur.
- NFPA Instability Rating 0: Is normally stable even under fire conditions.

It could be a potential fire hazard when in storage as cylinders exposed to fire may explode. Therefore, pressure relief devices can be used to vent to release toxic and/or corrosive gas. Anhydrous ammonia at high concentrations in confined spaces, presents a flammability risk if a source of ignition is introduced.

4.4. Water

4.4.1. Main Characteristics and Description

Water appears as a transparent fluid, nontoxic liquid composed of hydrogen and oxygen. It forms the world's streams, lakes, oceans and rain. Moreover, is the major constituent of the fluids of organisms. Its molecular formula is H₂O.

Water is a liquid at STP, but it often co-exists on Earth with its solid state (ice) and gaseous state (water vapor).

4.4.2. Physical Properties

- Molecular Weight: 18,015 g/mol.
- Boiling Point: 100°C (373,15K) at 1 atm.
- Melting Point: 0°C (273,15K) at 1 atm.
- Critical Temperature: 374,2 °C (647,35K).
- Critical Pressure: 218 atm.
- Heat of Vaporization: 9,717 kcal/mol.
- Liquid Density: 1000 kg/m³ at 0°C (273,15K) and 1 atm.

4.4.3. Sources

Water is the most widespread substance to be found in the natural environment. It can be found in many places among the earth, such as oceans, seas, lakes, rivers, glaciers, the underground waters found in the top layers of the Earth's crust, soil cover and the atmosphere. Water can also be included in many compounds, minerals, food, etc.

Current estimations show that the Earth's hydrosphere contains about 1318 million cubic kilometres, which is a big amount. However, only 2,5 % corresponds to fresh water. A significant amount of fresh water (68,7 %) can be found as ice and snow in the Antarctic, Arctic and mountainous regions. Another 29,9 % exists as fresh groundwaters, while only 0,26 % is concentrated in lakes, reservoirs and river systems, which are the most accessible sources for our needs.

In the case of Chile, the central agency controlling the study, monitoring and use of water resources is "Dirección General de Aguas (DGA)", which belongs to the "Ministerio de Obras Públicas". DGA divides the country in 101 River basins.

In Chile there are 1.251 rivers, 12.784 lakes and lagoons, and 24.114 glaciers. Average annual precipitation over the territory and the corresponding runoff are estimated to be 1.525 and 1.220 mm/year, respectively. Overall, Chile is a privileged country in terms of water resources. The average annual runoff per capita is ~ 51.218 m³/person/year, value well above 1.000 m³/person/year, the limit that typically defines water scarcity.

In Figures 4.4 and 4.5 water availability (water available for use divided by the total population of the country [m³/population]) for years 1950, 1995 and expected for 2025 is shown. One can observe that Chile has an excellent water availability since 1950, and it is expected to continue in 2025.

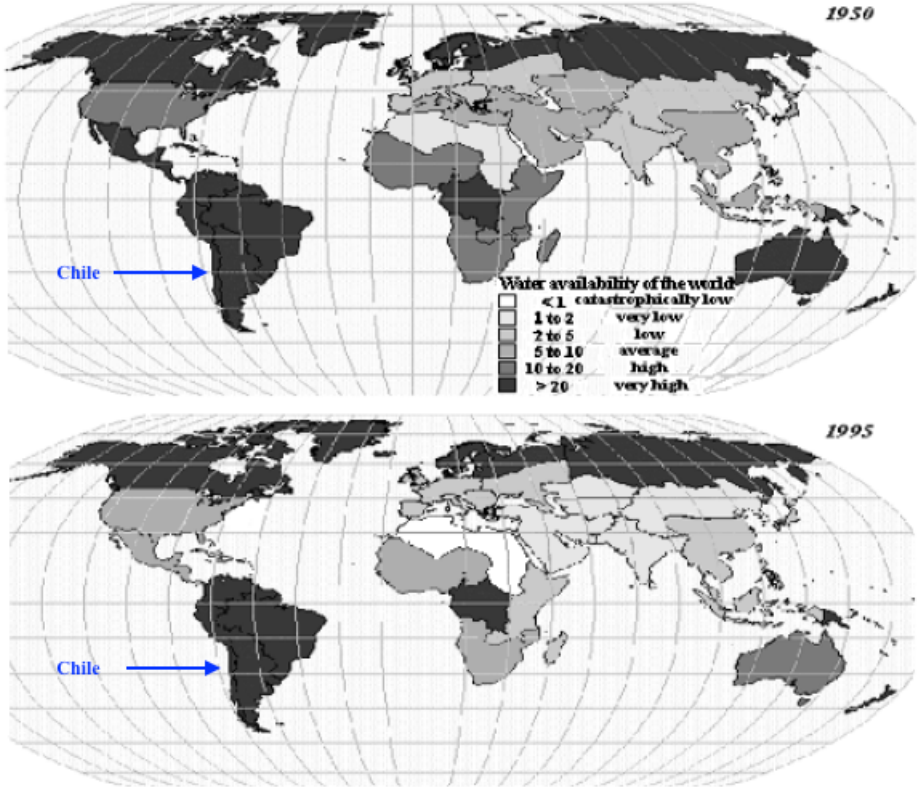


Figure 4.4: World’s Water Availability by country, 1950 and 1995, adapted from [37]

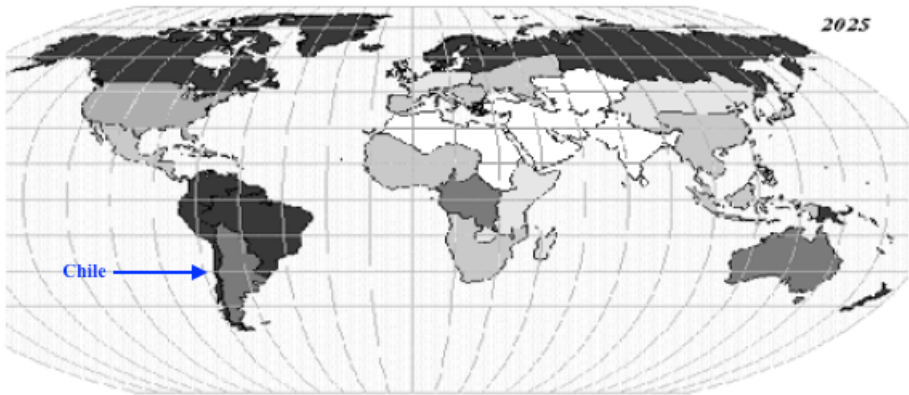


Figure 4.5: World’s expected Water Availability by country, 2025, adapted from [37]

4.4.4. Safety Aspects and Procedures

Reported as not meeting Globally Harmonized System of Classification and Labelling of Chemicals (GHS) hazard criteria, the chemical has been verified to be of low concern based on experimental and modeled data. Water itself is nontoxic and is in fact essential for life. Solutes dissolved in water may be toxic, but those interactions are covered by the reactive groups that the solute belongs to.

5. Main Processes for the Production of Green Ammonia

In the following sections, the dominant processes to produce green ammonia will be described. The majority of these processes will be simulated in Aspen Plus and described in a future section, while some will be described for didactic and comparative purposes. References [15], [16], [17], [18], [19], [20], [25], [27], [38], [55], [56], [59] and [60], were the main sources of information used to conduct this chapter.

5.1. Haber-Bosch Process

5.1.1. Haber-Bosch History and Schemes

In 1909, Fritz Haber and Carl Bosch developed the Haber-Bosch process, an artificial nitrogen fixation process, which enabled the large-scale production of ammonia. This process was a transformation for our society, leading the first chemical global revolution [15].

This process enabled the expansion of the world population from 2 billion to 7 billion in the last century, since the ammonia produced has been extensively used as fertilizer, making it possible to grow food faster than ever imagined [15].

In Figures 5.1 and 5.2 a general scheme of a Haber-Bosch process is shown. The first one uses hydrogen and nitrogen produced from SMR (steam methane reforming), while the second one uses hydrogen and nitrogen produced from an electrolyser and from PSA (pressure swing adsorption) respectively.

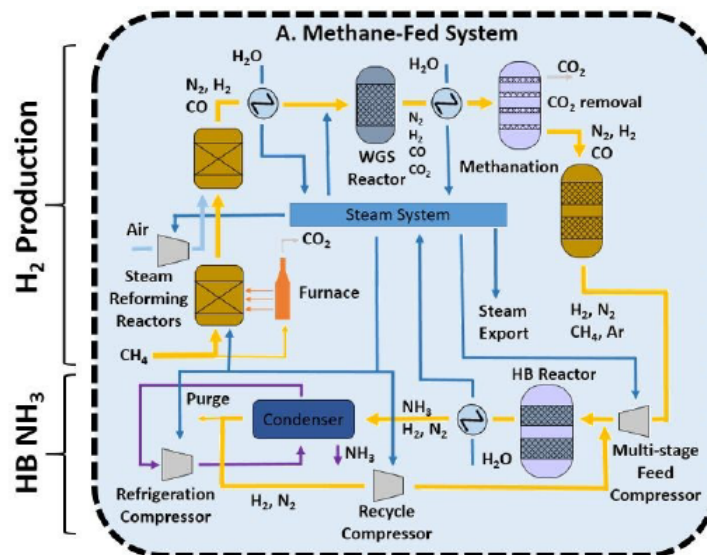


Figure 5.1: Methane fed Haber-Bosch process scheme [15]

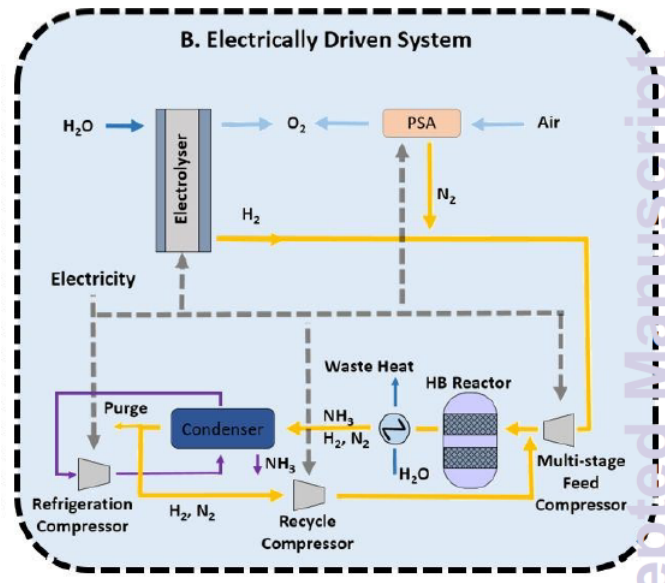


Figure 5.2: Electrically driven Haber-Bosch process scheme [15]

Each of the following parts of both schemes will be described in the following sections, except the Haber-Bosch reactor that will be described in this section.

5.1.2. Ammonia production kinetics

The overall stoichiometric equation for producing ammonia using the Haber-Bosch process is shown in equation (5.1),



Where ΔH^0 corresponds to the standard enthalpy of the reaction. As $\Delta H^0 < 0$, this corresponds to an exothermic reaction. The equilibrium constant can be calculated with the empirical equation (5.2),

$$\log_{10}k_a = -2,691122\ln(T) - 5,519265 \cdot 10^{-5}T + 1,848863 \cdot 10^{-6}T^2 + \frac{2001,6}{T} + 2,689 \quad (5.2)$$

In general the Haber-Bosch reaction is carried out by using iron based catalysts (magnetite or wüstite). Extensive studies on ammonia synthesis on iron catalysts suggest that the reaction follows the next steps:

1. $N_2(g) \rightarrow 2N(ads)$
2. $H_2(g) \rightarrow 2H(ads)$
3. $N(ads) + H(ads) \rightarrow NH(ads)$
4. $NH(ads) + H(ads) \rightarrow NH_2(ads)$
5. $NH_2(ads) + H(ads) \rightarrow NH_3(ads)$
6. $NH_3(ads) \rightarrow NH_3(g)$

This reactor operates based on the two kinetic reactions (5.3) and (5.4), based on reaction (5.1),



As found in paper [55], the reaction kinetics on iron catalysts can be expressed by means of the temkin-pyzhev equation (5.5), which can be expressed as,

$$\frac{dN_{N_2}}{dx} = -f \left[K_1 \frac{p_{N_2} p_{H_2}^{1,5}}{p_{NH_3}} - K_2 \frac{p_{NH_3}}{p_{H_2}^{1,5}} \right] \quad (5.5)$$

Where:

- $K_1 = k_1 \cdot \exp\left(\frac{-E_1}{RT_g}\right)$
- $K_2 = k_2 \cdot \exp\left(\frac{-E_2}{RT_g}\right)$
- $k_1 = 1,78954 \cdot 10^4 \left[\frac{kmol}{m^3 \cdot h \cdot atm^{1,5}} \right]$
- $k_2 = 2,5714 \cdot 10^{16} \left[\frac{kmol \cdot atm^{0,5}}{m^3 \cdot h} \right]$
- $E_1 = 20.800 \text{ kcal/kmol}$
- $E_2 = 47400 \text{ kcal/kmol}$
- Reaction rate = $-\frac{dN_{N_2}}{dx} \left[\frac{kmol_{N_2}}{s \cdot m^3} \right]$ (reactor volume basis)
- $f = \text{catalist activity} = 1$
- $p_{N_2}, p_{H_2}, p_{NH_3} = \text{partial pressure of } N_2, H_2 \text{ and } NH_3 \text{ respectively.}$

In order to put these parameters in Aspen Plus reactions all the units must be put in SI. Aspen defines SI units as length in meters, mass in kilograms, time in seconds, temperature in Kelvin, and pressure in Pascals. Therefore, we must convert k_1, k_2, E_1 and E_2 to SI, in order to agree with the reaction rate units. By doing this, the following values of these parameters are obtained:

$$E_1 = 20.800 \frac{kcal}{kmol} \cdot 4,18 \frac{kJ}{kcal} = 86944 \frac{kJ}{kmol}$$

$$E_2 = 47.400 \frac{kcal}{kmol} \cdot 4,18 \frac{kJ}{kcal} = 198132 \frac{kJ}{kmol}$$

$$k_1 = 1,78954 \cdot 10^4 \frac{kmol}{m^3 \cdot \cancel{h} \cdot atm^{1,5}} \cdot \frac{1 \cancel{h}}{3600 s} \cdot \frac{1}{101.325^{1,5}} \frac{atm^{1,5}}{Pa^{1,5}}$$

$$k_1 = 1,54 \cdot 10^{-7} \frac{kmol}{m^3 \cdot s \cdot Pa^{1,5}}$$

$$k_2 = 2,5714 \cdot 10^{16} \frac{kmol \cdot atm^{0,5}}{m^3 \cdot \cancel{h}} \cdot \frac{1 \cancel{h}}{3600 s} \cdot 101.325^{0,5} \frac{Pa^{0,5}}{atm^{0,5}}$$

$$k_2 = 2,27 \cdot 10^{15} \frac{\text{kmol} \cdot \text{Pa}^{0,5}}{\text{m}^3 \cdot \text{s}}$$

5.1.3. Reaction Rate and Equilibrium

In terms of the reaction rate and equilibrium, we can analyze equation (5.1) in terms of the reaction heat (added or subtracted), temperature and pressure. The Haber-Bosch reaction is exothermic, which means that the reaction will release energy in form of heat. According to Le Chatelier's Principle, if heat is added to the system the reaction will shift to the left, and if heat is removed from the system the reaction will shift to the right.

Another important factor is how the pressure affects the kinetic of the reaction. In order for the reaction to occur the particles must collide. For a higher pressure, the chances of the gas molecules colliding is higher, which will give a higher reaction rate.

According to Le Chatelier's Principle if pressure is increased the system will react to reduce the stress (reduce the pressure) shifting the reaction in the direction which minimizes the number of molecules of gas. Since there is a fixed volume, a way to reduce the system's pressure is to reduce the number of molecules of gas.

For this reaction there are 4 molecules present in the reactants, while only 2 molecules in the products. Therefore, by increasing the system pressure, the system will shift to the products, since there are less molecules in the products.

The other important factor affecting the kinetics of this reaction is the temperature. How the temperature affects this reaction can be explained by the Van't Hoff equation (5.6), which under standard conditions can be written as,

$$\frac{d}{dT} \ln(K_{eq}) = \frac{\Delta H^0}{RT^2} \quad (5.6)$$

Where R is the ideal gas constant, ΔH^0 is the standard enthalpy of reaction, T is the temperature (K) and K_{eq} is the equilibrium constant. For an exothermic reaction in which $H^0 < 0$, the term $\frac{\Delta H^0}{RT^2}$ is < 0 for any temperature. Therefore, for a temperature increase, the K_{eq} will be lower, which for this case means that the ammonia production will be lower.

Consequently, the reaction should be conducted at the lowest possible temperature and highest possible pressure, by subtracting heat to maintain the reactor at a certain temperature or do an inter-refrigeration process between multiple reactors. Nevertheless, we must consider that the reaction rate increases by increasing the temperature, because the kinetic energy of the molecules will be higher.

Another important aspect to consider is that nitrogen gas is very unreactive because the atoms are held together by a triple bond, which means that is mandatory the use of catalysts in order to accelerate the reaction rate. Moreover, this reaction has a very high activation energy, which is another important factor for the use of catalysts. Since the catalyst is not efficient at temperatures below 400°C, the reaction must be carried out at at least 400°C [61].

Bases on all the previous information, the Haber-Bosch reactor has been optimized in terms of its temperature and pressure. Therefore, a Haber-Bosch reactor generally operates at temperatures between 400-450°C and at pressures between 150-250 bar, using an iron based catalyst, such as magnetite (Fe_3O_4) or wustite (FeO). In general, low equilibrium single-pass conversion is achieved ($\sim 15\%$), demanding the use of a gas recycle [15].

5.1.4. Environmental Concerns and Energy Use of the Haber-Bosch process

More than 96 % of the ammonia produced nowadays with this process uses fossil fuels as feedstocks. Of this 96 %, a 50 % is produced from natural gas, a 31 % from oil and a 19 % from coal. This causes the process to be responsible for 1,2 % of the global anthropogenic CO_2 emissions. This value is higher accounting for the extraction and transport of natural gas. This process could be carbon free if the following requirements are achieved:

- Hydrogen production is decoupled from methane reforming.
- Electric compressors replace condensing steam turbine compressors.
- Alternative ammonia separation techniques are adopted to decrease the operating pressure in the reactor, which would make it possible for renewable energy sources to give the sufficient amount of energy for the compressors to operate.

A modern, optimised and highly efficient methane-fed Haber-Bosch process emits 1,5-1,6 $\frac{t_{\text{CO}_2(\text{eq})}}{t_{\text{NH}_3}}$. Switching to hydrogen production method from methane reforming to hydropower-electrolysis reduces the emissions of CO_2 from 1,5 to 0,38 $\frac{t_{\text{CO}_2(\text{eq})}}{t_{\text{NH}_3}}$ (75 % decrease). The minimum energy requirement for the Haber-Bosch process, defined as the heat of combustion of ammonia, is 18,6 GJ/ t_{NH_3} based on ammonia's LHV. This is the amount of energy chemical stored and all energy consumed above this value is considered as energy loss.

In Figure 5.3, the minimum energy inputs to obtain H_2 are plotted in function of each technique.

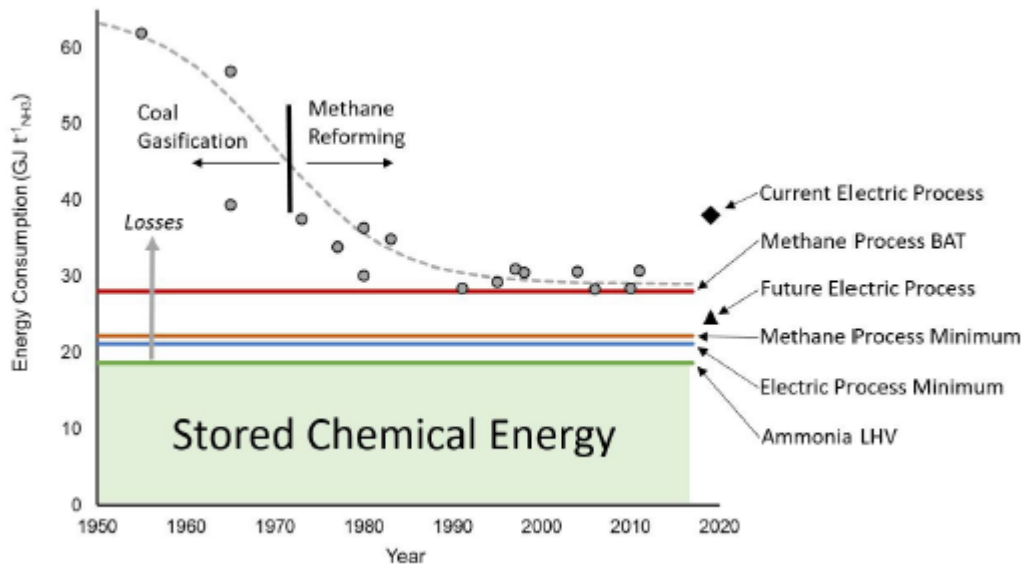


Figure 5.3: Improvement in the efficiency of ammonia production over the last decades [15]

One can observe that over the years the methane reforming process has switched from a $60 \text{ GJ}/t_{\text{NH}_3}$ to a $28 \text{ GJ}/t_{\text{NH}_3}$ minimum energy consumption to obtain H_2 using the best available technique (BAT). For the electrolyser process the minimum energy to produce H_2 is $\sim 40 \text{ GJ}/t_{\text{NH}_3}$ nowadays, but the minimum energy to supply an electric process is much lower (around the ammonia's LHV), which indicates that further improvements can be made.

5.2. Air Separation Process

In this section, three types of air separation processes are described. A deeper description of the cryogenic air separation process will be done respect to the other two, since this process will be the one simulated.

5.2.1. Air Separation Unit (ASU) for Cryogenic Distillation: Cryogenic Air Separation

The process of cooling a gas mixture to induce a phase change for effective separation is termed cryogenic distillation. This process separates the gaseous components in terms of their boiling points and volatilities in order to produce pure nitrogen, oxygen and argon, as well as other noble gases.

The amounts of nitrogen and oxygen that are produced may vary between 200 and 40.000 Nm^3/h and 1.000 and 150.000 Nm^3/h , respectively.

In general, for the treatment of large volumes of air, cryogenic distillation is the most cost-effective technology, and for smaller volumes, PSA is the most cost-effective. The N_2/O_2 purity generally dictates the cost associated with air separation [27]. This system consists of at least four blocks:

- Air compression and purification.

- Main heat exchanger.
- Cryogenic distillation column.
- Product compression.

The compressor selection depends mainly on the volumetric flow rate. For large volumetric flows, axial compressors are mainly used, whereas for high pressures with small volumetric flows, volumetric compressors (often reciprocating type) are used. In the case of lower volumetric flows and pressures, centrifugal compressors are used.

Heat exchangers are also very important to separate air using cryogenic distillation. In general, coil-wound, shell-and-tube and plate-and-fin are the most commonly used. The most important equipments are the cryogenic distillation columns since they conduct the air separation.

The cryogenic distillation process can be described by the following steps:

1. Air compression: dustless air is compressed in a multistage compressor with interstage cooling, in order to bring it to the desired pressure. (Table 4.1 gives the detailed composition of dustless air).
2. Air purification: All components that could potentially freeze in the air are removed (mainly CO₂ and H₂O) by thermal swing adsorption (TSA) or pressure swing adsorption (PSA).
3. Main heat exchanger: In this unit block, the air is liquefied to a temperature of -172°C. This heat transfer process is wide complex, since there are multiple streams in different passages with high number of channels and interactions.
4. Cryogenic distillation column: the air exits the main heat exchanger and enters the distillation column block, which consists of a double-column system. This system is made up of a high-pressure column (5-6 bar) and a low-pressure column (~1.3 bar). Both distillation columns operate at temperatures between the boiling points of N₂ and O₂. The reboiler of the low-pressure column and the condenser of the high-pressure column are thermally coupled.
5. Product Compression: The product is compressed in order to store it easier.

In Figure 5.4, a schematic of the double column for the cryogenic separation process is shown:

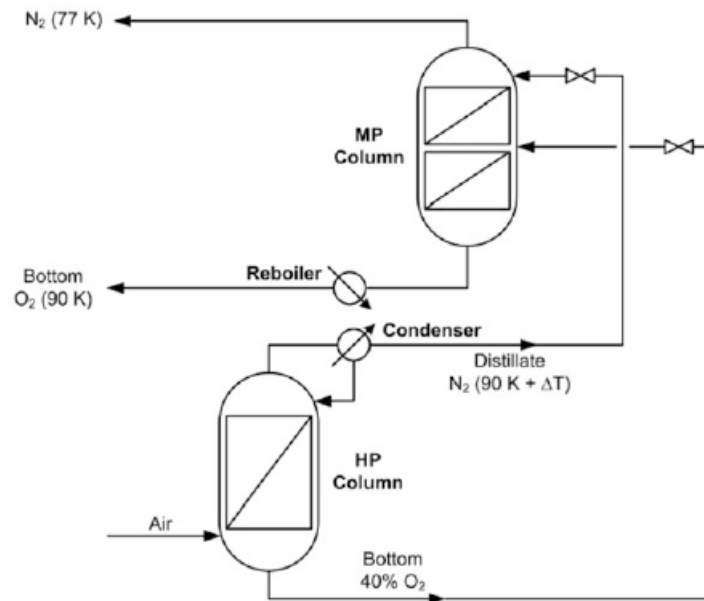


Figure 5.4: Scheme of the double distillation column [27]

In Figure 5.5 one can observe the process just mentioned in its main blocks:

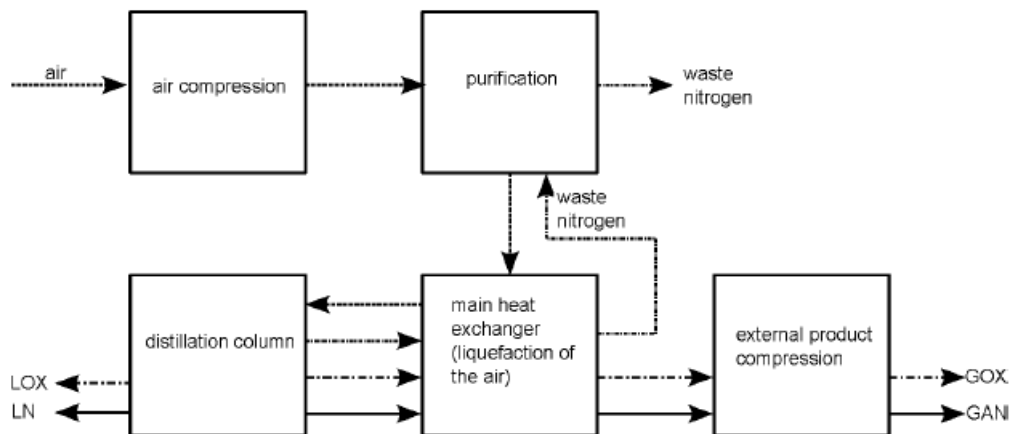


Figure 5.5: General Structure of an ASU [25]

Where LOX, LN, GOX and GAN accounts for liquid oxygen, liquid nitrogen, gaseous oxygen and gaseous nitrogen. In Table 5.1, an overview of the different types of air separation processes and their typical production rates and purities is shown.

Table 5.1: Different types of air separation processes, adapted from [25]

Component	Capacity (Nm ³ /h)	Purity mol %	Separation method	Load range %
Nitrogen	1-1.000	<99,5	Membrane	30-100
	5-5.000	<99,99	Pressure swing adsorption	30-100
	200-400.000	Any with residual concentrations down to ppb ^a range	Cryogenic air separation	60-100
	100-5.000	<95	Vacuum pressure swing adsorption	30-100
Oxygen	1.000-150.000	Any with residual concentrations down to ppb range, oxygen content mostly >95	Cryogenic air separation	60-100
Argon	-	-	Cryogenic air separation	-

^a parts per billion

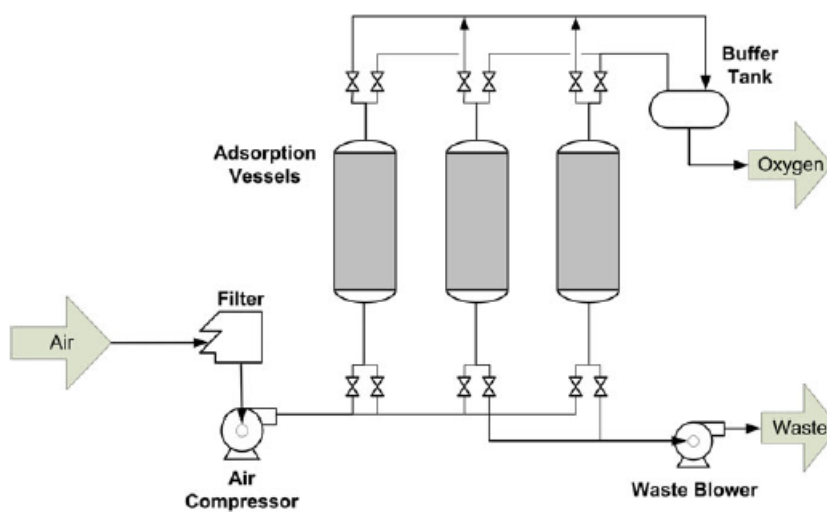
In addition, cryogenic air separation requires little refrigeration power, since both columns are thermally coupled.

5.2.2. Air Separation using Adsorption

Carbon molecular sieves (CMS) and zeolites are the typical sorbents used for air separation processes, since they are both selective towards the capture of N₂, allowing O₂ to pass freely through the sorbent bed.

The CMS works as a sieve to kinetically separate nitrogen and oxygen, since the kinetic diameter of O₂ is slightly smaller than N₂, only the oxygen passes through it.

In Figure 5.6, a scheme of an adsorption-based air separation process is presented, with the process description in the following paragraph.

**Figure 5.6:** Scheme of an adsorption-based air separation process [27]

Pressurized air enters one of the adsorber unit causing the sorbent bed to be saturated

with N_2 , therefore producing an outlet stream rich in O_2 . When the bed is saturated with N_2 , the air is fed to another sorbent bed while regeneration in the saturated bed begins. Regeneration may take place through addition of heat (TSA) or via pressure reduction (PSA). Due to faster recycling times, PSA is preferred respect to TSA.

5.2.3. Air Separation using Membrane Technology

The two primary types of membranes used for air separation are polymeric and ion transport. Both membranes use a separation mechanism called the solution/diffusion model, which mainly consists of three steps:

1. Gas is absorbed in the high-pressure side of the membrane.
2. Gas diffuses across a concentration gradient through the polymeric separating layer.
3. Gas desorbs from the low-pressure side of the membrane.

One of the main advantages of the membrane systems is that they can operate at near-ambient conditions, which implies less costs in utilities, heat exchangers and compressors.

In Figure 5.7, a scheme of an air separation process by membrane is shown.

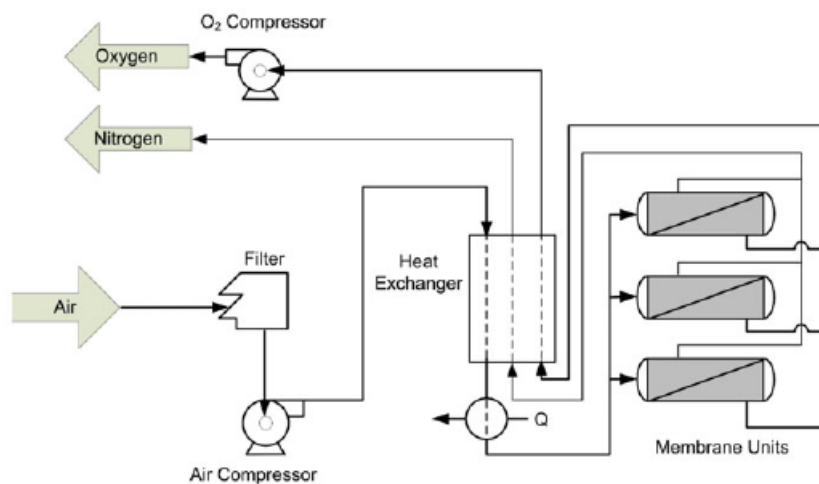


Figure 5.7: Scheme of an air separation process by membrane [27]

In Figure 5.8, one can observe the competitive ranges of the various N_2 production systems.

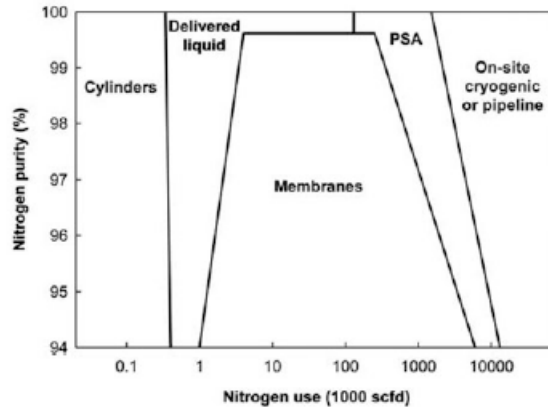


Figure 5.8: Competitive ranges of the various nitrogen production methods [27]

In function of the N_2 purity and N_2 required per time, one can select the best air separation method.

5.3. Steam Methane Reforming

Steam Methane Reforming (SMR) is the most common industrial process for producing hydrogen and synthesis gas. In particular, almost 50% of the global demand of hydrogen is currently produced via SMR. This process consists mainly of a conventional reformer (CR), two water gas shift reactors (WGSR) and a purification/separation equipment. In Figure 5.9, a scheme of a typical SMR process is shown:

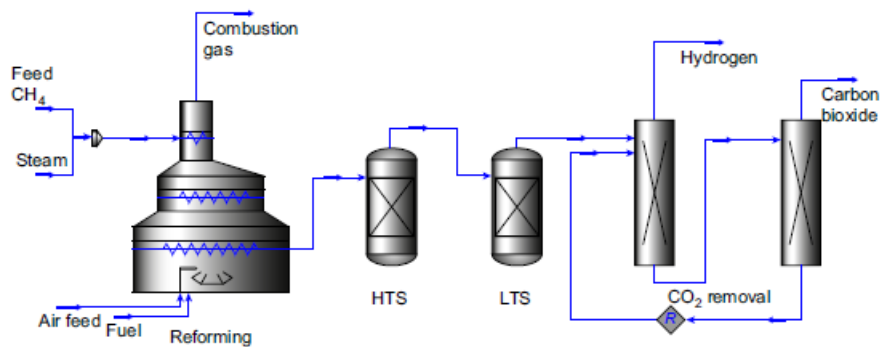
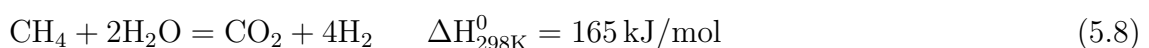


Figure 5.9: Scheme of a conventional SMR process [16]

In the CR, methane and steam react under harsh operating conditions, that is, temperatures between 1073-1273K and pressures between 14-20 bar. A Ni-based catalyst is used to perform reactions (5.7), (5.8) and (5.9).





These three reactions occur in the main reformer in order to produce H_2 . Since the CO concentration at the reformer is relatively high, it needs to be reduced in the subsequent WGSR, where the reaction 5.9 occurs.

The first WGSR is loaded with high temperature catalyst, generally chromium-promoted iron oxide and operates at temperatures between 623-673 K, while the second one is loaded with low temperature catalyst, generally copper-promoted zinc oxide and operates at 473 K.

The stream coming out of the second WGSR contains about 80 % of H_2 , ~ 12 % CO_2 , and very low methane (CH_4) and carbon monoxide (CO). Since the final stream contains only a purity of about 80 % H_2 , subsequent separations and purifications methods are used. In Table 5.2 the different techniques for H_2 purification are shown.

Table 5.2: Different techniques for H_2 purification [16]

Technique	Principle	H_2 Recovery (%)	H_2 Purity (%)
Cryogenic separation	Partial condensation of gas mixtures at low temperatures	Up to 98	90-98
PSA	Selective adsorption of impurities from gas stream	70-85	99,99
Dense palladium membrane	Selective diffusion of hydrogen through a palladium-alloy membrane	Up to 99	>99,999
Polymer membrane	Differential rate of diffusion of gases through a permeable membrane	>85	92-98
Metal hybrid separation	Reversible reaction of hydrogen with metals to form hydrides	75-95	99
Solid polymer electrolyte cell	Electrolytic passage of hydrogen ions across a solid polymer membrane	95	99,8

In Figure 5.10, an scheme of the just described SMR process is shown with heating and materials integration:

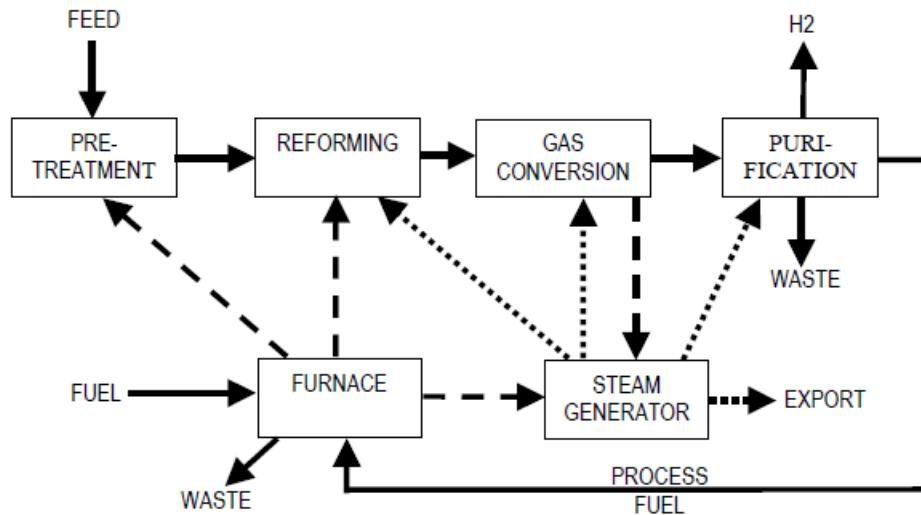


Figure 5.10: Schematic of an SMR process showing heat and materials integration [62]

5.3.1. Carbon Capture and Storage (CCS)

As nowadays the world is taking conscious about the GHG, new methods to reduce CO₂ emissions are being developed everyday. One of these is called carbon capture and storage, which mainly consists of capturing and storage of the CO₂ produced. However, the decision making of when to capture it (in which part of the process) and where to store it are not trivial in energy and economic terms.

A SMR process has three CO₂ containing streams, which can be identified as:

- Shifted synthesis gas upstream of the hydrogen purification unit.
- PSA tail gas from hydrogen production.
- Flue gas from steam reformer furnace system.

Each stream has different specifications and potentials for removing CO₂ (different pressures and CO₂ concentrations), therefore, an optimization must be conducted to decide when to capture it. In Figure 5.11, the three different CO₂ streams are identified.

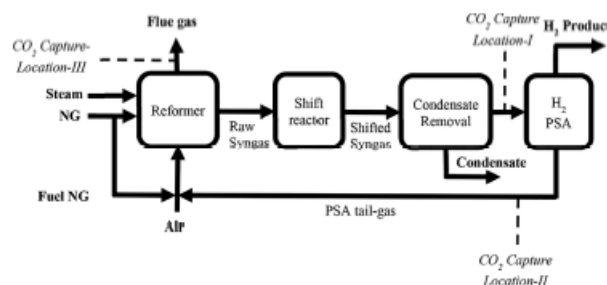


Figure 5.11: Typical processing steps in SMR with CO₂ capture [39]

In general, CO_2 is stored as geo-sequestration. This method involves injecting CO_2 , generally in supercritical form, directly into underground geological formations.

In [38], an analysis of pressurising CO_2 to obtain supercritical CO_2 for fracking of natural gas is analysed. After the SMR the CO_2 obtained is pressurised to obtain supercritical CO_2 (sCO_2). This sCO_2 is then piped in well locations in the general vicinity of the SMR in order to obtain methane (CH_4) for further SMR. In general, this fracking process is done by using water.

The potential amount of sCO_2 that could be used for fracking may be estimated from the amount of water currently used for this purpose. The density of sCO_2 is approximately equal to that of water. Assuming this, and taking into account the water used for fracking nowadays, it would result in a usage of 340 million tonnes of sCO_2 annually. The amount of CO_2 sequestered using the above estimate would be equivalent to the carbon avoided by 60 nuclear power plants, 30.000 large utility-scale wind turbines, or 1.000.000.000 solar panels.

In Figures 5.12 and 5.13, schemes of fracking process with sCO_2 are shown. The first scheme illustrates H_2 production as direct use to end users, while the second one illustrates H_2 production as a feedstock for producing electricity to end users.

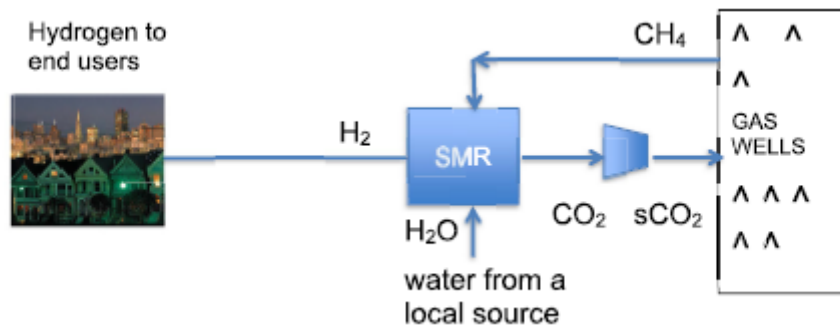


Figure 5.12: Hydrogen Output System [38]

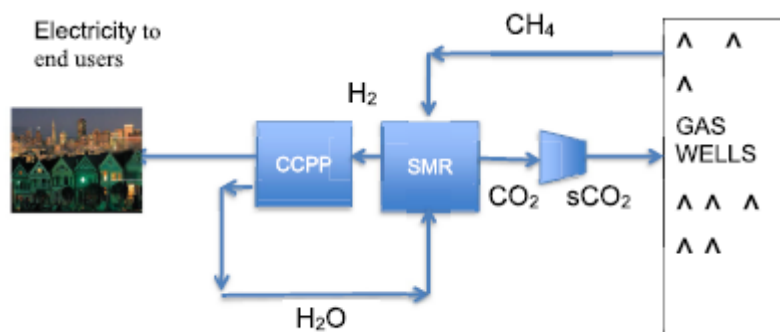


Figure 5.13: Electric-Output System Configuration [38]

In [39], Zeolite 13X (NaX) and NaY were used as CO_2 adsorbent materials for Vacuum

Pressure Swing Adsorption (VPSA). It was demonstrated that zeolite 13X has a higher working capacity and selectivity compared to NaY for CO₂ capture. The CO₂ capture using zeolites can be carried out in different parts of the process. In general, due to thermodynamic and economic arguments, CO₂ must be captured at the outlet stream with the highest partial pressure. Moreover, CO₂ capture by using this method must be done after condensate removal and dehydration since the adsorbents have a higher selectivity to water compared to CO₂.

The process just described is done by feeding the gas mixture (mainly H₂ and CO₂ into an 8-bed adsorbent system). When the process is finished, a H₂ purity >99,999% by mol is achieved, adsorbing almost all the CO₂. This is a cycle process, implying that at the end has an evacuation step where the CO₂ is desorbed and stored for later use (for example, for methanol production). The cycle time of a typical H₂ PSA employing pelleted adsorbents is around of 800 seconds, whereas for this VPSA process is of 200 seconds.

In Figure 5.14, a diagram of the process just described is shown,

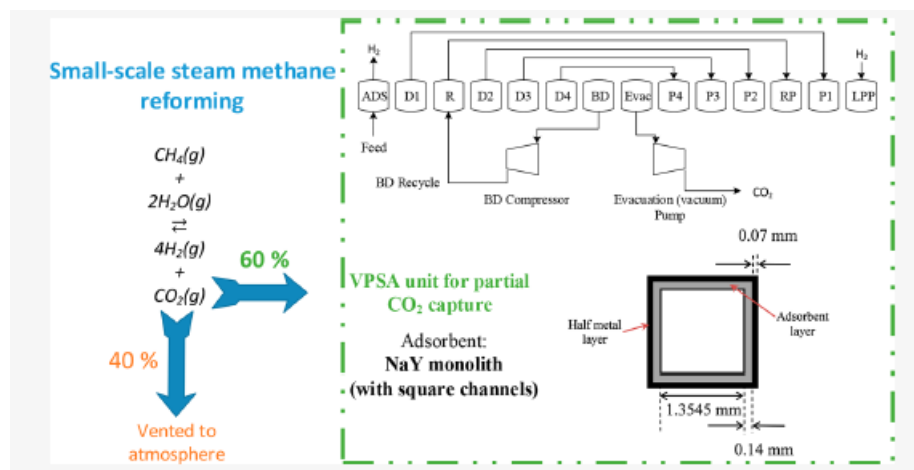


Figure 5.14: Small-Scale steam methane-reforming with CCS by using adsorbents [39]

Another method to capture CO₂ is to use amine adsorbents, a mature technology nowadays, as it is shown in papers [40] and [41]. This capture process consists in using an amine-based capturing method known as the monoethanol-amine (MEA) process. The CO₂ absorption process on MEA just described is shown in Figure 5.15.

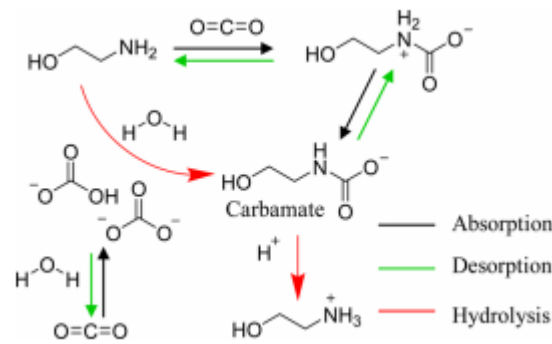


Figure 5.15: Mechanism of CO₂ capture into MEA solution [41]

5.4. Electrolyser

The process in which a direct electric current (DC) passing between two electrodes through an ionic substance to perform a non-spontaneous chemical reaction and to separate reaction products is called electrolysis. The electrolyser is the device that carries out the electrolysis, and is made by the interconnection of several elementary electrolysis cells. The key component of the electrolysis cell is the interface between a metal and an electrolyte (electron conductor or electrode and an ionic conductor).

From a thermodynamic viewpoint, an electrolyser can be seen as a device which converts electrical energy into chemical energy. The required reaction is mainly non spontaneous, therefore, a membrane is introduced in order to avoid recombination of the chemical products produced at the anode and cathode.

One of the most common type of electrolysis is water electrolysis, which transforms liquid water into gaseous hydrogen and oxygen [4]. This accounts as a renewable hydrogen energy system (RHES) [3].

When the amount of electricity that can be produced through renewable energy sources is higher than the electricity required, it can be stored as hydrogen (produced in an electrolyser) or as methane (in a reactor). This method is known as Power to gas (P2G), which is expected to play a key role as a storage technology able to exploit excess electricity from renewables to produce clean fuels [26].

Although several methods have been and are being developed for production of hydrogen different from water electrolysis by means of renewable energy sources, the only state-of-the-art practical technique is water electrolysis. Water electrolysis has in general the following characteristics [3]:

- Relatively high efficiency (above 70 %).
- Very pure H₂ can be produced since the gases are physically separated during their evolution at the electrodes.
- Require relatively very little space.
- Produce H₂ free from CO₂.

- Production costs are relatively high based on electricity cost, although, they can be much lower if produced on off-peak rates.
- Low maintenance costs.

5.4.1. Cell Types: Gap cells, Zero-gap Cells and Solid Polymer Electrolyte (SPE) cells

As described before, an electrolyser is made by an interconnection of several elementary electrolysis cells. The most common types of these cells will be described below.

The first one is called gap-cells, which is the most conventional configuration. Two planar electrodes are placed face-to-face in an electrolyte and a membrane is inserted in the liquid electrolyte, to prevent recombination of products. Since transport of electric charges in an electrolyte follow Ohm's law, the larger the distance between the two electrodes, the larger the ohmic losses and the lower the cell efficiency. This type of cell has low efficiency when gaseous products are formed, since these ones limit the maximum current density due to the fact they are non conducting.

The second type is the zero-gap cell. In this one, porous electrodes are pressed onto the membrane separator to reduce as much as possible the distance between anode and cathode in order to reduce the ohmic losses. In this case, significant current densities can be achieved, although liquid electrolyte is mandatory.

The third type is called solid polymer electrolyte (SPE) cell. In these ones, since the membrane acts as a solid electrolyte, ions which convey electric charges from one electrode to the other are immobilized inside it. Therefore, there is no liquid electrolyte in circulation in the electrolyser. This is the type of cell used in Proton Exchange Membrane (PEM) water electrolyzers.

In Figure 5.16, the three types of cells are shown:

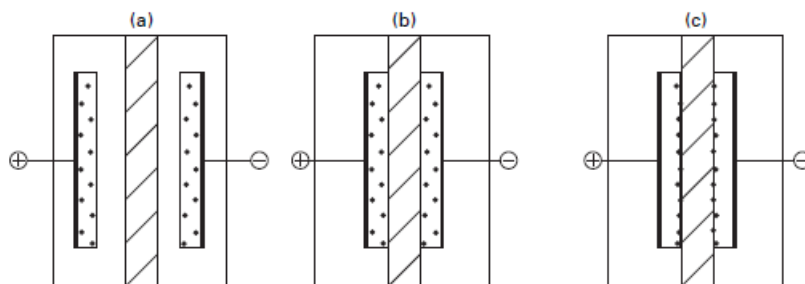


Figure 5.16: Two dimensional schematic diagrams of (a) gap-cell, (b) zero-gap cell and (c) SPE cell [17]

5.4.2. Membranes

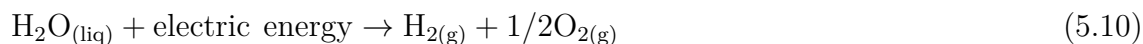
A membrane is defined as a thin sheet of natural or synthetic material that is permeable to substances in solution. It is impregnated with the solvent while the solute moves freely across the membrane.

The membrane present in electrolyzers is usually called ion-exchange membrane, designed as a thin sheet or film of ion-exchange material used to separate ions by allowing the preferential transport of either cations or anions. These membranes are used in electrolyzers for the double purpose of carrying electric charges (ions) between electrodes and separating the products of the electrochemical reaction.

5.4.3. Basic principles of Water Electrolysis

In this thesis, the water electrolysis will be described, since is one of the main important processes for producing hydrogen, which is one of the reactants for producing ammonia.

In a water electrolysis cell, electricity is used to separate water into hydrogen and oxygen molecules. Electric current (direct) passes between two electrodes separated by an aqueous electrolyte with good ionic conductivity. The splitting occurs following the full reaction (5.10):



The half reactions occurring at the anode and cathode will vary in function of the type of electrolyzer used.

In standard conditions, this reaction is a non-spontaneous (endergonic) transformation, since the standard Gibbs energy of the reaction (ΔG°) is a lot higher than 0. Moreover, a T of at least 2000 K at a pressure of 1 bar is required to shift this equation to a negative value.

The energy requirements for carrying out this reaction in function of operating temperature are plotted in Figure 5.17.

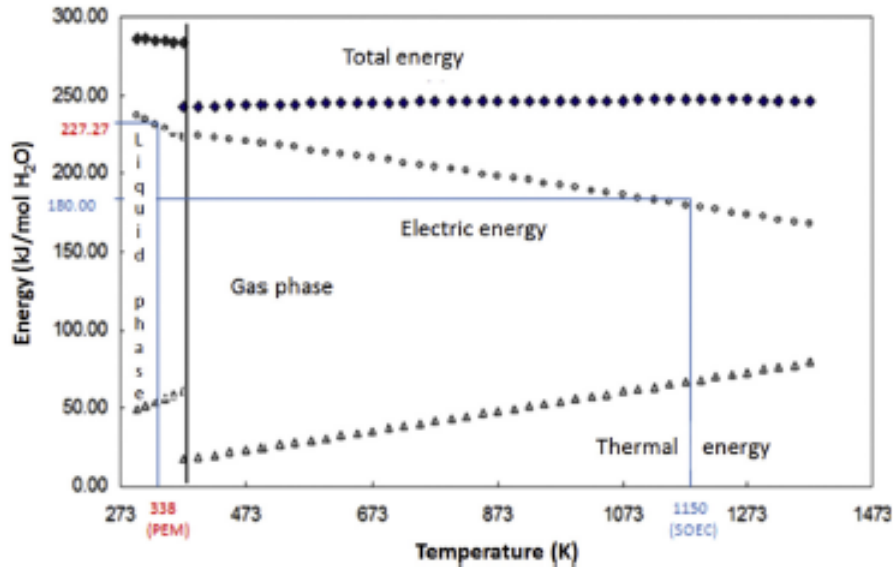


Figure 5.17: Energy Requirements for water splitting as function of operating temperature [4]

The total energy required for the transformation is the reaction enthalpy ΔH_r . For example, at 338 K, $\Delta H_r^{338K} = 287$ kJ/mol, 80% of that energy is supplied as electric power ($\Delta G_r^{338K} = 227$ kJ/mol), where the rest is supplied as heat demand, which is required to assist the positive entropy change $\Delta S_r^{338K} = 60$ kJ/mol. At higher temperatures, one must give less electric power but higher heat demand in order to carry out the reaction. During the operation, the energy consumption is always higher respect to the theoretical one due to the different sources of dissipation, charge transfer, overpotentials, cell resistance, etc. [4].

Based on the electrochemical reaction (5.10), a minimum electrical voltage called reversible voltage must be applied to both electrodes. By using the Gibbs equation, the reversible voltage that must be applied to carry out this reaction at standard temperature and pressure (STP) can be calculated by using equations (5.11), (5.12) and (5.13):

$$\Delta G = zFV_{rev} \quad (5.11)$$

$$V_{rev} = \Delta G / zF \quad (5.12)$$

$$V_{rev} = \frac{237,2 \text{ kJ/kmole}}{2 \cdot 96485 \text{ C/mole}} = 1,229 \text{ V} \quad (5.13)$$

Where: $\Delta G(\text{H}_2\text{O}) = 237,2$ kJ/kmol (STP) is the Gibbs Energy, $z = 2$ is the number of electrons transferred and $F = 96485$ C/mol is the Faraday's constant.

5.4.4. Alkaline Water Electrolysis (AWE)

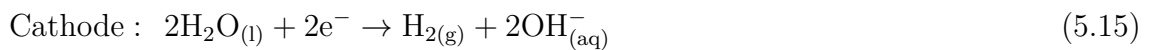
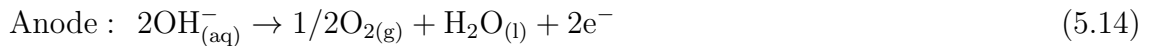
Is the most widely used technology for producing hydrogen. An alkaline electrolyser consists mainly of a cell frame, an electrolyte, an anode, a cathode and a separating diaphragm. The diaphragm is a key component, as it is needed to achieve the required hydrogen purity as a product of the electrolysis. Currently, with the development of the diaphragms and by using catalytic purification systems the purity of hydrogen obtained is $> 99,999\%$.

A typical alkaline electrolysis has two Ni-based electrodes immersed in a liquid electrolyte. Usually a 30-35 wt. % aqueous potassium hydroxide (KOH) solution is used, because of its optimal conductivity and remarkable corrosion resistance of stainless steel in the concentration range. However, sodium hydroxide (NaOH) and sodium chloride (NaCl) have also been used as electrolytes with interesting results.

Since at elevated current densities the generated gas bubbles that tend to flow upwards along the electrode surface can form a continuous and non conductive film over the entire electrode surface, advanced commercial alkaline electrolysers run with current densities in the range 100-400 mA/cm², with only a maximum of 450 mA/cm². One way to solution this problem is to use a porous diaphragm, which has the advantage of allowing higher current densities compared to a gap cell.

An AWE generally operates at temperatures between 60°C and 90°C and the pressure is commonly between 1-30 bar.

The semi reactions that are carried out in an AWE are (5.14) and (5.15),



AWE is the most mature electrolysis technology and is commercially available for large-scale hydrogen production. Nowadays, installations up to the MW scale of electric power are commercially available [3].

5.4.5. Proton Exchange Membrane Electrolyser (PEM)

Low temperature PEM water electrolysers operate in between 20-90°C, very similar compared to AWE, but can operate at much higher pressures (1-200 bar). The electrodes are usually metals, where the most commonly used is titanium (Ti). The solid electrolyte used is in general iridium (Ir)/ruthenium (Ru) oxide for the anode, whereas for the cathode platinum (Pt) is used. The electric consumption is in general of 5 kWh/Nm³_{H₂}. In Figure 5.18, the cross section of an elementary PEM water electrolysis cell is shown:

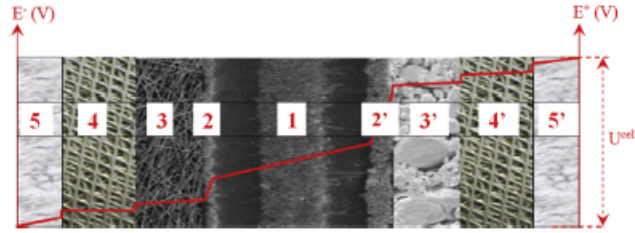


Fig. 5 – Schematic representation (cross-sectional view) of a PEM water electrolysis cell. 1 – PTFE-reinforced membrane, 2/2' – catalytic layers, 3/3' – porous transport layers, 4/4' – spacers and flow disrupters, 5/5' – end-plates [26].

Figure 5.18: PEM Electrolysis Cell [20]

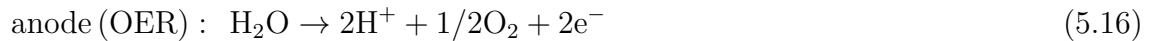
This unit cell is usually made of titanium and is quite compact (between 5-7 mm thick). Number 1 represents the cell core component, where water splitting takes place. 2-2' are the porous catalytic layers, while 3-3' are the porous transport layers, which both favor homogeneous distribution of current lines. 4-4' represent both cathodic and anodic cell compartments, where liquid water is pumped across to feed the reaction on the anode side.

These electrolyzers have many advantages respect to AWE in terms of simplicity, higher current densities, solid electrolyte and higher working pressures. Higher working pressures are an excellent advantage since it is not necessary to compress the products. Therefore, the compressors can operate at less pressures incurring in fewer expenses.

The main advantages of integrating a PEM with renewable resources are:

- No need for hazardous liquid electrolyte.
- Fast dynamic response (easier start-up) since higher current densities are possible.
- Possibility of more compact designs.

Water is fed into the anode unlike the AWE, where water is fed into the cathode. The reaction carried out in the anode is called oxygen evolution reaction (OER), while the reaction carried out in the cathode is called hydrogen evolution reaction (HER), which both can be represented by the following equations.



The electrolyte (acidic) that separates the electrodes is a polymeric membrane, which function is to enable the transport of charge carriers (H^+) from anode to cathode where hydrogen is produced. In general, Nafion ® is used as membrane, since it gives high proton conductivity and low gas crossover, summed up that its low thickness and the possibility of achieving high current densities (up to 20 A cm^{-2}) allow for a compact design.

The electrolyser is in general composed of many cells connected in series to form a stack, thus allowing to operate with higher voltage at the external connections, while keeping the same current flowing across the cells.

In Table 5.3, a comparison between these two technologies is reported. The solid oxide electrolysis, another type of water electrolysis, will not be accounted in this thesis, since it is in research and development (R&D) stage.

Table 5.3: Comparison of main water electrolysis technologies [18]

Comparison of main water electrolysis technologies		
Types of water electrolyzers	Alkaline	PEM
Technology status	mature technology	
T range (°C)	ambient - 120	
Electrolyte /pH	25-30 wt % (KOH) _{aq}	perfluorosulfonic acid
Charge carrier	OH ⁻	H ⁺
Overall reaction	H ₂ O → H ₂ + 1/2O ₂	H ₂ O → H ₂ + 1/2O ₂
Anode reaction	2OH ⁻ → 1/2O ₂ + H ₂ O + 2e ⁻	H ₂ O → 1/2O ₂ + 2e ⁻ + 2H ⁺
Cathode reaction	2H ₂ O + 2e ⁻ → H ₂ + 2OH ⁻	2H ⁺ + 2e ⁻ → H ₂
Anode catalyst	Ni ₂ CoO ₄ , La - Sr - CoO ₃ , Co ₃ O ₄	Ir/Ru oxide
Cathode catalyst	nickelfoam/Ni - stainlesssteel Ni - Mo/ZrO ₂ - TiO ₂	platinum
Separator	asbestos, polysulfone-bonded polyantimonic acid, ZrO ₂ on polysulfone, NiO, polysulfone impregnated with Sb ₂ O ₅ polyoxide	polymer membrane
Sealant	metallic	synthetic rubber/fluoroelastomer
Current distributor	Ni	titanium
Containment material	nickel plated steel	stainless steel
P range (bar)	1-200	1-350 (700)
Conventional current density (A/cm ²)	0,2-0,5	0-3 (up to 20)
Efficiency (/ %)	60-80	80
(at i A/cm ² /Ucell V/T°C)	0,2-0,5/2,0/80	1,0/1,8/65
Capacity (Nm ³ /h)	1-500	1-250
Durability (hours)	100.000	10.000-50.000
H ₂ O specification	liquid	>10 MΩ.cm
Load cycling	medium	good
Stop/go cycling	weak	good
T cycling	weak	good

5.5. Ammonia Separation Process

The gases present in the reactor outlet flow are N₂, H₂ and NH₃ principally. The most common way to separate ammonia is by condensation, since NH₃ has a higher boiling point respect to nitrogen and oxygen. The product flow passes through a condenser, where ammonia is condensed, while the tail gases (nitrogen and hydrogen) are recycled to enter one more time to the Haber-Bosch (H-B) reactor. In order to obtain a more concentrated ammonia, an absorber/membrane could be used after the condenser.

As it is described in [15], the condenser usually operates between -25°C and -33°C in order to separate ammonia from hydrogen and nitrogen. On [58], the condenser is operated at -20°C for less thermal requirements, although achieving less ammonia recovery. The temperature at which the condenser operates is in function of the pressure and the recovery of ammonia required by the Haber-Bosch process. The condenser cannot operate at temperatures below -33°C at atmospheric pressure, since it is the boiling point of ammonia.

As it is described in [2], another way to separate ammonia is to pass it through a 1M con-

centration boric acid trap solution with a pH of 3,7. This traps the ammonia synthesized and allows its separation from unreacted gases.

Instead of using a condenser, in [29] absorbers for ammonia separation are studied. The main driver of the H-B process is the high pressure, which leads to expensive compressors. By using an absorber, higher concentrations of ammonia have been reported at the reactor product flow, which could lead to the use of lower pressures in the full H-B process while maintaining the yield. In this simulation a fixed bed of magnesium chloride supported on silica was used, which serves to remove ammonia selectively through its absorption into the solid.

In terms of storage, ammonia in large quantities is stored refrigerated at -33°C in cylindrical double-walled storage tanks [1]. Another way to store ammonia is by mixing it with water, called ammonium hydroxide or household ammonia. In general, this mixture is stored at $15,5^{\circ}\text{C}$ in a 30 % w/w solution [30].

A comparison between the ammonia separation by condensation and absorption is shown in the Figure 5.19,

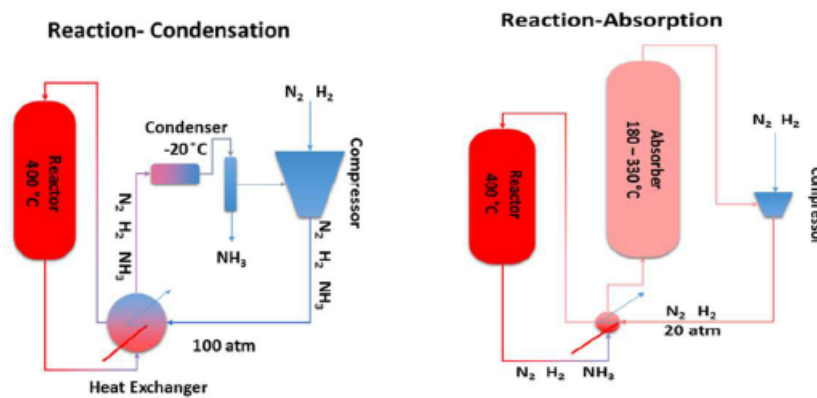


Figure 5.19: Conventional ammonia separation versus absorption based ammonia separation [63]

6. Chile's Geographical Context and Saltpetre History

In this chapter the main characteristics of Chile along with its potential of renewable energy resources will be described, along with a section to report the Chilean History about saltpetre. References [23], [34] and [36] were the main sources of information in order to conduct this chapter.

6.1. Chile's Geography and Economy

In this section, a brief description of Chile's geography will be done with the purpose of showing the potential that Chile has for green hydrogen and ammonia production.

Chile is a long, narrow strip located on the southwestern region of South America, between the Pacific Ocean to the west and the Andes mountains to the east. Chilean Territory also includes the "Juan Fernández archipelago", the "Salas y Gómez island", the Desventuradas islands and Easter island in the Pacific Ocean. A section called Chilean Antarctic Territory located in Antarctica is also claimed as part of Chile.

Chile has a length of 4.300 km and a surface of approximately 756.700 km². Chile possesses a very unique geographical configuration featuring a wide variety of climates, geomorphology, soil and vegetation. This contextual richness produces a diverse hydrological and hydrogeological setup, in which a large diversity of climates are present from north to south continental Chile.

Chile is a high urbanized country, with 87,8 % of the population living in urban areas. The economy is based on the exploitation of agricultural, fishing, forest, and mining resources, while many manufactured products must be imported. Since 2010, the country is a full member of the Organization for Economic Cooperation and Development (OECD).

The primary economic sector constitutes 21 % of the gross domestic product (GDP), showcasing the mining industry as the main contributor.

6.2. Chile's Renewable Energy Potential

Chile has the world's strongest solar resource, an exceptional wind in the south, and a very good wind in the north.

The solar potential in the North of Chile was estimated to be 1260 GW for photovoltaics (PV) and 550 GW for concentrated solar power (CSP). For wind power, in several areas of the north are shown potential capacity factors of above 40 %. Moreover, some areas can reach wind speeds of 10m/s at 80m height. The available wind potential in the north was estimated of about 14,5 GW, whereas in the south (from Bio-Bio to Chiloé) about 23 GW was estimated. In Figure 6.1, the different capacity factors for solar and wind energy in the North of Chile are shown,

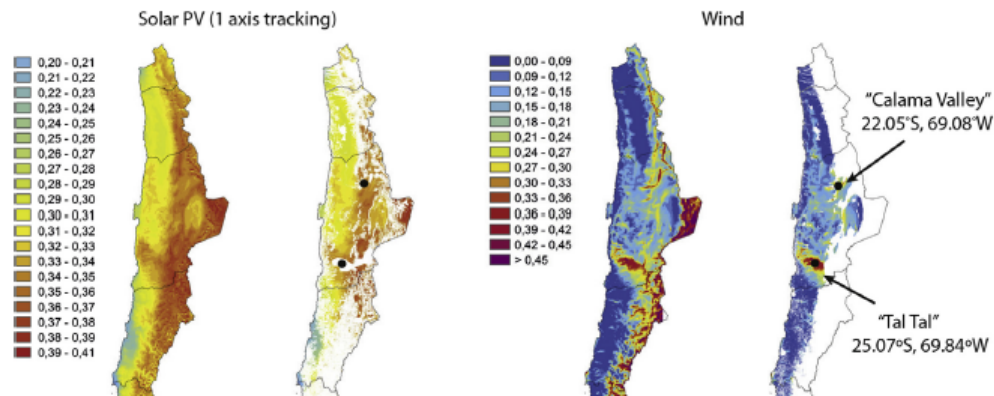


Figure 6.1: Potential Capacity factors for solar and wind energy in the North of Chile. Maps on the right side take into account the land restrictions such as high altitude, vicinity to national parks, etc. [36]

In Chile, 70 % of the matrix energy is provided by fossil fuels, 18,5 % by biomass, 5 % by hydroelectric and the rest by other types of energy sources.

The electrical installed capacity in Chile is 23,3 GW, with already 2,3 GW of solar, 1,5 GW of wind, 6,8 GW of hydroelectric and 500 MW of biomass, while the rest is produced from fossil fuels. Due to rapid development of variable renewable energies (VRE) in recent years, electricity prices have fallen strongly in the northern part of Chile. In example, the spot price in Diego de Almagro (City in Atacama region) averaged 7 USD/MWh in December 2017 between 11pm and 6 am [36].

In Chile, the Long-Term Energy Planning foresees a doubling of the energy consumption 2016 and 2050. Moreover, a carbon tax at 5USD/t_{CO₂} is already applied in the electricity generation sector, and some scenarios consider it could raise to 30 USD/t_{CO₂} in 2050.

In Chile, the hydrogen production is being promoted by the Chilean Economic Development Agency (CORFO), while the production of green ammonia is being pursued by ENAEX, in order to use it in the mining context. This company imports 360.000 tonnes of NH₃ each year to produce explosives.

6.3. Chile's Saltpetre History

In the following section, the Chilean's saltpetre history will be described, along with a brief description of the saltpetre and its main uses. This section has the didactic purpose of describing one of the first natural compounds used for a long time as a fertilizer, along with a brief of history from my country. All the events took part in between 1880 to 1930, where the great depression and the invention of the synthetic saltpetre put an end to the Chilean's saltpetre economy.

Potassium nitrate (saltpetre) is a crystalline salt with the chemical formula KNO₃. It is one of the several nitrogen-containing compounds, and therefore, a source of nitrogen. It is a strong oxidizer, typically used in making gunpowder, as a fertilizer and in medicine

[10].

The saltpetre industry was the main economic activity in Chile between 1880 and 1930. After the War of the Pacific, the State annexed the territories of Tarapacá (Peru) and Antofagasta (Bolivia), where the largest reserves of this mineral were found. During this period, its exploitation went through different stages in which foreign investment, technological innovation and the migration of Chilean and foreign labour were of great importance.

The first evidence of saltpetre exploitation dates back to the colonial period, when it was used to make gunpowder. At the beginning of the 19th century, saltpetre from Tarapacá began to be known in Europe due to its use in the chemical industry as a base for the manufacture of explosives and the creation of fertilisers. At that time, some Chilean explorers and businessmen discovered and exploited the saltpetre in the *Salar del Carmen*, through the Saltpetre and Antofagasta Railway Company.

In the 1880s, Chile defeated Peru and Bolivia in the War of the Pacific and incorporated the provinces of Tarapacá and Antofagasta into its territory. In these provinces, particularly in the Tamarugal pampas and the Atacama Desert, saltpetre was found in large quantities. The extraction of this mineral was quickly integrated into the national industrialisation drive and its export made Chile the world's leading producer.

The high quality and abundant caliche blankets extended from the Camarones ravine to Taltal and were easily accessible thanks to traditional roads and the construction of railway lines and branches. The large amount of resources and good connectivity made it easy for the country to have a monopoly on its production. However, this did not ensure sustained development, as the saltpetre industry went through periods of boom and crisis.

The Chilean government decided to leave the exploitation of saltpetre in private hands, but applied a high export tax, generating large resources for the public coffers. At first, the capital that predominated was Chilean and Peruvian, but later, German, Italian, French, Spanish and Croatian capital was incorporated. However, the entrepreneurs who managed to dominate the saltpetre industry were mostly English. In fact, one of the most important businessmen, John Thomas North, was known at this time as the "King of Saltpetre".

The industry began to specialise and innovate technologically to make saltpetre mining more efficient. In addition, during the turn of the century, saltpetre entrepreneurs organised themselves into trade unions to develop marketing and advertising strategies to keep saltpetre consumption levels high abroad, especially in Europe and North America. One of the main promoters of these commercial development policies was the engineer Alejandro Bertrand, who in 1910 warned of the possible consequences that one or several consecutive economic crises could have on the saltpetre industry.

Thanks to the saltpetre industry, and because of the migration of men and women in search of work, numerous populated areas were formed on the pampas and in the ports and coves where people embarked. An extensive railway network was also built.

Despite the development that saltpetre brought, the 1920s saw a major recession, which

reached its peak in the Great Depression of 1929. Another issue was the invention of the synthetic saltpetre, which was much more easier to produce than to extract saltpetre, while also being a lot cheaper. These two aspects favoured the end of the expansion cycle of Chilean saltpetre, which forced the country to reorganize the mining industry.

Today, these, mining settlements persist as ghost towns. These ruins can be visited and the testimony of that period of splendour can be seen in them.

The Santiago Humberstone and Santa Laura saltpetre offices are two former saltpetre offices, currently the best known. Nowadays, they are managed by the Saltpetre Museum Corporation and have been declared National Monuments and World Cultural Heritage.

The Figure 6.2 shows one of the Atacama saltpetre camps in 1890, where workers from all over the country came to work as miners to extract this precious mineral:

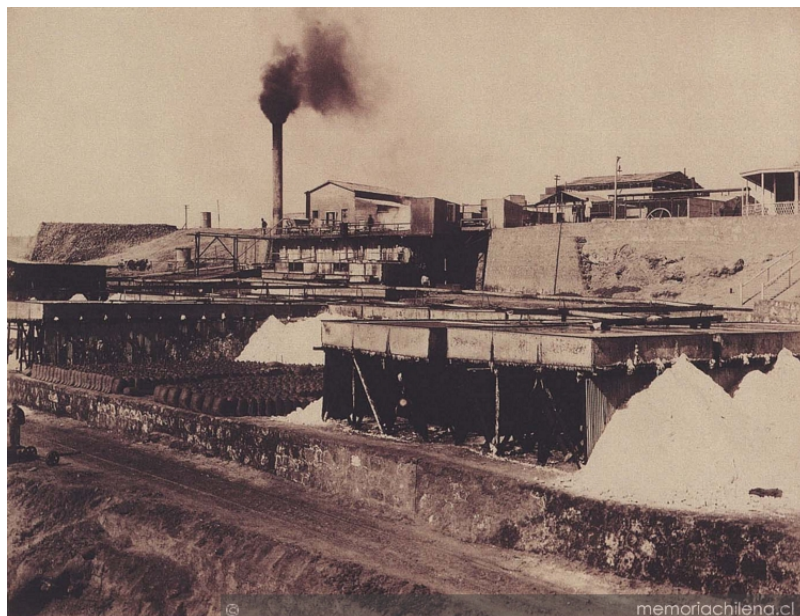


Figure 6.2: Saltpetre Office Jaspampa, Tarapaca. 1889 [34]

The Figure 6.3 shows the *Santa Laura* saltpetre office nowadays, which is now declared as official heritage:



Figure 6.3: *Santa Laura* saltpetre office [35]

7. Market Research and Availability

In this chapter the main ammonia producing countries, along with a description of the main green and conventional ammonia plants will be described. Reference [9] was the main source of information for conducting this chapter.

7.1. Ammonia Worldwide Production

In this section, the amount of ammonia produced in the whole world along with the amount of ammonia imported and exported in Chile will be reported. This will have the purpose of comparing the amount of ammonia produced of the simulated plant with the amount of ammonia that Chile needs every year.

In USA, most of the ammonia consumption was for fertilizer use as ammonia for direct application. Also urea, ammonium nitrates and ammonium phosphates were used. Ammonia was also used to produce explosives, plastics, and many other compounds.

Global ammonia capacity is expected to increase by a total of 4% from 2020 to 2025. Demand for ammonia is expected to increase in all regions with the largest increases expected in Africa and Eastern Europe.

In terms of nitrogen reserves, there is abundant atmospheric nitrogen to produce ammonia in every country for many years, since the availability of nitrogen from the atmosphere for fixed nitrogen production is unlimited. There is no substitute for nitrogen nowadays.

In Table 7.1 and Figure 7.1, the main ammonia production countries with their ammonia production by tonnes and percentage are shown:

Table 7.1: Principal Ammonia Production Countries, adapted from [9]

Principal Ammonia Production Countries	
Countries	Production [thousand tonnes]
China	40.000
Russia	15.000
United States	14.000
India	12.000
Indonesia	5.000
Saudi Arabia	4.300
Germany	4.100
Egypt	4.100
Trinidad & Tobago	4.000
Canada	3.800
Pakistan	3.100
Qatar	3.100

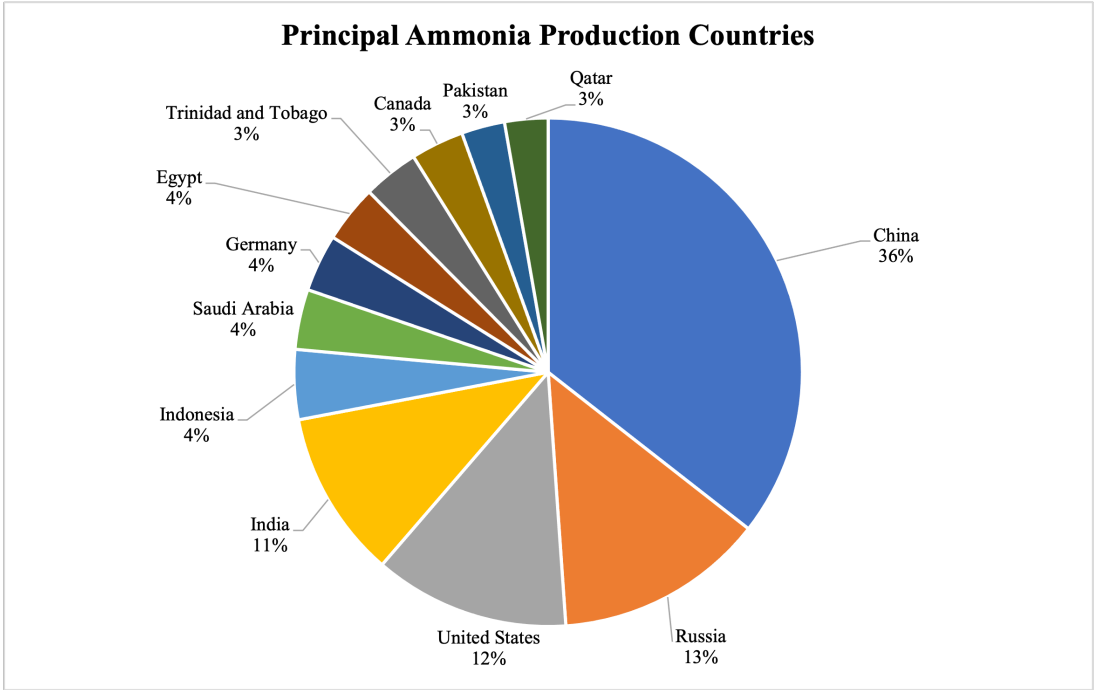


Figure 7.1: Main Ammonia Production Countries, adapted from [9]

As it is shown the main countries that produce ammonia worldwide are China (36%), Russia (13%), United States (12%) and India (11%). In Chile, 347.184 tonnes of ammonia were imported in 2019, while the amount of ammonia exported was of 342 tonnes [42]. This is an important factor, since more than 10 times of the ammonia needed is imported.

As described in section 6.2, Chile has an incredible potential of renewable energy sources (RES)[42]. Therefore, as the technology continues to advance, Chile could potentially substitute in the future almost all the ammonia imported by using RES to produce green ammonia.

As data of 2007, 90% of the ammonia produced in Chile is used for synthesizing ammonium nitrate, product used as an explosive in the mining industry, a 9,8% is used for fertilizer production and the rest 0,2% is exported [8].

In Figures 7.2 and 7.3, the principal countries from which Chile exports and imports ammonia are shown, with the percentage of ammonia exported/imported from each country.

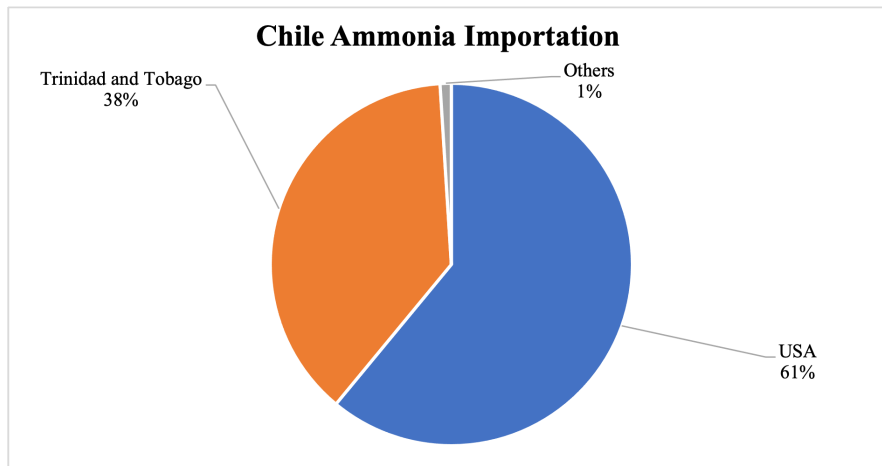


Figure 7.2: Main Chilean ammonia importers [42]



Figure 7.3: Main Chilean ammonia exporters [42]

As it is shown, the two main countries from which Chile imports ammonia are Peru (64%) and Bolivia (32%), while the principal countries from which Chile exports ammonia are USA (61%) and Trinidad & Tobago (38%).

7.2. Green Ammonia Plants

In this section, current and future ammonia renewable plants will be described in terms of ammonia production and energy use. In this way, we can compare the simulated plant with existent plants and explore future technologies that the companies will implement.

A first case is the UK, which did a £390 million investment in hydrogen technologies. £500,000 of all these money were awarded to ITM, Ørsted and Element Energy for the project "GigaStack". This project is focused on producing 5 MW stack modules of electrolyzers in series, in order to develop 100 MW+ electrolyser systems [43].

A very known company that constructs ammonia plants is Thyssenkrupp. This company, with decades of expertise in alkaline water electrolysis and ammonia production, is constructing and revamping conventional ammonia plants by replacing them with green ammonia plants. Conventional ammonia plants are plants which use fossil fuel as a feedstock.

This company has developed a 50 metric tons per day (mtpd) green plant based on 20 MW power input (small electrolyser) and 100% availability, and a 300 mtpd green plant based on 120 MW power input (big electrolyser). As it is approaching industrial scale, it could be an interesting revamping option for existing ammonia plants [44].

Another company, Siemens Pacific, described a project of a 10.000 km² solar field in Australia that would generate 500 GW of renewable energy, with a production capacity of 1 million tonnes of ammonia per day. This could be the world's largest green ammonia plant powered by renewable hydrogen.

On behalf of the Australian Government, ARENA today announced \$980.000 for Dyno Nobel Moranbah Pty Ltd, a business of Incitec Pivot Limited, to conduct and assess the feasibility of building a renewable ammonia facility at its existing Moranbah ammonia plant. If feasible, the proposed green ammonia facility would include a 160 MW electrolyser and a 210 MW solar farm co-located at Moranbah [45].

In Chile there is a project called "HyEx" that will be done by ENGIE and ENAEX, two very important companies. ENGIE focuses on energy generation, while ENAEX focuses on the production of explosives for the mining industry.

This project will be able to produce more than the 350.000 tonnes of ammonia that ENAEX imports every year to produce ammonium nitrate, with the possibility of exporting the rest. "HyEx" will have a 2.000 MW renewable energy capacity to produce energy for a 1.600 MW electrolyser plant that produces green hydrogen. This plant will produce the feedstock necessary for a subsequent ammonia factory.

This project has already the terrain for all the plants installation. Furthermore, Northern Chile is the best part in the world in terms of solar resources. Moreover, the interest of many mining companies of manufacturing green copper and lithium, both extracted by using ammonium nitrate synthesized from green ammonia, give an excellent sign in economic terms for this project revenue [46].

7.3. Conventional Ammonia Plants

In this section, the capacity of conventional ammonia plants will be described with the purpose of comparing a green ammonia plant with a conventional ammonia plant in terms of production capacity, costs and energy requirement.

Based on [50], the EU plants can be divided in three main types:

- Large size: with a capacity equal or higher than 600.000 tonnes/year.
 - Medium size: with a capacity between 400.000 and 600.000 tonnes/year.
-

- Small size: with a capacity lower than 400.000 tonnes/year.

In 2014 there were 42 ammonia production plants in the EU, where the number of plants in each division is shown in Table 7.2:

Table 7.2: EU statistics on plant size, 2013 [50]

EU plants size	# Plants	% Total
Large	10	24 %
Medium	15	36 %
Small	17	40 %
Total	42	

As in the production of green ammonia, Thyssenkrupp has developed and constructed conventional ammonia plants since 1928. In Chile, the first one was constructed in 1962 with a capacity of 50 mtpd.

This company offers two types of ammonia plants depending on the wanted capacity. Small-scale ammonia plants, with a production capacity ranging from 200 to 500 mtpd, and large-scale ammonia plants, with capacities ranging from 500 to 4.500 mtpd [47].

Another company is Linde, a leading industrial gas and engineering company. This company has developed a new concept for ammonia production, called Linde Ammonia Concept (LAC), which has, in general, the following advantages [49]:

- Elimination of three catalytic steps, reducing the catalyst volume to 50 % compared to a conventional plant.
- The generation of pure nitrogen, hydrogen, argon and other gases, which can be recycled and/or sold.
- Recovery of CO₂ through a washing unit.

The first LAC plant was built for Gujarat State Fertilizers & Chemicals Limited (GSFC) in Baroda, Gujarat, India. This plant went into operation in 1998 with a capacity of 1.350 mtpd.

Thus far, four plants based on the relatively new Linde Ammonia Concept have been constructed with capacities between 230 to 1.350 mtpd of ammonia [48].

8. Main Reasons to Conduct This Thesis

In this chapter, the main reasons to conduct this thesis will be described with the purpose of evidencing all the possibilities that Chile has to produce green hydrogen and ammonia. References [12] and [51] were the main source of information for conducting this chapter.

Energy is a key driver of industrialized societies. Its consumption is linked to living standards, lifestyles and population as well as its distribution between urban and rural areas. Population is growing in most countries driving increased consumption of energy globally. Nowadays, electricity is the main energy carrier used worldwide. However, the world can't sustain just by using electricity, it is mandatory to have chemical fuels and feedstocks. For example, many transportation vehicles such as airplanes cannot be economically flown using electricity. Consequently, H_2 could drive as an energy carrier in these situations.

To date, most research efforts have focused on advancing electrochemical systems to serve as stationary energy storage, buffering power delivery from variable energy sources on the electric grid, or displacing internal combustion engines in transportation [31].

One of the main reasons to conduct these researches is that hydrogen will be the energy carrier of the future. It can be obtained through many different ways and has a lot of applications such as fuel, precursor for other compounds, etc.

Hydrogen complements well electricity as an energy carrier since it can be stored over long periods of time. Furthermore, hydrogen production from intermittent renewable energy sources, such as solar energy sources, is only viable with an integration of a hydrogen storage system.

Many renewable energy resources are available intermittently, whereas nuclear power plants operate best at a constant power level. The possibility to operate nuclear power plants combined with renewable energies to produce electricity, and to use this electricity to produce H_2 as a green process is currently available. The current problem is that the hydrogen era will become available when fossil fuels become too expensive to recover economically and/or environmental or other imperatives cause modifications of our energy systems. Therefore, it is important to start developing more efficient technologies for today and the future.

One solution to reducing the prices is to produce and store H_2 by using the excess electric energy (in particular, the one generated in off-peak hours) produced by a nuclear power plant. Moreover, the hydrogen produced could be used for re-electrification (combustion in a fuel cell), thus, a so-called hydrogen cycle or hydrogen battery could be used for load shifting or nuclear power plants.

Another important reason is that electricity prices are getting lower throughout the years. The fall in electricity costs from utility-scale solar photovoltaic (PV) projects since 2010 has been remarkable. Driven by an 81 % decrease in solar PV module prices from 2009 to 2017, along with reductions in balance of system (BoS) costs, the global weighted average LCOE of utility-scale solar PV fell 73 % between 2010 and 2017, reaching a price of 0,10 USD/kWh.

Offshore wind power and concentrated solar power (CSP), though still in their infancy terms of deployment, both saw their costs fall between 2010 and 2017. The global LCOE of offshore wind projects commissioned in 2017 was 0,14 USD/kWh, while for CSP it was 0,22 USD/kWh. However, auction results in 2017, auctioned that in 2020 CSP and offshore wind LCOE will fall to 0,06 and 0,10 USD/kWh respectively.

In Figure 8.1, a comparison of the LCOE (USD/kWh) for years 2010 and 2017 for different renewable energy sources is plotted. Solar photovoltaic, CSP, offshore and onshore wind have decreased their LCOE, especially PV which decreased by a 72%. The band represents the fossil fuel-fired power generation cost range.

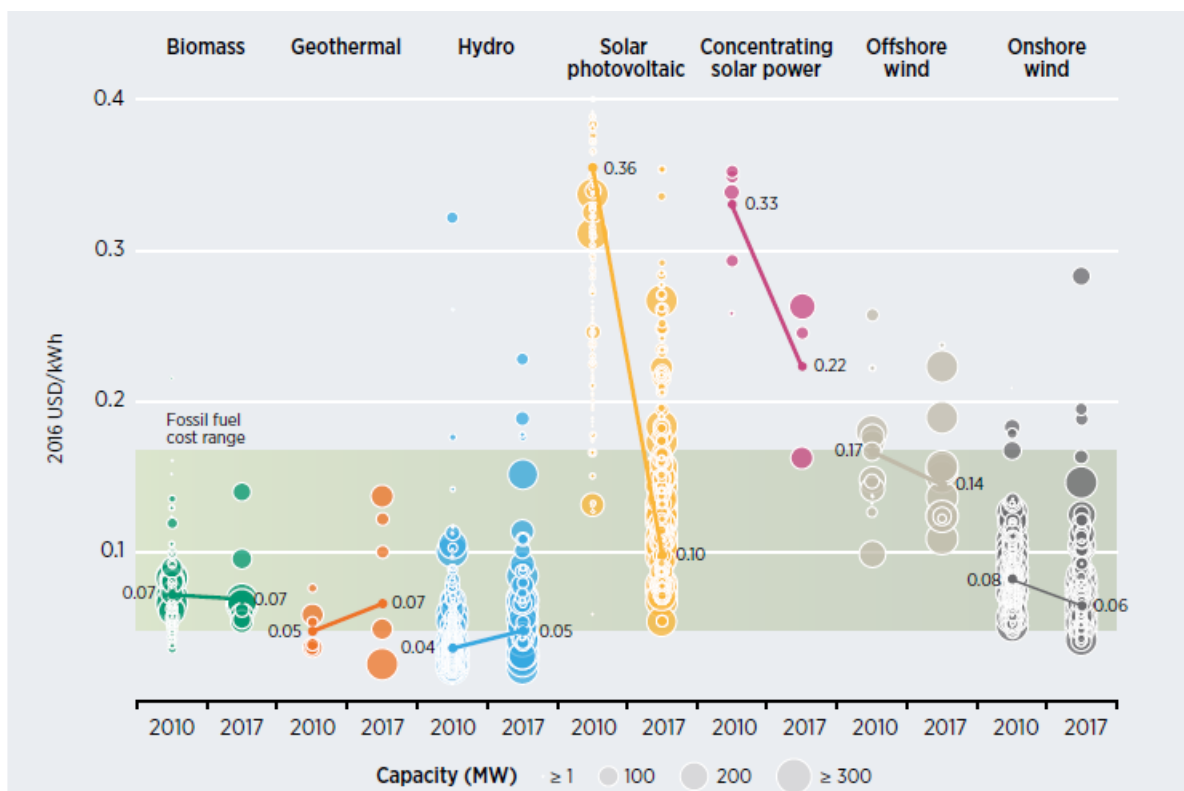


Figure 8.1: Global levelised cost of electricity from utility-scale renewable power generation technologies, 2010-2017 [51]

In Figure 8.2, it is plotted CSP, PV, onshore and offshore wind LCOE for different years in function of the cumulative capacity. Each circle represents an individual project, or, in some cases, auction result where there was a single clearing price at auction. It can be seen that the LCOE is getting lower each year, probably due to scale factors in constructing bigger renewable energy plants and better operational efficiencies that are being developed.

In the case of Chile, auction results around the world showed that Chile achieved record low prices for solar PV, with results around 0,03 USD/kWh on an LCOE basis now setting benchmark [51].

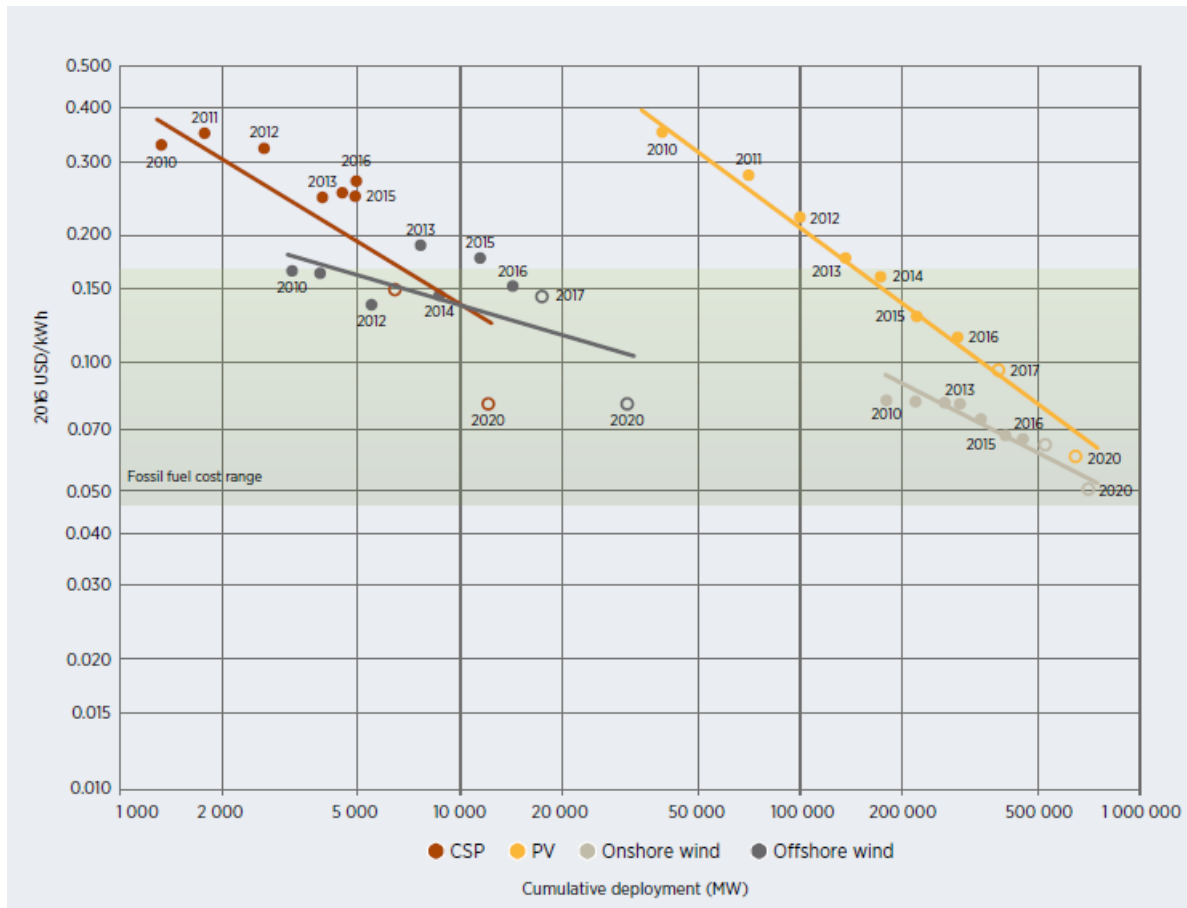


Figure 8.2: Learning curves for the global weighted average levelised cost of electricity from CSP, solar PV and onshore and offshore wind, 2010-2020 [51]

Another important reason is that ammonia is one of the most important and widely produced inorganic chemicals in the world. It has very important applications, mainly as a precursor for fertilizers and explosives for the mining industry.

As said before, hydrogen could be an excellent energy carrier complemented to electricity. Although, hydrogen has many challenges regarding storage due to its low energy density. Therefore, ammonia could be a perfect solution as storage of hydrogen, since it does not require high compression pressures or very low temperatures for liquefaction.

The conventional Haber-Bosch process accounts for 1,2% of the total anthropogenic CO₂ produced, and 96% of all ammonia produced uses fossil fuels as feedstock. Changing to a green ammonia production, that is, by using renewable energy sources integrated with an electrolyser, could lead in a future to a 0 greenhouse gas emission (GHG) Haber-Bosch process.

In Figure 8.3, the GHG emissions cycle is shown. If we can avoid from emitting more GHG by changing to a green ammonia production process, this cycle could be stopped in its first step: Anthropogenic activity.

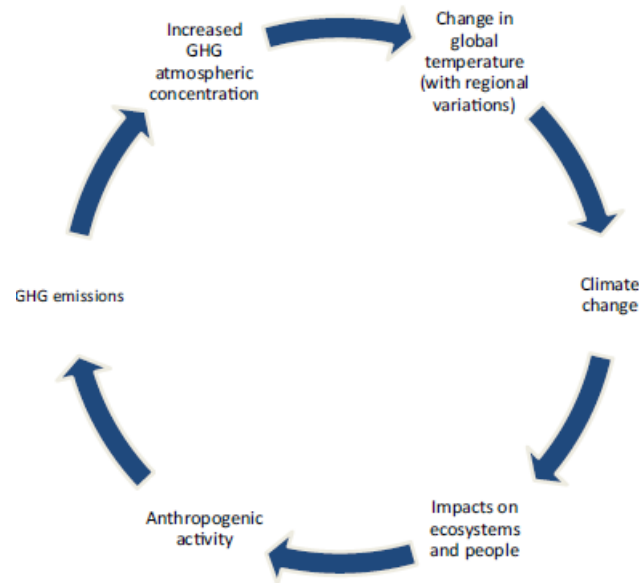


Figure 8.3: GHG cycle [12]

Another reason corresponds to the fossil fuels scarcity in the near future, leading to the requirement of changing to a renewable energy matrix. In Figure 8.4 we can notice that the use of fossil fuels is starting to decrease, while nuclear energy is starting to increase. Moreover, solfus (solar and nuclear fusion), will start increasing soon, leading the possibility of integrating renewable energy sources with nuclear energy.

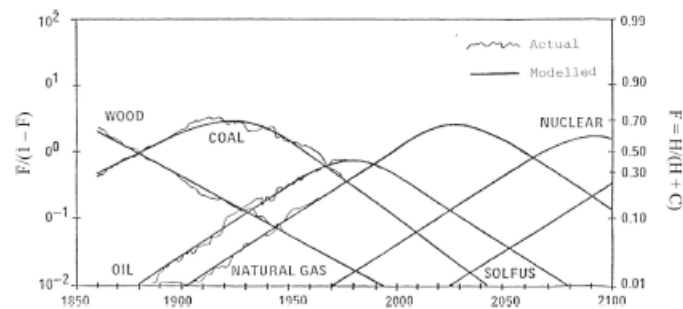


Figure 8.4: World Primary energy substitution in terms of the fraction F of total resources by the identified source [12]

9. Process Simulation of the Base Case

In this chapter, the Aspen Plus process simulation for producing green ammonia will be described by using a base case, which consists of a green ammonia plant with a production capacity of 50 mtpd. A detailed description of the properties, chemical methods, inputs, outputs, equipments, parameters and necessary calculations will be done.

9.1. First Simulation to Determine Required Nitrogen and Hydrogen Inputs

The first step is to conduct the simulation of the Haber-Bosch reactor and ammonia separation by condensation, in order to determine their conversion and ammonia recovery respectively. A first tentative of a current of nitrogen and hydrogen will be simulated in a molar proportion 1:3, as the reaction stoichiometry demands. As said before, the plant produces 50 tonnes/day of ammonia, or, in kmol/h:

$$n_{NH_3,prod} = 50 \text{ mtpd} = 50 \left(\frac{\text{tonnes}}{d} \right) \cdot 1000 \left(\frac{kg}{\text{tonnes}} \right) \cdot \frac{1}{17,031} \left(\frac{kmol}{kg} \right) \cdot \frac{1}{24} \left(\frac{d}{h} \right) = 122,33 \left(\frac{kmol}{h} \right)$$

$$n_{NH_3,prod} = 122,33 \left(\frac{kmol}{h} \right)$$

Therefore, following the reaction stoichiometry (5.1), the amount of nitrogen and hydrogen simulated as feed will be (assuming 100% nitrogen conversion and recovery).

$$n_{N_2,feed} = 61,165 \text{ kmol/h}$$

$$n_{H_2,feed} = 183,495 \text{ kmol/h}$$

The reaction kinetics from subsection 5.1.2 were simulated in an RPlug configuration in Aspen Plus through the kinetics reaction. In Figures 9.1, 9.2, 9.3 and 9.4, the inputs for Aspen Plus are shown for each kinetic reaction:

1) N2 + 3 H2 --> 2 NH3(MIXED)

Reacting phase: Vapor Rate basis: Reac (vol)

Power Law kinetic expression

If To is specified Kinetic factor = $k(T/T_0)^n e^{-(E/R)[1/T - 1/T_0]}$

If To is not specified Kinetic factor = $kT^n e^{-E/RT}$

k: 1,54122e-07

n: 0

E: 86944 kJ/kmol

To: C

[C] basis: Partial pressure

Edit Reactions

Solids

Figure 9.1: Parameters for first kinetic equation

Reaction No. 1 Reaction type *Kinetic*

Reactants

Component	Coefficient	Exponent
N2	-1	1
H2	-3	1.5

Products

Component	Coefficient	Exponent
NH3	2	-1

Figure 9.2: Coefficients and exponents for first kinetic equation

2) 2 NH3 --> N2(MIXED) + 3 H2(MIXED)

Reacting phase *Vapor* Rate basis *Reac (vol)*

Power Law kinetic expression

If To is specified Kinetic factor = $k(T/T_0)^n e^{-(E/R)[1/T-1/T_0]}$

If To is not specified Kinetic factor = $kT^n e^{-E/RT}$

k

n

E *kJ/kmol*

To *C*

[Ci] basis *Partial pressure*

Figure 9.3: Parameters for second kinetic equation

Reaction No. 2 Reaction type *Kinetic*

Reactants

Component	Coefficient	Exponent
NH3	-2	1

Products

Component	Coefficient	Exponent
N2	1	0
H2	3	-1.5

Figure 9.4: Coefficients and exponents for second kinetic equation

A problem is generated by following the kinetics described just before inserted in Aspen Plus, because when there is no ammonia in the feed current the program does not simulate the corresponding reaction. Therefore, an ammonia stream on the order of $1 \cdot 10^{-8}$ in mole fraction is also given as a feed for the Haber-Bosch process.

Consequently, the feed current simulated consists of the calculated amounts of nitrogen, hydrogen and ammonia. The temperature and pressure of the feed current will be equal to 450 °C and 250 bar respectively, in order to carry out the reaction properly with a relatively good conversion respect to the theoretical maximum, as explained in section 5.1.

The mixed current of nitrogen and hydrogen enters the Haber-Bosch reactor, with a diameter of 2 meters and a length of 6 meters as inputs for the first simulation. In Figure 9.5, the first simulation conducted in Aspen Plus is shown:

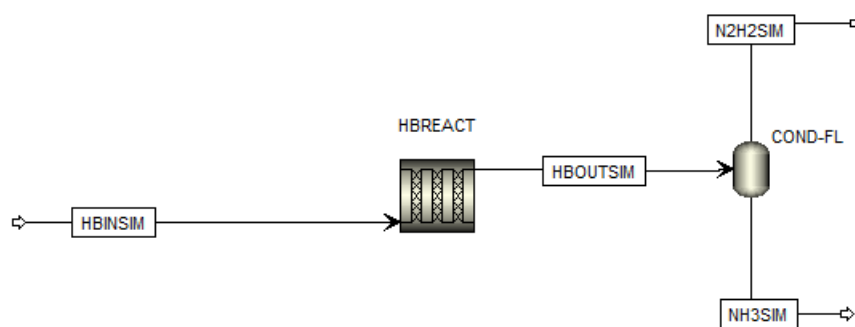


Figure 9.5: First tentative simulation in Aspen Plus to obtain the required nitrogen and hydrogen inputs

9.1.1. Optimization of the Haber-Bosch Reactor's Temperature and Pressure

As described in subsection 5.1, the Haber-Bosch reactor operates between 400-450°C and between 150-250 bar. In Aspen Plus, an optimization was conducted in order to determine the maximum ammonia conversion from the reactor in function of the temperature and pressure.

A sensitivity analysis was conducted by varying the discharge pressure of the compressor and the temperature of the heater previous to the Haber-Bosch reactor. It was found that the maximum conversion of ammonia produced from the reactor was at $T = 400$ °C and $P = 250$ bar, which agrees with the principles described in subsection 5.1.3. Hence, the reactor operating temperature was changed from $T = 450$ °C to 400 °C. In Figure 9.6, the sensitivity analysis conducted is shown:

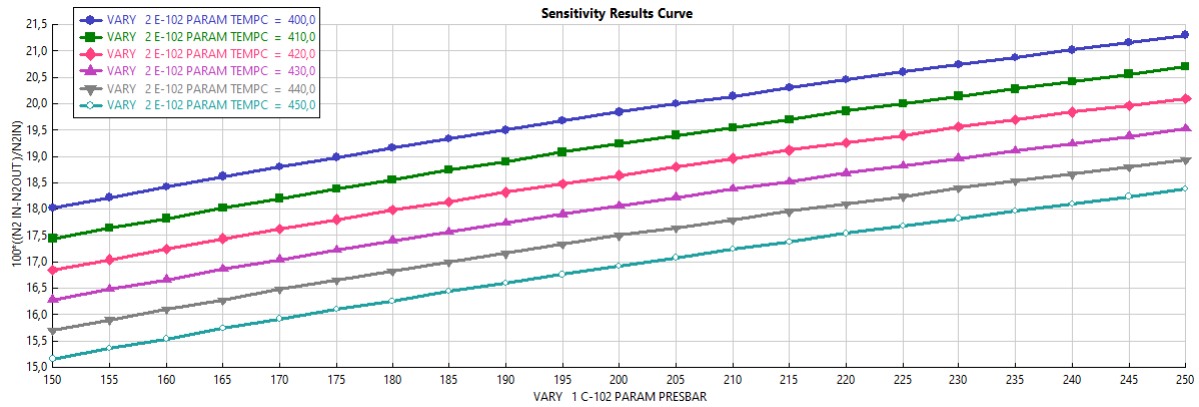


Figure 9.6: Sensitivity analysis conducted in Aspen Plus

As it can be seen, there is a higher amount of ammonia produced at higher pressures and lower temperatures.

Finally, the amount of nitrogen, hydrogen and ammonia that exit the reactor are:

$$n_{N_2,out} = 48,25 \text{ kmol/h}$$

$$n_{H_2,out} = 144,75 \text{ kmol/h}$$

$$n_{NH_3,out} = 25,83 \text{ kmol/h}$$

Therefore, the nitrogen conversion can be calculated by using equation (9.1),

$$\text{Conv} = \frac{n_{N_2,feed} - n_{N_2,out}}{n_{N_2,feed}} = 0,21 = 21\% \quad (9.1)$$

9.1.2. Ammonia Recovery Calculation

As stated in paper [58], the condensation occurs at a temperature around $-20\text{ }^\circ\text{C}$ in a condenser by using R-404A as the cooling current, which has a boiling point of $-46\text{ }^\circ\text{C}$ at 1 atm. Ammonia could also be used as a cooling current, with a boiling point of $-33\text{ }^\circ\text{C}$ at 1 atm.

The flash simulated operates at $-20\text{ }^\circ\text{C}$ with negligible pressure drop. At this flash enters the output stream from the Haber-Bosch reactor, and comes out a vapor stream (mainly containing hydrogen and nitrogen) and a liquid stream (mainly containing ammonia), as shown in Figure 9.5.

The importance of this step is to determine the recovery of ammonia obtained at the flash at $-20\text{ }^\circ\text{C}$, in order to obtain the real hydrogen and nitrogen inputs for our simulation. Figure 9.7 obtained from Aspen Plus represents the stream table, which shows the amount of hydrogen, nitrogen and ammonia in each of the streams.

	Units	HBINSIM	HBOUTSIM	N2H2SIM	NH3SIM
– Mole Flows	kmol/hr	244,66	218,832	196,198	22,6343
N2	kmol/hr	61,165	48,2511	48,206	0,0451533
H2	kmol/hr	183,495	144,753	144,619	0,134748
NH3	kmol/hr	1,49e-05	25,8277	3,37335	22,4544

Figure 9.7: Stream table corresponding to the simulation carried out to obtain the required nitrogen and hydrogen inputs

The recovery of NH_3 obtained from the flash bottom can be calculated by equation (9.2), (the stream names correspond with the names given in the Aspen Plus simulation, as shown in figure 9.5):

$$\text{NH}_{3,\text{recov}} = 100 \cdot \frac{n_{\text{NH}_3,\text{NH3SIM}}}{n_{\text{NH}_3,\text{HBOUTSIM}}} \quad (9.2)$$

Where $n_{\text{NH}_3,\text{NH3SIM}}$ represents the moles of NH_3 in the stream NH_3SIM and $n_{\text{NH}_3,\text{HBOUTSIM}}$ represents the moles of NH_3 in the stream HBOUTSIM . In other words, this represents the useful moles of NH_3 divided by the total moles of NH_3 that enter the flash. For a flash that operates at -20°C , the recovery obtained using equation (9.2) was:

$$\text{NH}_{3,\text{recov}} = 87\%$$

Therefore, the amount of hydrogen and nitrogen needed, taking into account the reactor's conversion and the flash recovery is:

$$n_{\text{N}_2,\text{feed}} = 61,165 \cdot \frac{1}{0,21} \frac{1}{0,87} = 334,784 \text{ kmol/h}$$

$$n_{\text{H}_2,\text{feed}} = 183,495 \frac{1}{0,21} \frac{1}{0,87} = 1004,35 \text{ kmol/h}$$

9.2. Alkaline Electrolyser

One of the main feedstocks to produce ammonia is hydrogen. In order to produce it, a simulation of an electrolyser was done by using an Excel calculator block integrated with Aspen Plus. This calculator block receives the required inputs, either manually or from Aspen Plus and through given formulas calculates the required outputs, one of which is the amount of H_2 produced.

Most of the parameters and formulas used for this simulation were retrieved from [19], which describes an alkaline water electrolyser model done in Aspen Custom Modeler following the equation (5.10). An Electrolyte NRTL (Non-Random Two-Liquid) model was used for the parameters calculation at the simulation as it was used on the base model.

In order for this reaction to occur a minimum voltage must be supplied known as reversible voltage (V_{rev}), which has a value of 1,229 V at STP (calculated in equation (5.13)). However, the cell voltage is always higher due to irreversibilities, called overvolta-

ges. Therefore, the real cell voltage (V_{cell}) can be defined as the sum of reversible voltage plus each of the overpotentials. In the case of an AWE these overpotentials are:

- Activation overpotentials ($\hat{\eta}_{\text{cat}}$ and $\hat{\eta}_{\text{an}}$).
- Ohmic overpotentials ($\hat{\eta}_{\text{ohm}}$).
- Concentration overpotentials ($\hat{\eta}_{\text{conc}}$).

9.2.1. Calculation of the Real Cell Voltage and the Amount of Water Required

The polarisation curve displays the necessary voltage to conduct the electrochemical reaction for a given current density loading. In [53], a semi-empirical model to determine the polarisation curve of an AWE is developed. This model calculates the real cell voltage in function of the temperature (T), pressure (P), current density (i) and diverse parameters. Since the concentration overpotentials occur at very high current densities (which is not the case of an AWE), they were neglected. Equation (9.3) represents the semi-empirical model just described:

$$V_{\text{cell}} = V_{\text{rev}} + [(r_1 + d_1) + r_2 \cdot T + d_2 \cdot P]i + s \cdot \log \left[\left(t_1 + \frac{t_2}{T} + \frac{t_3}{T^2} \right) i + 1 \right] \quad (9.3)$$

Where T is temperature ($^{\circ}\text{C}$), P is pressure (bar), i is current density (A/m^2) and r_1 , r_2 , d_1 , d_2 , s, t_1 , t_2 , t_3 are parameters.

It is also possible to measure the efficiency of the electrolyser by using the Faraday efficiency. This parameter compares the moles of H_2 produced and the theoretical moles that should have been produced through equation (9.4):

$$\eta_{\text{F}} = \frac{n_{\text{H}_2, \text{prod}}}{n_{\text{H}_2, \text{th}}} \quad (9.4)$$

Analogue to the polarization curve, this efficiency can be modelled by an empirical expression (9.5) for a given temperature and current density by using four parameters. The pressure is not included due to its slightly influence on the amount of H_2 produced.

$$\eta_{\text{F}} = \left(\frac{i^2}{f_{11} + f_{12} \cdot T + i^2} \right) \cdot (f_{21} + f_{22} \cdot T) \quad (9.5)$$

Where T is in $^{\circ}\text{C}$, i in A/m^2 and f_{11} , f_{12} , f_{21} , f_{22} are parameters.

In addition, a model for the diffusion of hydrogen to oxygen (HTO) has been proposed, in function of the temperature (T), current density (i) and pressure (P) in the electrolyser (9.6). This value represents irreversibilities, since some amount of the H_2 that should have been produced will be diffused into the oxygen. The diffusion of oxygen to hydrogen will

be considered negligible, since it reaches at most values of 0,5 %.

$$HTO = \left[C_1 + C_2 \cdot T + C_3 \cdot T^2 + (C_4 + C_5 \cdot T + C_6 \cdot T^2) \cdot \exp\left(\frac{C_7 + C_8 \cdot T + C_9 \cdot T^2}{i}\right) \right] + \left[E_1 + E_2 \cdot P + E_3 \cdot P^2 + (E_4 + E_5 \cdot P + E_6 \cdot P^2) \cdot \exp\left(\frac{E_7 + E_8 \cdot P + E_9 \cdot P^2}{i}\right) \right] \quad (9.6)$$

Where T is in °C, P in bar, i in A/m², and C₁, C₂, C₃, C₄, C₅, C₆, C₇, C₈, C₉, E₁, E₂, E₃, E₄, E₅, E₆, E₇, E₈, E₉ are constants.

In order to determine the moles of hydrogen diffused to oxygen, we must multiply this value (9.6) with the moles of oxygen produced (9.7),

$$n_{HTO} = n_{O_2,prod} \cdot HTO \quad (9.7)$$

The hydrogen production rate at the cathode depends on the electrochemical behaviour of the cells and can be determined through the Faraday efficiency (9.8),

$$n_{H_2,output} = \eta_F \cdot \frac{I}{z \cdot F} \cdot N \quad (9.8)$$

Where I is the current (A), z is the number of electrons exchanged (2 for water electrolysis), F is the Faraday constant (96485 C/mol) and N is the number of cells in the electrolyser stack.

The amount of oxygen and water produced are determined according to the reaction stoichiometry. We must also take into account the mass balance of hydrogen that is diffused across the diaphragms (HTO). Therefore, the mass balances can be expressed using formulas (9.9), (9.10), (9.11), (9.12), (9.13) and (9.14).

$$n_{H_2,cat} + n_{H_2,an} = n_{H_2,prod} \quad (9.9)$$

$$n_{H_2,an} = n_{HTO} \quad (9.10)$$

$$n_{O_2,an} = n_{O_2,prod} = \frac{1}{2} n_{H_2,prod} \quad (9.11)$$

$$n_{H_2O,feed} = \frac{n_{H_2,prod}}{\eta_F} \quad (9.12)$$

$$n_{H_2,cat} = n_{H_2,output} \quad (9.13)$$

$$n_{H_2O,prod} = n_{H_2O,feed} - n_{H_2,prod} \quad (9.14)$$

Where $n_{H_2,cat}$ are the moles of hydrogen produced at the cathode, $n_{H_2,an}$ are the moles of hydrogen produced at the anode, $n_{H_2,prod}$ is the amount of hydrogen produced in total in the electrolyser, $n_{O_2,an}$ are the moles of oxygen produced at the anode, $n_{H_2O,feed}$ is the amount of water that must be fed into the electrolyser in order to produce an amount of hydrogen equivalent to $n_{H_2,prod}$. Since not all the water fed to the electrolyser reacts to convert into H_2 , we must use the Faradaic efficiency to calculate this value, and $n_{H_2,output}$ is the total amount of hydrogen that exits through the cathode, which corresponds to the useful moles of hydrogen available to produce ammonia in the following steps.

The last step is to calculate the electric power input for the stack operation (W_{stack}), which can be calculated with the equation (9.15),

$$W_{stack} = V_{stack} \cdot I = (V_{cell} \cdot N) \cdot (i \cdot A_{cell}) \quad (9.15)$$

Where V_{cell} is the voltage that must be applied to the electrolyser (V), N is the electrolyser number of cells, i is the current density (A/m²) and A_{cell} is the active electrode area (m²).

The parameters used for calculating all these values are listed in Table 9.1:

Table 9.1: Coefficients considered for the electrochemical model of an alkaline water electrolysis cell

Model	Coefficient	Value	Unit
Polarization Curve	r_1	$4,45153 \cdot 10^{-5}$	$\Omega \text{ m}^2$
	r_2	$6,88874 \cdot 10^{-9}$	$\Omega \text{ m}^2 \text{ }^\circ\text{C}^{-1}$
	d_1	$-3,12996 \cdot 10^{-6}$	$\Omega \text{ m}^2$
	d_2	$4,47137 \cdot 10^{-7}$	$\Omega \text{ m}^2 \text{ bar}^{-1}$
	s	0,33824	V
	t_1	-0,01539	$\text{m}^2 \text{ A}^{-1}$
	t_2	2,00181	$\text{m}^2 \text{ }^\circ\text{C} \text{ A}^{-1}$
	t_3	15,24178	$\text{m}^2 \text{ A}^{-1}$
Faraday efficiency	f_{11}	478645,74	$\text{A}^2 \text{ m}^{-4}$
	f_{12}	-2953,15	$\text{A}^2 \text{ m}^{-4} \text{ }^\circ\text{C}^{-1}$
	f_{21}	1,03960	-
	f_{22}	-0,00104	$^\circ\text{C}^{-1}$
Gas purity (hydrogen in oxygen)	C_1	0,09901	-
	C_2	-0,00207	$^\circ\text{C}^{-1}$
	C_3	$1,31064 \cdot 10^{-5}$	$^\circ\text{C}^{-2}$
	C_4	-0,08483	-
	C_5	0,00179	$^\circ\text{C}^{-1}$
	C_6	$-1,1339 \cdot 10^{-5}$	$^\circ\text{C}^{-2}$
	C_7	1481,45	A m^{-2}
	C_8	-23,60345	$\text{A m}^{-2} \text{ }^\circ\text{C}^{-1}$
	C_9	-0,25774	$\text{A m}^{-2} \text{ }^\circ\text{C}^{-2}$
	E_1	3,71417	-
	E_2	-0,93063	bar^{-1}
	E_3	0,05817	bar^{-2}
	E_4	-3,72068	-
	E_5	0,93219	bar^{-1}
	E_6	-0,05826	bar^{-2}
E_7	-18,38215	A m^{-2}	
E_8	5,87316	$\text{A m}^{-2} \text{ bar}^{-1}$	
E_9	-0,46425	$\text{A m}^{-2} \text{ bar}^{-2}$	

Additionally, the base case conditions for the AWE simulated in [53] are shown in Table 9.2,

Table 9.2: AWE base case conditions used in the paper

Parameter	Value	Unit
Stack working temperature, T_{stack}	75	°C
Operating system pressure, P_{stack}	7	bar
Electrolyte concentration	35	wt % KOH
Active electrode area, A_{cell}	1000	cm ²
Cell number, N	12	cells
Input power stack, W_{stack}	10	kW

The working temperature, pressure, number of cells and electrolyte concentration of the electrolyser model were used as parameters for our base case simulation. In addition, the AWE designed in the paper is able to operate between 40-80°C and 1-10 bar. The electrode area and input power stack will be modified in order to achieve the desired amount of ammonia produced. Therefore, by knowing this value, the electrolyser parameters can be modified in order to achieve it. Moreover, by fixing the electrolyser parameters, all the mass balances can be resolved.

Finally, some assumptions were considered in order to simplify the simulation process:

- All processes operate at steady state.
- All the gases in the system behave like ideal gases.
- Liquid deionised H₂O is fed to the system in a reference environment condition at 298 K.
- The hydrogen and oxygen outputs are the same temperature and pressure as the electrolyser stack.
- AWE stack is operated at balanced anode and cathode pressure.

9.2.2. Aspen Plus AWE Simulation

Firstly, the feed current is simulated. This consists of a mixture of water-KOH with a 0,65 mole fraction of water and a 0,35 mole fraction of KOH at STP. The mass flow of feed current will be obtained by a calculator block given a desired amount of ammonia.

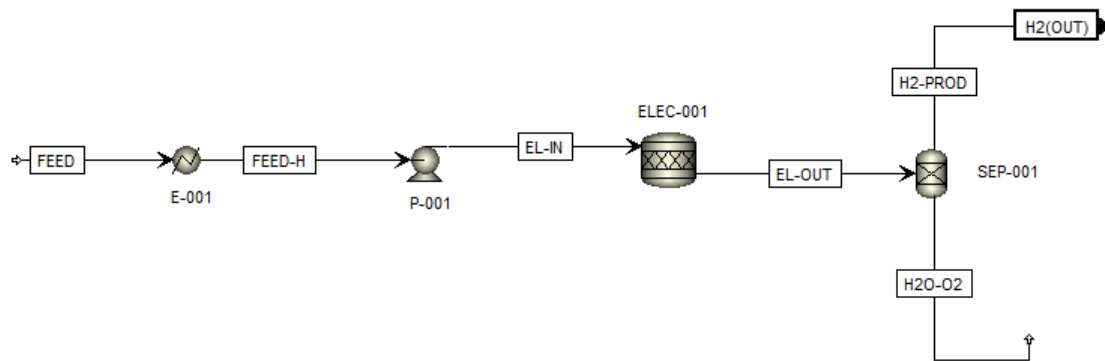
Secondly, the current is heated by means of a heater to the desired temperature, which corresponds to 75°C. Afterwards, it is pressurised by means of a pump to the wanted pressure of 7 bar.

Thirdly, the heated and pressurised current enters the electrolyser stack. This electrolyser stack works by means of an Excel calculator block, which gives as main outputs the hydrogen production and the necessary amount of water that must be fed to the electrolyser, in addition to the required electric power input. The Table 9.3 shows the different inputs that must be inserted into the calculator block in order to obtain the desired outputs. Some inputs will be taken from Aspen, while some others will be inserted directly on the calculator block.

Table 9.3: Inputs for AWE Electrolyser simulation in Aspen Plus

Inputs	Value	Unit
Electrolyser temperature (T_{elect})	75	$^{\circ}\text{C}$
Electrolyser pressure (P_{elect})	7	bar
Number of electrons transferred (z)	2	-
Cell number (N)	12	cells
Current Density (i)	5000	A/m^2
Faraday constant (F)	96485	C/mol
Electrolyte concentration in feed	0,35	-

The Aspen Plus simulation process for the electrolyser just described is presented in Figure 9.8:

**Figure 9.8:** Alkaline water electrolyser model in Aspen Plus

9.2.3. Aspen Plus AWE: Voltage calculation

As the electrolyser does not operate at STP, equation (5.13) does not apply for this case. In [54] an empirical equation for calculating the reversible voltage V_{rev} for an alkaline water electrolysis cell for a given temperature and pressure is described. Pressure effects are neglected since they are not relevant when coupled with renewable energies.

A current density of $i = 5000 \text{ A}/\text{m}^2$ was used as the base case, since it is the highest current density that can be delivered to an AWE, in addition to obtaining the highest possible Faraday efficiency for an allowable range between 2000 and 5000 A/m^2 . Using equation (9.16) for an electrolyser at $T = 348\text{K}$ and $P = 7 \text{ bar}$ gives the following value:

$$V_{rev} = 1,5184 - 1,5421 \cdot 10^{-3}T + 9,523 \cdot 10^{-5}T \ln(T) + 9,84 \cdot 10^{-8}T^2 = 1,19 \text{ V}. \quad (9.16)$$

Where T is in K and V_{rev} in V. Substituting this value in equation (9.3) the cell voltage is equal to:

$$V_{cell} = 2,039 \text{ V}$$

The Faradaic efficiency can be obtained from equation (9.5):

$$\eta_F = 0,952 = 95,2 \%$$

9.2.4. Aspen Plus AWE: Amount of Water Feed Required

In order to obtain the amount of water feed required, we must consider the amount of H_2 that must be produced in order to obtain 50 mtpd. As calculated in section 9.1.2, the amount of H_2 needed (output from electrolyser) is:

$$n_{H_2,output} = 183,495 \frac{1}{0,21} \frac{1}{0,87} = 1004,35 \text{ kmol/h}$$

We must consider from equations (9.6) and (9.7) the amount of hydrogen that is diffused to oxygen. From equation (9.6):

$$HTO = 0,0073$$

With the values of $n_{H_2,output}$ and HTO , the $H_{2,prod}$ can be calculated by using equations (9.9), (9.10), (9.11), (9.13) following the next steps:

$$n_{H_2,prod} = n_{H_2,output} + n_{HTO}$$

$$n_{H_2,prod} - n_{HTO} = n_{H_2,output}$$

$$n_{H_2,prod} - n_{O_2,prod} \cdot HTO = n_{H_2,output}$$

$$n_{H_2,prod} - n_{H_2,prod} \cdot \frac{1}{2} \cdot HTO = n_{H_2,output}$$

Therefore, the amount of H_2 can be obtained using (9.17),

$$n_{H_2,prod} = \frac{n_{H_2,output}}{\left(1 - \frac{HTO}{2}\right)} = 1008,051 \text{ kmol/h} \quad (9.17)$$

Consequently, the amount of water necessary to drive the full system can be calculated with equation (9.12):

$$n_{H_2O,feed} = 1059,09 \text{ kmol/h.}$$

By using equations (9.11) and (9.14), the amount of oxygen and water produced are:

$$n_{O_2,prod} = 504,03 \text{ kmol/h}$$

$$n_{H_2O,prod} = 51,04 \text{ kmol/h}$$

Knowing that the feed current has a 65 % of water, the fresh feed mole flow that enters the system is:

$$n_{feed} = 1629,37 \text{ kmol/h} \quad (9.18)$$

9.2.5. Aspen Plus AWE: Electricity Input Requirement

By knowing all these values, it is necessary to calculate the electrolyser area which gives the necessary electricity input in order to obtain the amount of water necessary just calculated ($n_{H_2O,feed}$). As said in equation (9.15), the relation between electrolyser area and W_{stack} is lineal, therefore, the relation between hydrogen produced and W_{stack} is also lineal, as hydrogen produced depends linearly on the current input. Consequently, as we know the hydrogen output from last calculation, we can calculate the necessary W_{stack} and the electrolyser active area (A_{cell}). From equation (9.8), we can calculate the necessary current that must be given to the electrolyser:

$$I = 4.713.481,22 A = 4713,48 kA$$

Therefore, by knowing $I = \frac{i}{A_{cell}}$,

$$A_{cell} = 942,7 m^2$$

Finally, by using equation (9.15), the electric power that must be given to the electrolyser to produce the required amount of H_2 is:

$$W_{stack} = 115.332,033 kW = 115,33 MW$$

9.3. Air Separation Unit

A typical ASU unit with cryogenic distillation uses a multistage compressor with intercooling, in addition to multi heat exchangers with different passages and high numbers of channels and interactions. The ASU modelled in Aspen Plus will be a simplification of this process, which includes a compressor, a cooler and one distillation column.

9.3.1. Aspen Plus ASU Model

The simulated air is fed to the distillation column at a temperature of 298K and at a pressure of 1 bar. It consists of a mixture of 78,1 % of N_2 , 20,96 % of O_2 and 0,94 % of Ar, all in volume basis. As calculated in section 9.1, the amount of hydrogen needed is $n_{H_2,output} = 1004,35$ kmol/h. Therefore, as the stoichiometry demands (5.1), the amount of nitrogen needed is:

$$n_{N_2,feed} = \frac{1004,35}{3} = 334,9 kmol/h$$

Based on the air composition just mentioned, the amount of air needed is:

$$n_{Air,feed} = \frac{334,9}{0,781} = 428,8 kmol/h$$

Therefore, the amount of oxygen and argon in the feed air stream is:

$$n_{O_2,feed} = 89,88 kmol/h \quad n_{Ar,feed} = 4,03 kmol/h$$

The other components of the air have been omitted since they are not relevant for this simulation.

The first step is the compression of the air by means of an isentropic compressor, which increases the pressure of the air stream up to 6,5 bar. The second step is to cool the compressed air. The critical point of air is $-140,7\text{ }^{\circ}\text{C}$, therefore, the air must be cooled to a temperature lower than this value in order to condense. For an air current with a pressure of 6,5 bar, the air was cooled by means of a cooler to $-172\text{ }^{\circ}\text{C}$, value taken from [25]. The third step is the separation process. For a process which requires big amounts of N_2 it is advised to use cryogenic distillation. For this case, one distillation column was simulated in order to separate N_2 from O_2 and Ar. In this column, gaseous nitrogen exits as distillate from the top of the column, since nitrogen has the lower boiling point among the three compounds, meanwhile oxygen and argon exit from the bottom part. O_2 and Ar separation will not be modelled, as it is not necessary for the ammonia production process.

In order to simulate the distillation column, first a DSTWU column is simulated. The DSTWU column calculates the required amount of plates, the feed stage, the distillate to feed ratio, the reflux ratio, the reboiler and condenser heating required and the distillate and bottom temperature. In order to calculate these values, one must insert the required number of stages or the desired reflux ratio, the condenser and reboiler pressure, the condenser specifications (total or partial), and the desired recovery of the light and heavy components. As a base case, a desired 1,5 times the minimum reflux ratio is chosen as reflux ratio, a condenser and reboiler pressure of 6,5 bar (assuming negligible pressure drop along the column), and a recovery of 99,99 % of N_2 as distillate.

With these parameters, the following requirements were calculated in order to achieve a recovery of 99,99 %:

- Molar reflux ratio: 1,3282
- Number of stages: 37
- Feed stage: 19 (on stage)
- Reboiler heating required: 1292,92 kW
- Condenser cooling required: 681,012 kW
- Distillate temperature: $-175,6\text{ }^{\circ}\text{C}$
- Bottom temperature: $-160,8\text{ }^{\circ}\text{C}$
- Distillate to feed ratio: 0,781

The Aspen Plus model of the ASU unit just described is shown in Figure 9.9:

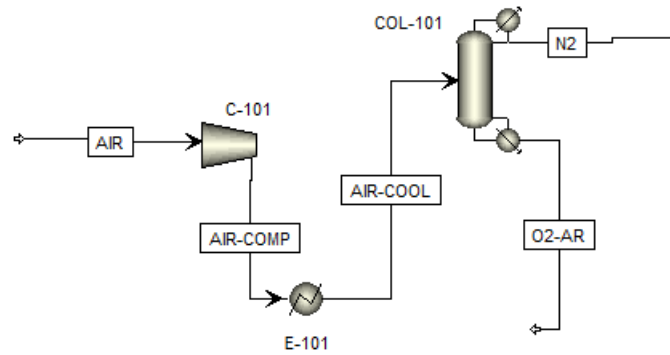


Figure 9.9: Aspen Plus Air Separation Unit model

The DSTWU column must be replaced by a RADFRAC column unit in order to conduct a design specification. This design specification will be carried out in order to determine the specific distillate to feed ratio and reflux ratio to obtain a purity of nitrogen gas as distillate of 99,99 % and a nitrogen recover of at least 99,99 %.

After conducting the design specification, the required distillate to feed ratio and molar flux ratio in order to obtain the desired purity and recovery of 99,99 are:

$$\text{Distillate to feed ratio} = 0,781$$

$$\text{Molar reflux ratio} = 1,96$$

After conducting the design specification, the following requirements for the distillation column were determined:

- Molar reflux ratio: 1,96
- Number of stages: 37
- Feed stage: 19 (on stage)
- Reboiler heating required: 1610 kW
- Condenser cooling required: 998,19 kW
- Distillate temperature: -175,6 °C
- Bottom temperature: -160,8 °C
- Distillate to feed ratio: 0,781

Finally, the composition of the outlet stream of the distillation column (distillate) is:

$$n_{N_2, dist} = 334,868 \text{ kmol/h} \quad n_{O_2, dist} = 0,009 \text{ kmol/h} \quad n_{Ar, dist} = 0,023 \text{ kmol/h}$$

Which meets the requirements for a stream entering a Haber-Bosch reactor (99,99 % mole purity).

9.4. Haber-Bosch Process

In this subsection, the Aspen Plus process simulation of a Haber-Bosch reactor will be simulated. As stated in section 9.1, the reactor operates at $T = 400\text{ }^{\circ}\text{C}$ and $P = 250\text{ bar}$ for maximum ammonia production. The simulated reactor will be adiabatic for simplification purposes.

The hydrogen stream outlet from the electrolyser exits at $25\text{ }^{\circ}\text{C}$, whereas the nitrogen stream outlet from the distillation column exits at $-175,6\text{ }^{\circ}\text{C}$. Therefore, it must be heated by means of a heater to $25\text{ }^{\circ}\text{C}$. Afterwards, both currents are mixed by means of a mixer.

This mixed current enters a compressor to bring it to the desired pressure of 250 bar. Subsequently, by means of a cooler, (since the stream outlet at the compressor exit is higher than $400\text{ }^{\circ}\text{C}$) the stream is brought to $T = 400\text{ }^{\circ}\text{C}$. Finally, the stream current enters the Haber-Bosch reactor, where the Haber-Bosch reaction takes place.

In Figure 9.10, the Aspen Plus simulation for the Haber-Bosch process is shown:

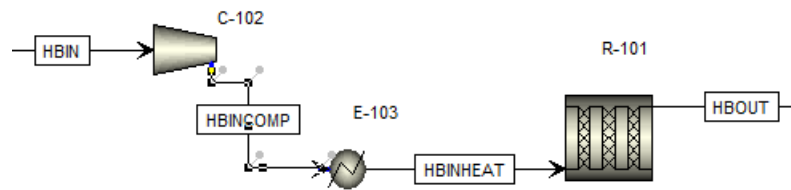


Figure 9.10: Aspen Plus Haber-Bosch process model

9.4.1. Optimization of the Reactor's Dimension

In this subsection, the reactor's dimension will be optimized in order to maximize the conversion with the minimum required volume, since in [56] the reactor length is chosen based on how the conversion changes, selecting its optimum value when the conversion starts changing too little.

As reported in [57], the reactor is constrained to length-to-diameter ratio of at least two (9.19),

$$\frac{L_{reactor}}{D_{reactor}} \geq 2 \quad (9.19)$$

In addition to this, the reported optimization conducted that the optimal point for operation is when the constraint (9.19) is equal to 2. Therefore, constraint (9.20) was used for the simulation:

$$\frac{L_{reactor}}{D_{reactor}} = 2 \quad (9.20)$$

The procedure to determine the reactor's dimension was the following:

1. Select a base case for the sensitive analysis. Diameter equal to 0,5m and length equal to 1m were chosen as base values.
2. Conduct a sensitivity analysis by fixing the diameter and changing the length by 0,05m in each iteration and calculate the conversion until the length is 4m.
3. Graph the curve conversion vs length.
4. Select the length when the change in conversion significantly decreases (for this case, when a change in conversion $<0,01\%$ was detected that value is chosen).
5. Calculate the volume obtained with this length and diameter.
6. Calculate the length and diameter that fulfill the constraint (9.20) for the volume obtained in the previous step.

In Figures 9.11 and 9.12, the sensitivity analysis conducted is shown:

Row/Case	Status	VARY 1 R-101 PARAM LENGTH METER	$((N2IN-N2OUT)/N2IN)*100$
▶ 11	OK	1,5	19,689
▶ 12	OK	1,55	20,0614
▶ 13	OK	1,6	20,3633
▶ 14	OK	1,65	20,6013
▶ 15	OK	1,7	20,7843
▶ 16	OK	1,75	20,9225
▶ 17	OK	1,8	21,0254
▶ 18	OK	1,85	21,1011
▶ 19	OK	1,9	21,1562

Figure 9.11: Sensitivity analysis conducted in Aspen Plus to optimize the Haber-Bosch reactor dimensions

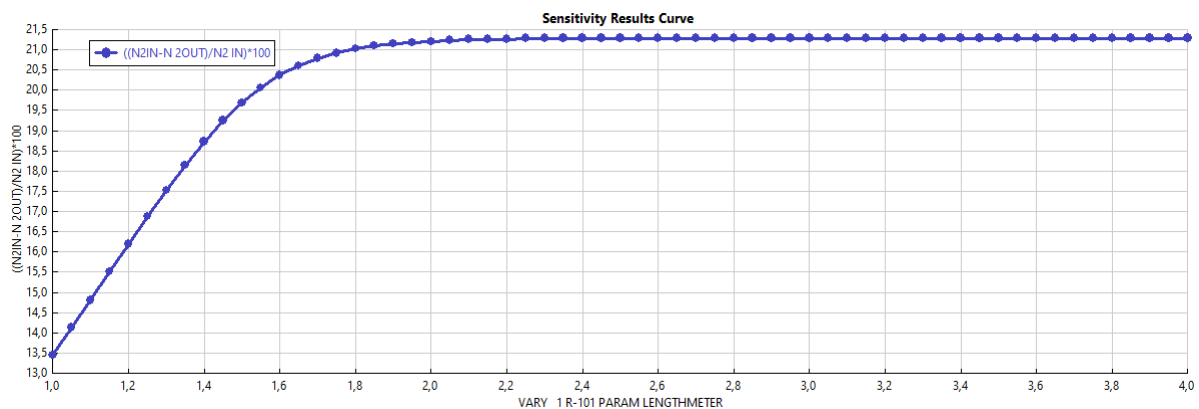


Figure 9.12: Conversion versus reactor length

Finally, with the sensitivity analysis conducted in Aspen Plus, the reactor dimensions and volume obtained are shown in Table 9.4:

Table 9.4: Optimization of the Haber-Bosch reactor's dimension

Optimization of the reactor's dimension		
Parameter	Value	Unit
Length	1,22	m
Diameter	0,61	m
Volume	0,35	m ³

With these parameters, the amount of ammonia produced at the Haber-Bosch reactor is:

$$n_{NH_3,prod} = 140,902 \text{ kmol/h} = 57,59 \text{ t/d}$$

9.5. Ammonia Separation Process by Condensation

After the Haber-Bosch process, the outlet stream enters the ammonia separation block. This block will separate the ammonia from the nitrogen and hydrogen tail gases, in order to fulfill the requirement of 50 mtpd of ammonia produced.

For the base case in Aspen Plus, the ammonia separation process will consist of a cooler (condenser) and a flash. The condenser condenses the ammonia, which has a higher boiling point compared to nitrogen and hydrogen. Afterwards, the flash unit separates the liquid ammonia from the nitrogen and hydrogen gases.

For this simulation, the cooler will operate at $-20 \text{ }^\circ\text{C}$ with no pressure drop, with a subsequent adiabatic flash with also no pressure drop and operating at the same temperature.

In Figure 9.13, the ammonia separation process by condensation carried out in Aspen Plus is shown:

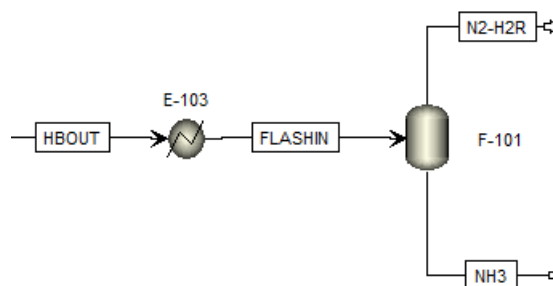


Figure 9.13: Ammonia separation section modelled in Aspen Plus

The amount of ammonia produced in the liquid stream outlet of the flash is:

$$n_{NH_3,outlet} = 122,538 \text{ kmol/h} = 50,085 \text{ t/d}$$

Value that meets the requirements established for the green ammonia production plant.

10. Improvements of the Base Case

10.1. PEM Electrolyser

In this section, the model of a PEM electrolyser will be described. The purpose of developing this PEM electrolyser is to compare it with the alkaline electrolyser in terms of required electricity input and costs. The development will be done using an Excel calculator block as a subroutine for Aspen Plus calculations in order to obtain the H₂ needed for the green ammonia plant, same procedure as in section 9.2.

10.1.1. Calculation of the Real Cell Voltage and the Amount of Water Required

In this subsection, the necessary equations in order to determine the real cell voltage and the amount of water required in order to fulfill the ammonia plant requirements is shown.

Firstly, some assumptions must be made for the voltage calculation in order to use the following equations [20].

- Pressure effects are neglected since they are not relevant when coupling with renewable energies.
- Temperature uniform among all stacks.
- Identical PEM electrolytic cells connected in series. Total stack working voltage is obtained by multiplying the cell voltage by the number of series-connected cells.

The minimum voltage to conduct the reaction is affected mainly by temperature and pressure. In real systems, a higher potential must be applied due to kinetics losses at bipolar plates, electrodes and internal resistances in the cell. Therefore, the required potential can be written as the sum of the reversible voltage plus overpotentials. Most of the equations and relations employed in this section to calculate the required voltage (real) were retrieved from [52].

The required voltage for PEM electrolysis can be expressed in function of different terms (10.1),

$$V_{cell} = E + \eta_{\Omega} + \eta_{electrodes} + \eta_{conc} \quad (10.1)$$

Where one of the expression can be expressed as (10.2)

$$\eta_{electrodes} = \eta_{act,a} + \eta_{act,c} \quad (10.2)$$

Where E is the equilibrium voltage, η_{Ω} is the ohmic overpotential across the proton exchange membrane, $\eta_{electrodes}$ is the activation overpotential at the electrodes, which is the sum of the activation overpotential at the anode and cathode ($\eta_{act,a}$ and $\eta_{act,c}$ respectively) and η_{conc} is the concentration overpotential, which can be neglected because the gas transport limitations in thin electrodes are insignificant for PEM electrolysis under

normal operation conditions. Consequently, the required voltage can be through equation (10.3),

$$V = E + \eta_{\Omega} + \eta_{act,a} + \eta_{act,c} \quad (10.3)$$

Firstly, the equilibrium voltage must be calculated, which for PEM electrolysis can be empirically expressed by equation (10.4),

$$E = 1,23 - 0,9 \cdot 10^{-3}(T - 298) + 2,3 \frac{RT}{4F} \ln(P_{H_2}^2 P_{O_2}) \quad (10.4)$$

Where R is the universal gas constant = 8,314 (J/mol·K), F is the Faraday constant = 9,65 · 10⁴ (C/mol), T is Temperature (K) and P_{H_2} and P_{O_2} are the partial pressures of hydrogen and oxygen respectively (atm).

Secondly, the ohmic overpotential must be considered across the PEM. This overvoltage is caused by the resistance of the membrane to the hydrogen ions transporting through it. In order to determine this value, we must find the ionic resistance of the membrane, which is related to the degree of humidification and thickness of the membrane as well as the membrane temperature.

It is easier to find the ionic conductivity and calculate the ionic resistance from that value. A way to calculate it is to use an empirical model (10.5) to determine the total ionic conductivity $\sigma(x)$ of the membrane:

$$\sigma[\lambda(x)] = [0,5139\lambda(x) - 0,326]exp \left[1268 \left(\frac{1}{303} - \frac{1}{T} \right) \right] \quad (10.5)$$

Where x is the location in the membrane measured from cathode-membrane interface (m) and $\lambda(x)$ is the water content at location x in the membrane. This value can be expressed linearly in terms of water content at the membrane-electrode interfaces using equation (10.6),

$$\lambda(x) = \frac{\lambda_a - \lambda_c}{L}x + \lambda_c \quad (10.6)$$

Where L is the Membrane thickness (m) and λ_a and λ_c are the water contents at the anode-membrane and cathode-membrane interface respectively. Therefore, the overall ohmic resistance can be determined through (10.7),

$$R_{PEM} = \int_0^L \frac{dx}{\sigma[\lambda(x)]} \quad (10.7)$$

Consequently, the ohmic overpotential can be expressed in terms of the ohm's law (10.8),

$$\eta_{\Omega} = J \cdot R_{PEM} \quad (10.8)$$

Where J is the current density (A/m²).

Thirdly, the activation overpotential must be determined. This overvoltage is a mea-

sure of the activity of the electrodes. It represents the overpotential required for the electrochemical reaction, which can be expressed by the Butler-Volmer equation (10.9),

$$J = J_{0,i} \left[\exp\left(\frac{\alpha z F \eta_{act,i}}{RT}\right) - \exp\left(\frac{(1-\alpha) z F \eta_{act,i}}{RT}\right) \right], \quad i = a, c \quad (10.9)$$

Where $J_{0,i}$ is the exchange current density (A/m²) and subscripts a, c represent anode and cathode respectively, α is the symmetrical factor and z is the number of electrons involved per reaction. Therefore, taking into account that for water electrolysis z and α take the values of 2 and 0,5 (assuming perfect symmetry) respectively, the activation overpotential can be defined through equation (10.10),

$$\eta_{act,i} = \frac{RT}{F} \sinh^{-1} \left(\frac{J}{2J_{0,i}} \right), \quad i = a, c \quad (10.10)$$

The exchange current density is an important parameter in calculating the activation overpotential, since it represents the electrode's readiness to proceed with the electrochemical reaction (electrodes with higher reactivity have higher exchange current densities). The exchange current density can be determined using equation (10.11),

$$J_{0,i} = J_i^{ref} \exp\left(\frac{-E_{act,i}}{RT}\right), \quad i = a, c \quad (10.11)$$

Where J_i^{ref} is the pre-exponential factor (A/m²) and $E_{act,i}$ is the activation energy (J/mol) for anode and cathode, respectively.

Finally, in order to calculate the required voltage for the electrochemical reaction, we must substitute equations (10.4), (10.8) and (10.10) in equation (10.3) to obtain it. This value will be a function of the temperature, the vapor pressures of H₂ and O₂, the current density, the water contents, the membrane thickness and the exchange current densities (which are a function of the temperature). The typical values that one can assume for the water contents, the activation energies and the vapor pressures are shown in Table 10.1,

Table 10.1: PEM Electrolyser Parameters [52]

Parameters	Values	Units
P_{O_2}	1	atm
P_{H_2}	1	atm
λ_a	14	$\frac{mol_{H_2O}}{mol_{SO_3}}$
λ_c	10	$\frac{mol_{H_2O}}{mol_{SO_3}}$
$E_{act,a}$	76000	J/mol
$E_{act,c}$	18000	J/mol

In order to determine the amount of water required to obtain the desired amount of hydrogen calculated in subsection 9.1.2, models, equations and relations were retrieved from [26], [64], [65] and [66].

Firstly, we must determine the hydrogen production rate from the electrolyser at the cathode, which depends on the electrochemical behavior of the electrolyser cells and di-

verse parameters. Equation (10.12) can be used to determine it:

$$n_{H2,prod,PEM} = \frac{iAN_{cells}}{zF} \quad (10.12)$$

Where $n_{H2,prod,PEM}$ is the amount of moles of hydrogen produced at the cathode (mol/s), i is the current density (A/m²), A is the active electrode area (m²), N is the number of cells, z is the number of electrons exchanged = 2 for water electrolysis, and F is the Faraday constant = 96485 C/mol.

The total amount of water needed and oxygen produced can be determined through equations (10.13), (10.14), (10.15) and (10.16).

$$n_{H2,cat,out,PEM} = n_{H2,cat,in,PEM} + n_{H2,prod,PEM} \quad (10.13)$$

$$n_{O2,an,out,PEM} = n_{O2,an,in,PEM} + n_{O2,prod,PEM} \quad (10.14)$$

$$n_{H2O,an,out,PEM} = n_{H2O,an,in,PEM} - n_{H2O,cons,PEM} - n_{H2O,PEM}^{eo} - n_{H2O,PEM}^{diff} + n_{H2O,PEM}^{PE} \quad (10.15)$$

$$n_{H2O,cat,out,PEM} = n_{H2O,cons,PEM} + n_{H2O,PEM}^{eo} + n_{H2O,PEM}^{diff} - n_{H2O,PEM}^{PE} \quad (10.16)$$

Therefore, the amount of water needed to enter the electrolyser in order to produce the required amount of hydrogen at the cathode can be determined using (10.17),

$$n_{H2O,in,PEM} = n_{H2O,an,in,PEM} = n_{H2O,out,an,PEM} + n_{H2O,cons,PEM} + n_{H2O,PEM}^{eo} + n_{H2O,PEM}^{diff} - n_{H2O,PEM}^{PE} \quad (10.17)$$

Where $n_{H2,cat,out,PEM}$ represents the moles of hydrogen that exit from the cathode, $n_{H2,cat,in,PEM}$ represents the moles of hydrogen that enter through the cathode, $n_{H2,prod,PEM}$ are the moles of hydrogen produced in the electrolyser, $n_{O2,an,out,PEM}$ are the moles of oxygen that exit through the anode, $n_{O2,an,in,PEM}$ are the moles of oxygen that enter through the anode, $n_{O2,prod,PEM}$ are the moles of oxygen produced in the electrolyser, $n_{H2O,an,out,PEM}$ are the moles of water that exit through the anode, $n_{H2O,an,in,PEM}$ are the amount of moles of water that enter through the anode and $n_{H2O,cons,PEM}$ are the moles of water that are consumed in the electrolyser. The terms $n_{H2O,PEM}^{eo}$, $n_{H2O,PEM}^{diff}$, and $n_{H2O,PEM}^{PE}$ account for electro osmotic drag (eo), diffusivity driven-transport and pressure driven cross flow. The electro osmotic drag is caused by the transport of water molecules by hydrogen ions, the diffusivity driven-transport due to concentration difference between anode and cathode and the pressure driven cross flow due to the pressure difference between both electrodes. The first two terms indicate water diffused from anode to cathode, as there is more water in the cathode side since water enters by the cathode, whereas the third one specifies transport from cathode to anode.

In literature ([26] [64] [65] [66]), H₂ diffusion through the membrane was not considered and a Faradaic efficiency of 99% was used, as similar to empiric results.

$$\eta_{F,PEM} = 0,99 = 99\%$$

The first diffusion term that accounts for electro-osmotic drag can be determined by equation (10.18),

$$n_{H_2O,PEM}^{eo} = \frac{n_d i A N_{cells}}{F} \quad (10.18)$$

Where n_d is a coefficient that depends on membrane humidification λ , which can be calculated through equation (10.19),

$$n_d = 0,0029\lambda^2 + 0,05\lambda + 3,4 \cdot 10^{-19} \quad (10.19)$$

The second diffusive term can be obtained in function of the concentration difference at the electrodes, by means of equation (10.20),

$$n_{H_2O,PEM}^{diff} = \frac{D_{w,eff}(C_w^{an} - C_w^{cat})AN_{cells}}{L} \quad (10.20)$$

Where $D_{w,eff}$ accounts for the effective diffusivity, which considers the effective binary diffusivity of H₂/H₂O and O₂/H₂O. For this simulation, both values will be considered equal for simplification. The effective diffusivity can be written in function of the water diffusion coefficient (D_w), the porosity of the electrodes (ϵ) and the percolation threshold (ϵ_p) using equation (10.21),

$$D_{w,eff} = D_w \cdot \epsilon \left(\frac{\epsilon - \epsilon_p}{1 - \epsilon_p} \right)^\alpha \quad (10.21)$$

Where $\epsilon = 0,3$, $\epsilon_p = 0,11$, $D_w = 1,28 \cdot 10^{-10}$ m²/s and $\alpha = 0,785$, which is an empirical coefficient.

The water concentration at both electrodes can be determined through equation (10.22),

$$C_w^i = \frac{\rho_{m,dry}}{M_{m,dry}} \lambda_i, \quad i = a, c \quad (10.22)$$

Where $\rho_{m,dry}$ is the density of a dry membrane (kg/m³) and $M_{m,dry}$ is the equivalent weight of a dry membrane (kg/mol).

In order to obtain the last diffusive term, the equation (10.23) can be used,

$$n_{H_2O}^{PE} = -\frac{K_{Darcy} A \rho_w (p_{cat} - p_{an})}{L \mu_w M M_w} \quad (10.23)$$

Where K_{Darcy} is the membrane permeability to water = $1,58 \cdot 10^{-18}$ m², ρ_w is the water density, MM_w is the molar mass of water = 17 g/mol and μ_w is the water viscosity. ρ_w and μ_w are values that depend on the temperature.

10.1.2. Aspen Plus Electrolyser Simulation PEM

The electrolyser simulated in this section has the same working temperature, pressure and feed composition as the AWE simulated in subsection 9.2.2.

Table 10.2 shows the different inputs that must be inserted into the calculator block in order to obtain the desired outputs. Some inputs will be inserted directly from Aspen, while some others will be inserted directly on the calculator block.

Table 10.2: Inputs for PEM Electrolyser simulation in Aspen Plus

Inputs	Value	Unit
Electrolyser temperature (T_{elect})	75	°C
Electrolyser pressure (P_{elect})	7	bar
Cell number (N)	12	cells
Current density (i)	5000	A/m ²
Membrane thickness (L)	$5 \cdot 10^{-6}$	m
Membrane porosity (ϵ)	0,3	-
Percolation threshold (ϵ_p)	0,11	-
Membrane humidity at anode (λ_a)	14	$\frac{mol_{H_2O}}{mol_{SO_3}}$
Membrane humidity at cathode (λ_c)	10	$\frac{mol_{H_2O}}{mol_{SO_3}}$
Density of a dry membrane ($\rho_{m,dry}$)	2000	kg/m ³
Equivalent weight of a dry membrane ($M_{m,dry}$)	1,1	kg/mol
Water diffusion coefficient (D_w)	$1,28 \cdot 10^{-10}$	m ² /s
Membrane permeability to water (K_{Darcy})	$1,58 \cdot 10^{-18}$	m ²
Hydrogen partial pressure (P_{H_2})	1	atm
Oxygen partial pressure (P_{O_2})	1	atm
Water density (ρ_w)	975	kg/m ³
Water molar mass (MM_w)	17	kg/kmol
Electrolyte concentration in feed	0,35	-
Number of electrons transferred (z)	2	-
Faraday constant (F)	96485	C/mol
Universal gas constant (R)	8,314	J/(K·mol)
Exchange current density at anode ($J_{A,0}$)	0,00001	J/mol
Exchange current density at cathode ($J_{C,0}$)	10	J/mol

The Aspen Plus simulation process for the electrolyser just described is presented in Figure 10.1:

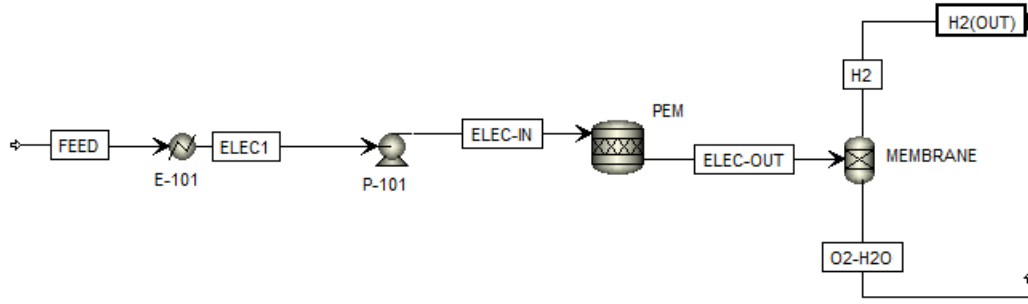


Figure 10.1: PEM electrolyser model in Aspen Plus

10.1.3. Aspen Plus Electrolyser PEM: Voltage Calculation

By using equation (10.4) for $T = 75^\circ\text{C}$ (348K) the equilibrium voltage in order to carry out the water electrolysis is equal to:

$$E = 1,185 \text{ V}$$

In order to determine the ohmic overpotential, one must calculate the integral value of equation (10.7) in function of the temperature and membrane thickness used in this simulation. For this calculation, the integral was solved by using numerical integration, due to the difficulty of evaluating the solution. In this case, the composite trapezoidal rule (10.24) was used, which in general can be defined as,

$$\int_a^b f(x)dx \approx \frac{b-a}{2m} \left[f(x_1) + 2 \sum_{i=2}^m f(x_i) + f(x_{m+1}) \right] \quad (10.24)$$

Where m is the number of intervals for $m+1$ nodes.

For this case, equation (10.24) can be written as (10.25) using 31 nodes,

$$R_{PEM} = \int_0^L \frac{dx}{\sigma[\lambda(x)]} \approx \frac{L-0}{2 \cdot 30} \left[f(x_1) + 2 \sum_{i=2}^{30} f(x_i) + f(x_{31}) \right] = 5,04 \cdot 10^{-6} \quad (10.25)$$

Where $f(x_i) = \frac{1}{\sigma[\lambda(x_i)]}$.

Therefore, the ohmic overpotential can be calculated using equation (10.8), obtaining the following value,

$$\eta_{ohm} = 0,0252 \text{ V}$$

For the activation overpotentials, the pre-exponential factor must be obtained. At $T = 353 \text{ K}$, the values of exchange current density for anode and cathode are 10^{-5} A/m^2 and 10 A/m^2 respectively. Therefore, by substituting the corresponding activation energy and the corresponding exchange current density for $T = 353 \text{ K}$ in equation (10.11) one can find that the pre-exponential factor for each one is:

$$J_a^{ref} = 1.763.563 \text{ A/m}^2$$

$$J_c^{ref} = 4.609,13 \text{ A/m}^2$$

By knowing the pre-exponential factor for the cathode and anode, the activation overpotential for the cathode and anode can be obtained by equation (10.10):

$$\eta_{act,c} = 0,186 \text{ V} \quad \eta_{act,a} = 0,6 \text{ V}$$

Finally, with the values of the equilibrium voltage, ohmic and activation overpotentials the required real cell voltage can be obtained by means of equation (10.3), obtaining the successive value:

$$V_{PEM} = 1,99 \text{ V}$$

10.1.4. Aspen Plus Electrolyser PEM: Amount of Water Required Calculation

As calculated before, the amount of ammonia required is 122,33 kmol/h while the amount of hydrogen output necessary is $n_{H_2,output,PEM} = 1004,35 \text{ kmol/h}$, as the reactor conversion and separation efficiency remain the same.

By using equation (10.12), the active electrode area necessary in order to obtain the required hydrogen output in order to achieve the ammonia demand can be calculated:

$$A_{cell} = n_{H_2,prod,PEM} \frac{nF}{iN_{cells}} \cdot \frac{1000 \text{ mol h}}{3600 \text{ kmol s}} = 897,27 \text{ m}^2$$

First, the water diffusion by electro osmotic drag is calculated. The membrane humidity was evaluated as $\lambda_a = 14$ and $\lambda_c = 10$ in the previous section for anode and cathode respectively. For simplicity, a mean of these two values will be used to evaluate the membrane humidity λ_m :

$$\lambda_m = \frac{\lambda_a + \lambda_c}{2} = 12 \tag{10.26}$$

Consequently, the constant n_d can be evaluated by using (10.19) and the value just obtained from (10.26),

$$n_d = 1,02$$

Therefore, the amount of water diffused by electro-osmotic drag is (10.18),

$$n_{H_2O,PEM}^{eo} = 2044,05 \text{ kmol/h}$$

Second, the water diffusion by the concentration gradient must be calculated. The effective diffusivity is calculated employing (10.21),

$$D_{w,eff} = 1,14 \cdot 10^{-11} \text{ m}^2/\text{s}$$

The concentration terms at the anode and cathode can be determined with equation (10.22),

$$C_{H_2O}^{an} = 25,45 \text{ kmol/m}^3 \quad C_{H_2O}^{cat} = 18,18 \text{ kmol/m}^3$$

Consequently, the amount of water diffused by concentration gradient is (10.20),

$$n_{H_2O,PEM}^{diff} = 64,42 \text{ kmol/h}$$

The amount of water diffused by pressure will not be considered in the simulations, since it can be neglected due to its low incidence [64].

Accordingly to equations (10.13), (10.14) (10.15) and (10.16) the oxygen and water produced can be calculated, along with the water consumed and the hydrogen that exits the electrolyser. For these calculations it is assumed that the feed current is pure water mixed with KOH, therefore, no hydrogen neither oxygen is entering through the electrolyser.

$$n_{H_2,cat,out,PEM} = n_{H_2,prod,PEM} = 1004,35 \text{ kmol/h}$$

$$n_{O_2,an,out,PEM} = n_{O_2,prod,PEM} = 502,18 \text{ kmol/h}$$

$$n_{H_2O,cons,PEM} = 1004,35 \text{ kmol/h}$$

$$n_{H_2O,cat,out,PEM} = 2108,47 \text{ kmol/h}$$

Finally, the amount of water entering the electrolyser through the anode can be calculated by (10.17):

$$n_{H_2O,in,PEM} = 3122,94 \text{ kmol/h} \tag{10.27}$$

Value which takes into account the Faradaic efficiency η_F .

10.1.5. Aspen Plus Electrolyser PEM: Electricity Input Requirement

By using (9.15), the electricity that must be applied to the electrolyser in order to carry out the equation is:

$$W_{stack,PEM} = 107,52 \text{ MW}$$

10.2. ASU with 2 Distillation Columns

The high refrigeration costs involving cryogenic processes demands heat integration for air separation units. It is important to conduct an optimization analysis for each different industry process, since each one has different feed and operation conditions and different purity targets.

In literature [69], designs based on 1, 2 and 3 distillation columns are usually reported. Using only one column process has the advantage of being a very simple design with an easy control system, but lacks of heat integration. The three distillation columns system is usually used when oxygen-argon separation with high purities is needed. Therefore, for this simulation a 2 distillation columns system will be conducted, in order to compare the heat energy requirements between this configuration and the last reported.

In this section, the improvement of the ASU is done by implementing a high pressure

and a low pressure distillation column energetically integrated instead of only one. In addition, the compressor and cooler will be changed by a multistage compression with intercooling system using cooling water at 25 °C and 1 bar. Each compressor will be simulated as isentropic, with an efficiency of 0,72 [67]. This change will be done with three purposes:

1. Achieve lower energy requirements for air compression and cooling.
2. The temperature at the compressor outlet cannot be higher than 150 °C, so as not to damage the components of the compressor [67].
3. The temperature of the cooling water outlet cannot be higher than 50 °C [67].

This ASU in Aspen Plus simulation will be done based in subsection 5.2.1, in addition to [68] and [69]. In Figures 10.2 and 10.3, the Aspen Plus simulation of the multistage compression of air with inter-cooling and the two cryogenic distillation columns are shown:

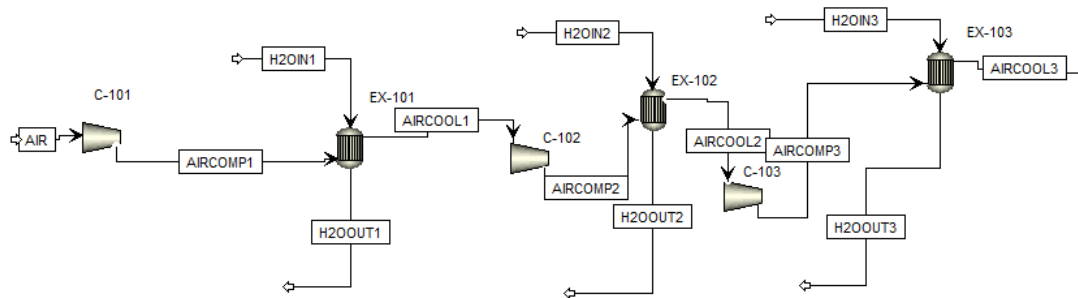


Figure 10.2: Aspen Plus model of the multistage compression of air with inter-cooling

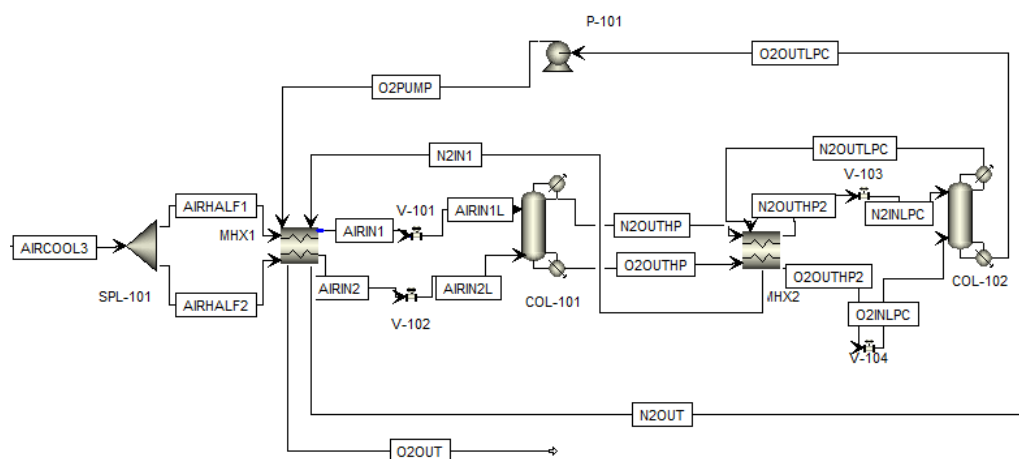


Figure 10.3: Aspen Plus model of a cryogenic double distillation column system with energy integration

In Table 10.3, the compression ratios fixed for compressors C-101, C-102 and C-103 are shown,

Table 10.3: Compression ratio for each compressor

Compressor	Compression Ratio
C-101	1,98 [68]
C-102	1,84 [68]
C-103	1,78 [68]

In addition, the fixed outlet temperatures of the air after each intercooling process are reported in Table 10.4,

Table 10.4: Outlet temperatures of the air after each intercooling

Stream	Outlet Temperature (°C)
AIRCOOL1	40
AIRCOOL2	40
AIRCOOL3	30

Regarding the cryogenic distillation columns, the pressure and number of staged fixed for each one can be seen in Table 10.5,

Table 10.5: Cryogenic distillation column parameters

Distillation Column	Parameter	Value	Unit
Low pressure column (LPC)	Pressure	1,5	bar
	# of stages	60	-
High pressure column (HPC)	Pressure	5,6	bar
	# of stages	60	-

In order to determine the amount of cooling water required to obtain the desired outlet temperatures of the air after each compression, we must obtain the amount of heat needed for this process. In Table 10.6, by using Aspen Plus, the amount of heat that must be subtracted from each air stream in order to achieve the desired temperatures are:

Table 10.6: Heat subtracted from each air outlet stream after compression

Heat Exchanger	Heat Subtracted (kW)
EX-101	257,9
EX-102	288,18
EX-103	308,96

Moreover, by using Aspen Plus, the amount of heat that must be given to an stream of 1 kg/h of water at 25 °C and 1 bar to bring it to 50 °C is:

$$Q_w = 0,031 \text{ kW} \quad (10.28)$$

Therefore, by dividing the heat that must be subtracted from each stream 10.6 by the value calculated in equation (10.28) the amount of water needed in each heat exchanger can be obtained, as shown in Table 10.7,

Table 10.7: Amount of water needed in each heat exchanger

Heat Exchanger	Water needed (kg/h)
EX-101	8209,34
EX-102	9173,2
EX-103	9834,66

Therefore, by fixing the compression ratio of each compressor and the required amount of cooling water, the temperatures at the outlet of each stream can be obtained, as shown in Table 10.8,

Table 10.8: Stream outlet temperature after compression and cooling water temperature after intercooling

Stream	Temperature (°C)
AIRCOMP1	114
AIRCOMP2	122
AIRCOMP3	118
H2OOUT1	50
H2OOUT2	50
H2OOUT3	50

Values that accomplish the constraints that the outlet temperature at each compressor must be lower than 150 °C and the temperature of cooling water cannot be higher than 50 °C, as described in 10.2.

After the multistage compression with intercooling, the feed air is splitted into two streams with the same composition and mass flow. Both currents enters a multi-stream heat exchanger, where they are cooled with the nitrogen and oxygen streams exiting the LPC distillation column. By fixing that the nitrogen stream N2OUT must exit at $T = 25^{\circ}\text{C}$ and that the oxygen-argon stream O2OUT must exit as vapor stream, the outlet temperature of the streams AIRIN1 and AIRIN2 reached -174°C , which is perfect in order to conduct the distillation process at the HPC (which operates between -177°C and -172°C). Afterwards, both streams enter the HPC in different feed stages so as to achieve the separation between nitrogen and oxygen with argon.

The nitrogen liquid distillate and the liquid oxygen bottom exiting the HPC enter a multi heat exchanger, where they are further cooled by the gaseous nitrogen stream exiting through the LPC. The gaseous nitrogen distillate and the oxygen liquid exiting through the bottom are further heated in the multi-heat exchangers mentioned before.

Valves V-101, V-102, V-103 and V-104 are called JT valves since they operate by the Joule-Thomson effect. They are used to depressurize the stream exiting the distillation columns so as to decrease their temperature while keeping it insulated. Therefore, no heat is exchanged with the ambient. The valves cool further down so as to achieve the desired temperature in the streams entering the distillation columns [68].

An optimization was conducted in each distillation column. For the HPC, the distillate to feed ratio and reflux ratio varied in order to obtain an oxygen purity of 40% at

the bottom and a nitrogen purity of 99,99% at the distillate. Instead, for the LPC, the distillate to feed ratio and reflux ratio varied too towards obtaining a recovery and purity of nitrogen at the distillate of 99,99%.

The distillate to feed ratio and the reflux ratio obtained in each column are shown in Table 10.9:

Table 10.9: Design specification for both distillation columns

Distillation Column	Parameter	Value
Low pressure column (LPC)	Distillate to feed ratio	0,476
	Molar reflux ratio	1,35
High pressure column (HPC)	Distillate to feed ratio	0,781
	Molar reflux ratio	0,852

In Tables 10.10 and 10.11, the parameters used for each distillation column are shown and the desired targets for both multi-stream heat exchangers are shown. The parameters for each distillation column were based on obtaining the same energy requirements for the reboiler of the LPC and the condenser of the HPC.

Table 10.10: Parameters for distillation columns COL-101 and COL-102

Equipment	Parameter	Value	Unit
Column COL-101	# of stages	60	-
	Feed stage AIRIN1	50	-
	Feed stage AIRIN2	60	-
	Pressure	5,6	bar
	Pressure drop	0,2	bar
Column COL-102	# of stages	45	-
	Feed stage AIRIN1	1	-
	Feed stage AIRIN2	38	-
	Pressure	1,5	bar
	Pressure drop	0,3	bar

Table 10.11: Desired output specifications for both multi-heat exchangers

Equipment	Specification	Value	Unit
MXH1	Cold outlet stream O2OUT	25	°C
	Cold outlet stream N2OUT	25	°C
	Pressure drop	0,1	bar
MXH2	Hot outlet stream N2OUTH2P2	-182	°C
	Hot outlet stream O2OUTH2P2	-182	°C
	Pressure drop	0,1	bar

In Table 10.12, the heat requirements for each of the equipments used in the ASU process is shown:

Table 10.12: Energy requirements for each equipment in the ASU

Equipment	Energy necessary to be supplied or subtracted	Value (kW)
C-101	Supplied	309
C-102	Supplied	287
C-103	Supplied	271
COL-101 reboiler	Supplied	171,62
COL-101 condenser	Subtracted	643,44
COL-102 reboiler	Supplied	615,82
COL-102 condenser	Subtracted	157,16
P-101	Supplied	0,13

For this configuration, we can energetically integrate the condenser of the HPC with the reboiler of the LPC, since the condenser temperature is higher than the reboiler temperature. Therefore, the overall energy necessary for the air separation process in the distillation columns can be calculated using equation (10.29),

$$COL - 101_{cond} - COL - 102_{reb} = 27,62 \text{ kW} \quad (10.29)$$

10.3. Multi-bed Reactor System With Intercooling

The high energy requirements to drive the hydrogen and nitrogen streams after the ASU to the necessary temperature and pressure at the entrance of the Haber-Bosch reactor ($T = 400 \text{ }^\circ\text{C}$, $P = 250 \text{ bar}$), demands the use of multistage intercooling compressors and heat exchangers to control the temperature at the outlet of each compressor.

In Figures 10.4, 10.5 10.6 and 10.7 the full process is shown. Figures 10.4 and 10.5 corresponds to the process previous to the multistage compression, where hydrogen and nitrogen are brought to the same temperature and pressure through heat exchangers and compressors. Afterwards, both streams are mixed in a mixer (MIX-101). A small current of ammonia entering to the process is simulated, as said section 9.1 to avoid problems with Aspen Plus kinetics.

In Figure 10.6 is illustrated the process after the currents are mixed at the same pressure and temperature. The mixed current of mainly H_2 , N_2 and NH_3 enter a multistage compression with inter-refrigeration process, where they are brought to $T = 250 \text{ }^\circ\text{C}$ and 250 bar [70] [71]. Finally, in Figure 10.7, the heated and compressed mixed stream enters the multi reactor system with inter-refrigeration with one heat exchanger and three quenching splits is shown. This configuration was chosen from [70] and [71] proposed with the following objectives:

1. Maintain the temperature entering each reactor at $T = 400 \text{ }^\circ\text{C}$ to maximize ammonia conversion.

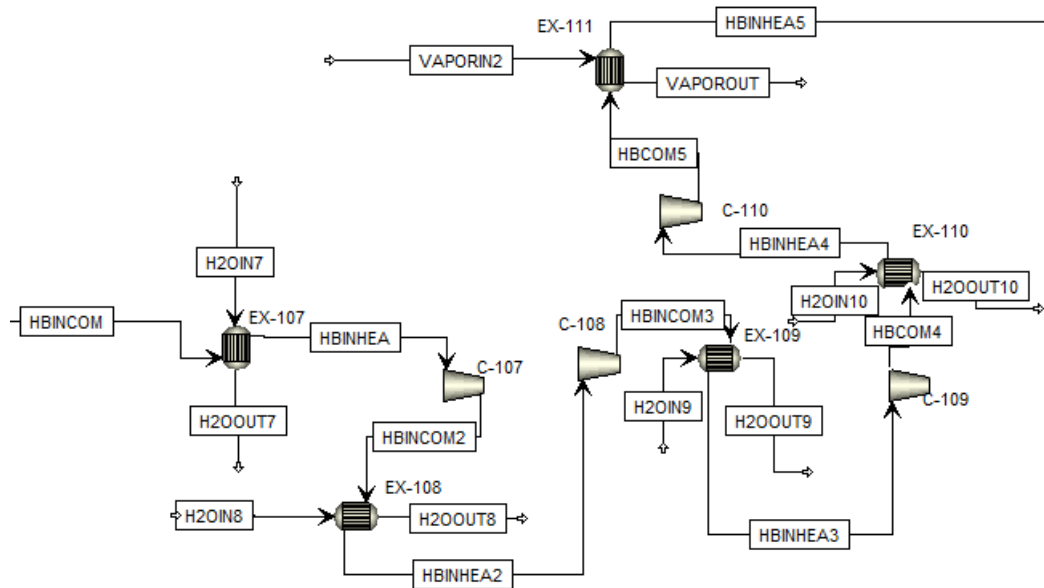


Figure 10.6: Aspen Plus model the multi stage compression system with inter cooling for the feed entering the Haber-Bosch reactor

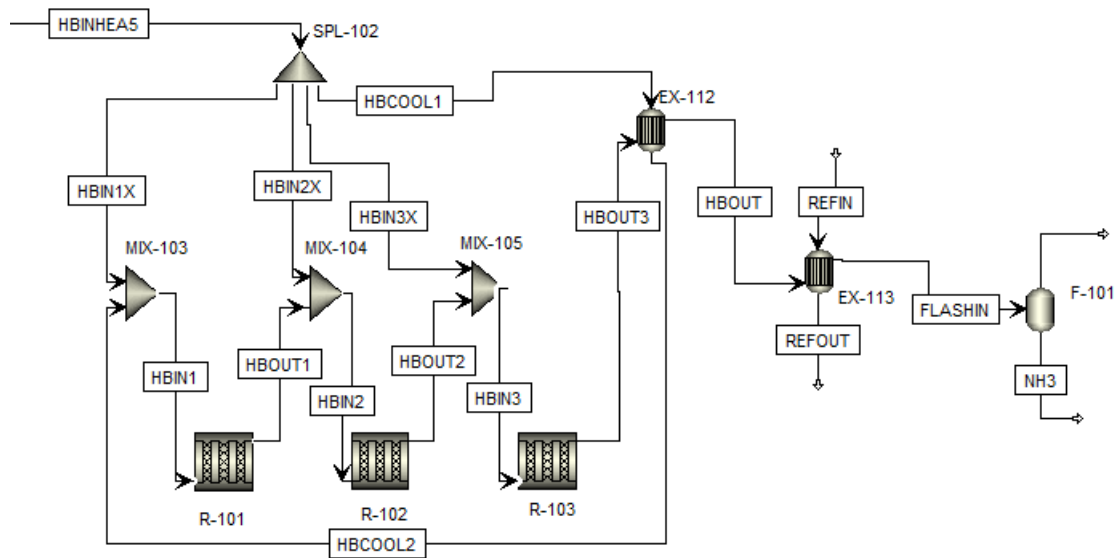


Figure 10.7: Aspen Plus model of the multi reactor system with intercooling, followed by the ammonia condensing and recovery process

10.3.1. Description of the process

First, the nitrogen current exiting the ASU at $P = 1,3$ bar and $T = 25$ °C is compressed in a two-stage compressing system, where it is brought to $P = 7$ bar, which corresponds to the hydrogen pressure exiting the electrolyser. Both currents are brought to $T = 30$ °C, where they are mixed with the ammonia entering current.

Second, the mixed current enters a five-stage multi compression system, where it is brought

to the desired temperature $T = 250\text{ }^{\circ}\text{C}$ and $P\ 250\text{ bar}$. After each compression exit, T must not be higher than $150\text{ }^{\circ}\text{C}$ so as to not compromise the compressor parts, as said before [67].

Finally, the mixed stream enters a quenching system, where it is splitted into four different streams. The first three currents enter each one to a different reactor, where the fourth one enters a heat exchanger to heat up before entering to the first reactor.

In Table 10.13, the parameters and configurations chosen for each equipment shown in the Figures 10.4, 10.5, 10.6 and 10.7 is described (except for the flash and reactor units, which will be described in further sections),

Table 10.13: Parameters established for multi stage compression with interrefrigeration system for feeding stream entering the multi stage reactor system

Equipment	Parameter/desired output	Value	Unit
C-104	Discharge pressure	3,2	bar
C-105	Discharge pressure	7	bar
C-106	Pressure ratio	2	-
C-107	Pressure ratio	2	-
C-108	Pressure ratio	2	-
C-109	Pressure ratio	2	-
C-110	Discharge pressure	250,1	bar
EX-104	Hot stream outlet temperature	30	$^{\circ}\text{C}$
EX-105	Hot stream outlet temperature	30	$^{\circ}\text{C}$
EX-106	Hot stream outlet temperature	30	$^{\circ}\text{C}$
EX-107	Hot stream outlet temperature	30	$^{\circ}\text{C}$
EX-108	Hot stream outlet temperature	30	$^{\circ}\text{C}$
EX-109	Hot stream outlet temperature	30	$^{\circ}\text{C}$
EX-110	Hot stream outlet temperature	30	$^{\circ}\text{C}$
EX-111	Cold stream outlet temperature	250	$^{\circ}\text{C}$
EX-112	Exchanger area	121,85 [72]	m^2
EX-113	Hot stream outlet temperature	-20	$^{\circ}\text{C}$

10.3.2. Optimization of the multi reactor system with inter-cooling using Aspen Plus

Six different design specifications were conducted in Aspen Plus so as to determine the optimal configuration for the multi reactor system. The parameters used as inputs are shown in Table 10.14,

Table 10.14: Input parameters for multi reactor system configuration

Equipment	Parameter	Value	Unit
EX-112	Area	121,853 [72]	m ²
	U	50 [72]	W/(m ² K)
R-101	Diameter	1	m
R-102	Diameter	1	m
R-103	Diameter	1	m

The first design specification varies the first reactor length in order to obtain a temperature $T = 500$ °C at its outlet stream. The second design specification does the same with the second reactor, while the third design specification varies the third reactor length to obtain a temperature $T = 487$ °C at its outlet stream. The length is varied since this parameter influences the conversion of nitrogen in each reactor, which influences the exiting temperature since it is an exothermic reaction.

The fourth design specification conducted varies the fraction of feed stream splitted to the first reactor so as to achieve a temperature of $T = 400$ °C at its inlet stream.

The fifth and sixth design specification does the same with the fraction of feed stream splitted to the second and third reactor respectively in order to achieve the same inlet stream temperature.

The system crushes when the six design specifications are conducted together since there are many variables at the same time that can be modified, in addition to the fact that sometimes it chooses split fractions which sum higher than 1, which is unfeasible. Therefore, the optimization was conducted following these stepsm

1. The first three design specifications were conducted at the same time, fixing flows equal to 0,25, 0,2 and 0,12 for the first three splits.
2. The sixth design specification is conducted along with the first three.
3. The fifth design specification is conducted along with the four just mentioned.
4. The six design specifications are conducted together, achieving the optimum requirements for this process.

In Tables 10.15 and 10.16, the outputs obtained after each step are shown:

Table 10.15: Outputs obtained with the optimization conducted in Aspen Plus for the first two steps

Step	Design Specifications Involved	Parameter	Value	Unit
1	1	R-101 length	0,082	m
		HBOUT1 temperature	500	°C
	2	R-102 length	0,22	m
		HBOUT2 temperature	500	°C
	3	R-103 length	0,767	m
		HBOUT3 temperature	487	°C
2	1	R-101 length	0,068	m
		HBOUT1 temperature	500	°C
	2	R-102 length	0,251	m
		HBOUT2 temperature	500	°C
	3	R-103 length	0,8	m
		HBOUT3 temperature	487	°C
	6	HBIN3X flow fraction	0,395	-
		HBIN3 temperature	400	°C

Table 10.16: Outputs obtained with the optimization conducted in Aspen Plus for steps three and four

Step	Design Specifications Involved	Parameter	Value	Unit
3	1	R-101 length	0,046	m
		HBOUT1 temperature	500	°C
	2	R-102 length	0,34	m
		HBOUT2 temperature	500	°C
	3	R-103 length	0,8274	m
		HBOUT3 temperature	487	°C
	6	HBIN3X flow fraction	0,394	-
		HBIN3 temperature	400	°C
	5	HBIN2X flow fraction	0,241	-
		HBIN2 temperature	400	°C
4	1	R-101 length	0,077	m
		HBOUT1 temperature	500	°C
	2	R-102 length	0,388	m
		HBOUT2 temperature	500	°C
	3	R-103 length	0,879	m
		HBOUT3 temperature	487	°C
	6	HBIN3X flow fraction	0,3934	-
		HBIN3 temperature	400	°C
	5	HBIN2X flow fraction	0,241	-
		HBIN2 temperature	400	°C
	4	HBIN1X flow fraction	0,073	-
		HBIN1 temperature	400	°C

With these configurations chosen, the amount of ammonia exiting at each Haber-Bosch reactor, with its conversion is illustrated in Table 10.17:

Table 10.17: Conversion and amount of ammonia exiting each reactor

Equipment	Parameter	Value	Unit
R-101	Ammonia at outlet	27,42	kmol/h
	Conversion	11,2	%
R-102	Ammonia at outlet	72,29	kmol/h
	Conversion	11,85	%
R-103	Ammonia at outlet	136,31	kmol/h
	Conversion	10,72	%

Finally, the amount of ammonia exiting the flash along with its recovery is reported in Table 10.18:

Table 10.18: Amount of ammonia exiting the liquid stream within the flash along with its recovery

Equipment	Parameter	Value	Unit
F-101	Ammonia at	117,49	kmol/h
	exiting liquid stream	48,02	t/d
	Ammonia recovery	86,2	%

10.4. Addition of a Recycle Loop

As reported in subsection 5.1.3, the low single-pass conversion of the Haber-Bosch process demands for a recycle stream so as to maximize the ammonia produced at each reactor. Therefore, in this subsection part of the gaseous stream exiting the flash will be recycled. In Figure 10.8, the simulation conducted in Aspen Plus with the recycle stream is shown,

3. The fifth design specification is conducted along with the four just mentioned.
4. The six design specifications are conducted together, achieving the optimum requirements for this process.

In Table 10.19, the different inputs inserted in Aspen Plus for the multi reactor system with a recycle loop are shown,

Table 10.19: Input parameters for multi reactor system configuration with addition of a recycle loop

Equipment	Parameter	Value	Unit
EX-112	Area	1500	m ²
	U	50 [72]	W/(m ² K)
R-101	Diameter	10	m
R-102	Diameter	10	m
R-103	Diameter	10	m

In Tables 10.20 and 10.21, the outputs for the optimization conducted using design specifications in Aspen Plus for this configuration is shown:

Table 10.20: Outputs obtained with the optimization conducted in Aspen Plus for the first two steps for the configuration with a recycle stream

Step	Design Specifications Involved	Parameter	Value	Unit
1	1	R-101 length	0,026	m
		HBOUT1 temperature	500	°C
	2	R-102 length	0,016	m
		HBOUT2 temperature	500	°C
	3	R-103 length	0,0057	m
		HBOUT3 temperature	487	°C
2	1	R-101 length	0,013	m
		HBOUT1 temperature	500	°C
	2	R-102 length	0,014	m
		HBOUT2 temperature	500	°C
	3	R-103 length	0,0052	m
		HBOUT3 temperature	487	°C
	4	HBIN1X flow fraction	0,154	-
		HBIN1 temperature	400	°C

Table 10.21: Outputs obtained with the optimization conducted in Aspen Plus for steps three and four with the addition of a recycle stream

Step	Design Specifications Involved	Parameter	Value	Unit
3	1	R-101 length	0,0092	m
		HBOUT1 temperature	500	°C
	2	R-102 length	0,035	m
		HBOUT2 temperature	500	°C
	3	R-103 length	0,0057	m
		HBOUT3 temperature	487	°C
	4	HBIN1X flow fraction	0,178	-
		HBIN1 temperature	400	°C
	5	HBIN2X flow fraction	0,349	-
		HBIN2 temperature	400	°C
4	1	R-101 length	0,0056	m
		HBOUT1 temperature	500	°C
	2	R-102 length	0,021	m
		HBOUT2 temperature	500	°C
	3	R-103 length	0,046	m
		HBOUT3 temperature	487	°C
	4	HBIN1X flow fraction	0,097	-
		HBIN1 temperature	400	°C
	5	HBIN2X flow fraction	0,24	-
		HBIN2 temperature	400	°C
	6	HBIN3X flow fraction	0,394	-
		HBIN3 temperature	400	°C

In Table 10.22, the calculated volume of each reactor with the diameters fixed in 10.19 and the lengths obtained in 10.21 after step 4 is shown,

Table 10.22: Volume of each reactor of the final case

Reactor	Volume (m ³)
R-101	0,44
R-102	1,65
R-103	3,61

Following the same procedure as in 9.4.1, the length and diameter of each reactor are modified in order to fulfill (9.20). In Table 10.23, the final length, diameter and volume of each reactor are shown,

Table 10.23: Length, diameter and volume of each reactor after the optimization

Reactor	Length (m)	Diameter (m)	Volume (m ³)
R-101	1,3	0,65	0,44
R-102	2,04	1,02	1,65
R-103	2,64	1,32	3,61

In Table 10.24, the amounts of ammonia exiting each reactor and its conversion are shown:

Table 10.24: Conversion and amount of ammonia exiting each reactor in the configuration with recycle stream

Equipment	Parameter	Value	Unit
R-101	Ammonia at outlet	139,6041685	kmol/h
	Conversion	11,9	%
R-102	Ammonia at outlet	342,57	kmol/h
	Conversion	12,61	%
R-103	Ammonia at outlet	635,94	kmol/h
	Conversion	11,38	%

Finally, the amount of ammonia exiting the flash along with its recovery is reported in Table 10.25:

Table 10.25: Amount of ammonia exiting the liquid stream within the flash along with its recovery in the configuration with recycle stream

Equipment	Parameter	Value	Unit
F-101	Ammonia at exiting liquid stream	560,64	kmol/h
		229,154	t/d
	Ammonia recovery	88,2	%

11. Results and Discussion

In this chapter the main results obtained from the previous chapters will be illustrated. The energy requirements from the base case and the final case will be compared in order to determine the most optimum design. Furthermore, the analysis of each unit block will be done in order to compare and analyse the most compromising equipments of the green ammonia production process.

A comparison of the amount of ammonia produced, conversion of each reactor, and feasibility will also be carried out between both cases, among other factors.

At last, an economic analysis of the final case plant cost will be done, considering capital expenses (CapEx) and operational expenses (OpEx) with the possible revenue of the plant.

11.1. Feasibility of each case

Regarding the feasibility of each case, in Figures 11.1, 11.2, 11.3, 11.4 and 11.5 the temperatures of the outlet stream exiting each compressor, reactor and heat exchangers (when cooling water is used) are shown. The red line in each graph indicates the maximum temperature that should be obtained at each outlet stream for security/efficiency reasons.

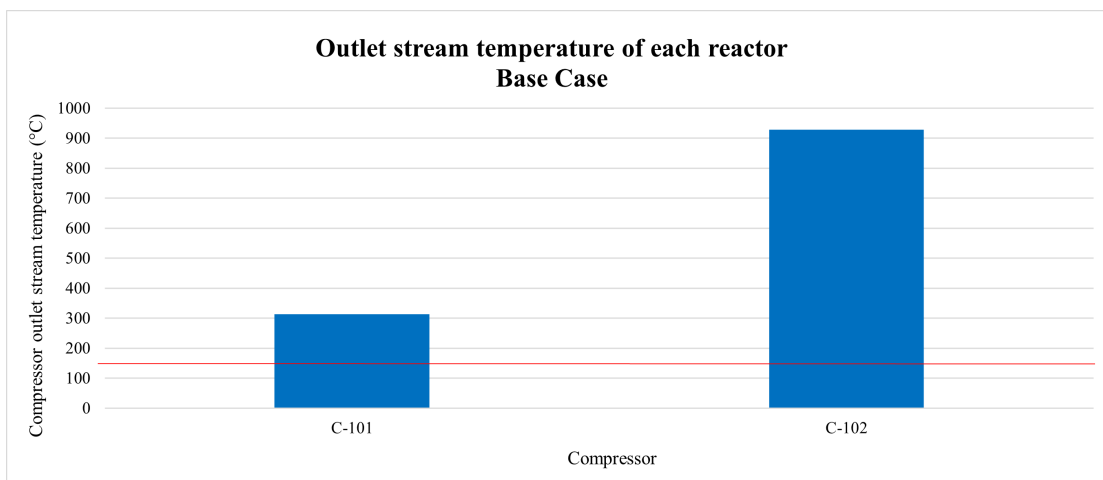


Figure 11.1: Outlet stream temperature of each compressor in the base case

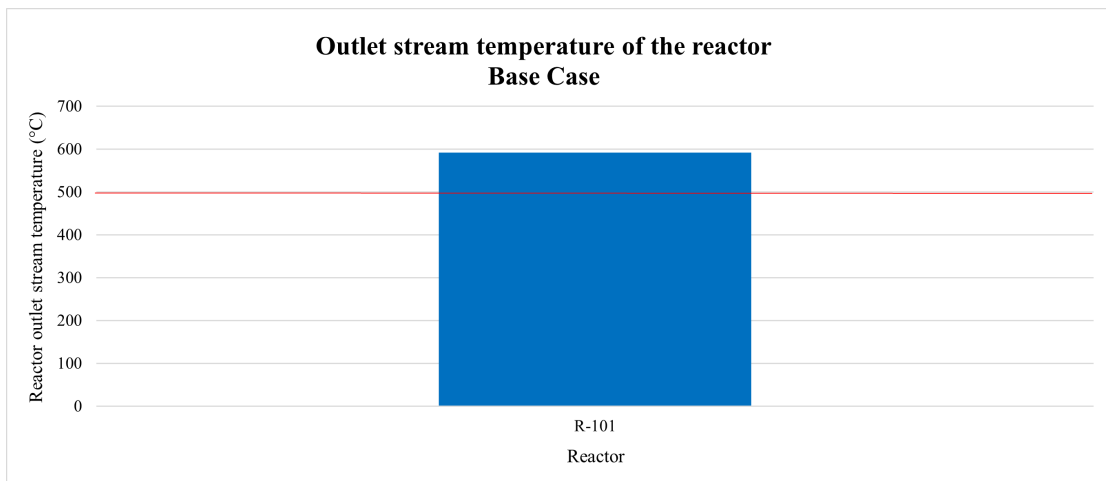


Figure 11.2: Outlet stream temperature of the reactor in the base case

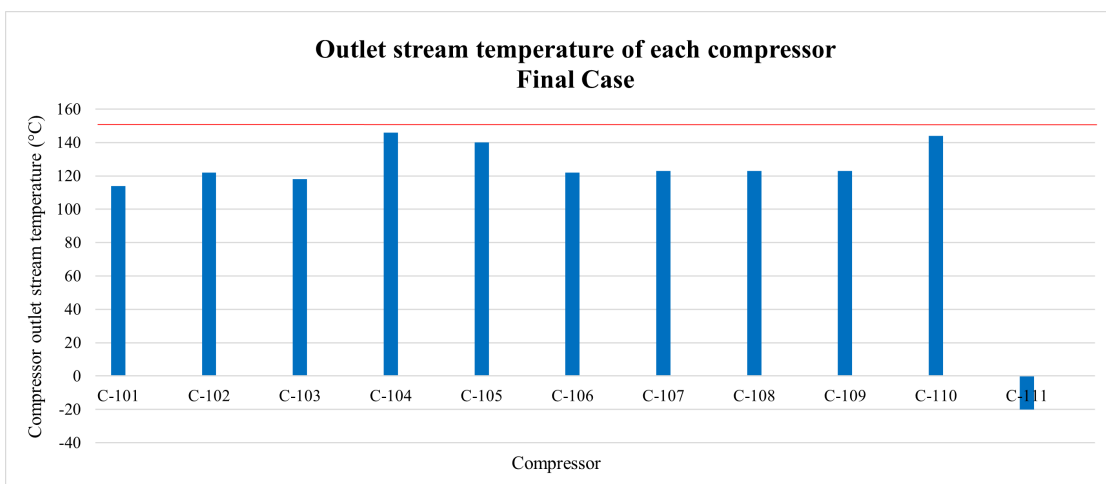


Figure 11.3: Outlet stream temperature of each compressor in the final case

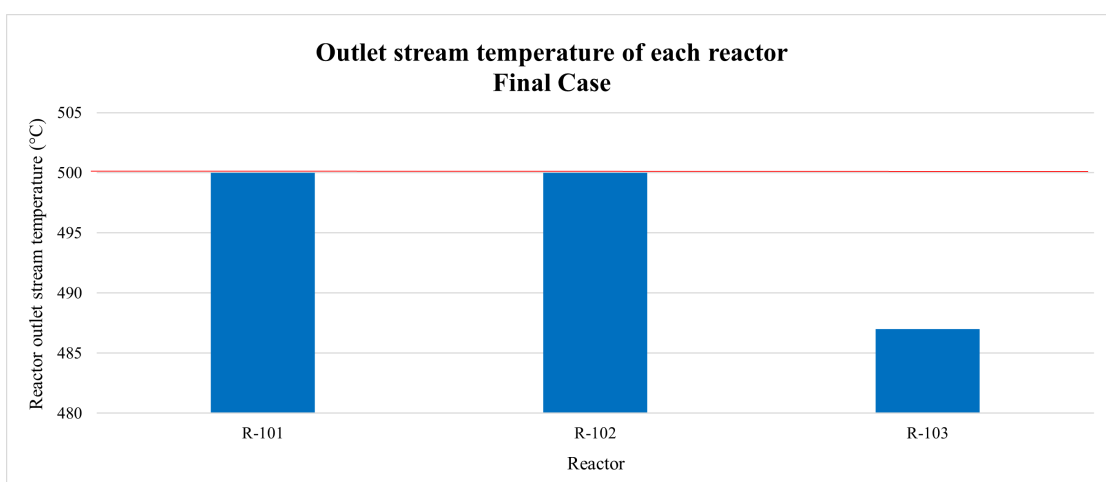


Figure 11.4: Outlet stream temperature of each reactor in the final case

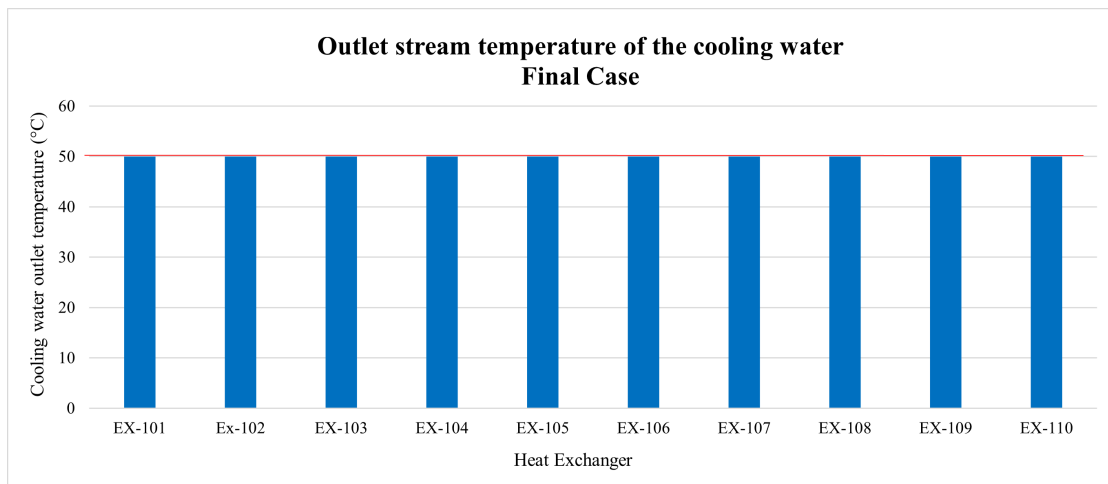


Figure 11.5: Outlet stream temperature of the cooling water exiting each heat exchanger in the final case

In Figures 11.1 and 11.2, it can be seen that both compressors and the reactor outlet streams temperature exceed the maximum imposed. Therefore, this case is not feasible.

However, regarding Figures 11.3, 11.4 and 11.5, it is observed that the temperature of every outlet stream from each equipment is less than the maximum imposed for security reasons. Consequently, this case is feasible in terms of security regarding temperature control in compressors, reactors and cooling utilities.

It is important to justify the use of cryogenic distillation instead of PSA for the final case. In Table 5.1, PSA is used for capacities between 5-5.000 Nm³/h of produced nitrogen, and cryogenic distillation for capacities between 200-400.000. In the final case, the amount of nitrogen that exits through the second column distillation, with a purity of 99,99 % is 6382,57 m³ at STP. Therefore, the use of PSA was not suitable for this simulation. Moreover, the purity needed of 99,99 % demands the use of cryogenic distillation, where purities with residual concentrations down to the ppb range can be obtained.

In addition, the amount of hydrogen that the electrolyser produces can also be justified in order to determine its feasibility. The reported electrolyser for the final case simulation has an electricity input requirement of 4,63 kWh/Nm³H₂ based on the values obtained in section 9.2 and calculating the amount of hydrogen at STP. In [53] the typical values obtained for AWE range from 4,3 to 5,5 kWh/Nm³H₂, indicating that our calculated value is feasible within the existing values. Moreover, in [81], the largest electrolysers have electricity input requirements around 4,5 kWh/NM³H₂, a value very near the one obtained in our simulation. Furthermore, developments of the order of MW and GW of electrolyser are being developed also in this company, which indicates that the use of a big electrolyser or electrolysers in series is feasible.

Regarding the PEM electrolyser, from the electricity input requirement obtained from subsection 10.1.5 and the hydrogen output necessary obtained from section 9.2 (bringing it to STP), the input requirement of the PEM electrolyser simulated is 4,32 kWh, which as seen before, is within the acceptable ranges.

It is also important to consider the amount of ammonia this plant produces regarding how much Chile needs. In section The green ammonia plant simulated in the final case produces 75915,6 t/day (assuming that the plant works 330 days a year, considering uncertainties in the renewable resources, maintenance, possible accidents, among other factors). Chile imports every year 347.184 tonnes of ammonia, which indicates that our plant could produce around the 21,87 % of the amount of ammonia Chile needs every year.

Finally, in section 6.2 it is described that the North of Chile has a potential of 1.260 GW for PV and 14,5 GW for wind power, achieving capacity factors higher than 40 %. Considering the AWE (which has the highest electricity input), the electricity input requirement for this electrolyser is around the 0,0092 % of the solar potential and 0,08 % of wind potential. Therefore, considering uncertainties and low capacity factors <30 %, this electrolyser (or electrolysers constructed in series) could be feasible. Furthermore, in section 7.2, a project to construct a 2.000 MW renewable energy plant and a 1.600 MW electrolyser for producing green hydrogen is being studied to produce almost all the ammonia Chile needs nowadays. This project electrolyser is almost 14 times bigger than the one simulated, which means that our electrolyser is feasible for constructing.

11.2. Amount of ammonia produced and conversion of each reactor comparison between both cases

In Table 11.1, the amount of ammonia that exits each reactor, the nitrogen conversion of each reactor, and the amount of ammonia that exits through the liquid flash are shown,

Table 11.1: Comparison of the amount of ammonia at each reactor outlet, amount of ammonia after the recovery and nitrogen conversion of each reactor between both cases

Base Case	Output	Value	Unit
R-101	Amount of ammonia at outlet stream	140,902	kmol/h
	Nitrogen conversion	0,21	-
F-101	Amount of ammonia at liquid outlet stream	122,538	kmol/h
Final Case	Output	Value	Unit
R-101	Amount of ammonia at outlet stream	139,6	kmol/h
	Nitrogen conversion	0,12	-
R-102	Amount of ammonia at outlet stream	342,57	kmol/h
	Nitrogen conversion	0,13	-
R-103	Amount of ammonia at outlet stream	635,94	kmol/h
	Nitrogen conversion	0,11	-
F-101	Amount of ammonia at liquid outlet stream	560,64	kmol/h

As it can be observed, the amount of ammonia that exits through the flash in the final case is 4,58 times the amount of ammonia produced at the base case, having the same feed concentrations, flow and purity entering the Haber-Bosch process. Furthermore, despite the less conversion of ammonia in each reactor (12% approx. in each one versus 21% in the base case), the amount of ammonia that exits from the first reactor is almost the same that exits the first reactor in the base.

11.3. Comparison of the Energy Requirements between Both Plants

In this section, the energy requirements from utilities and electricity between both plants will be compared. The analysis will be conducted regarding the total energy requirement for each process block (electrolyser, ASU, Haber-Bosch process and ammonia recovery) and for the equipments (electrolyser, compressors, heat exchangers or heaters/coolers and distillation columns).

In Tables 11.2, 11.3 and 11.4, the energy requirement for each equipment, for each process block unit and for the sum of the same equipments within the base case is shown,

Table 11.2: Energy requirements for every equipment in the base case simulated

Equipment	Energy requirement (kW)	Heat or Net duty
E-001	1416,12	Heat
P-001	10,33	Net
ELEC-001	115334,33	Net
SEP-001	-48,35	Heat
C-101	1001,87	Net
E-101	-2386,03	Heat
COL-101 condenser	-846,076	Heat
COL-101 reboiler	1364,7	Heat
E-102	699	Heat
MIX-101	0	-
MIX-102	0	-
C-102	9718,62	Net
E-103	-6036,68	Heat
R-101	0	-
E-104	-7274	Heat
F-101	0	-
Sum (of the absolute values)	146136,1	-

Table 11.3: Energy requirements for each block unit in the base case simulated

Process Block Unit	Energy Requirement (kW)
Electrolyser	116809,13
ASU	5598,68
Haber-Bosch	16454,30
Recovery	7274,00

Table 11.4: Energy requirements for the sum of all equal equipments in the base case simulated

Equipments	Energy Requirement (kW)
Electrolyser	115334,33
Compressors	10720,49
Heaters/Coolers	17811,826
Distillation columns	2210,776

In addition, in Tables 11.5, 11.6, 11.7 and 11.8 the energy requirements for every equipment, for every process block unit and for the sum of the same equipments within final case is illustrated,

Table 11.5: Energy requirements for every equipment in the final case simulated

Equipment	Energy requirement (kW)	Heat or Net duty
E-001	1416,12	Heat
P-001	10,33	Net
ELEC-001	115334,33	Net
SEP-001	-48,35	Heat
C-101	309,234	Net
EX-101	257,9	Heat
C-102	286,9	Net
EX-102	288,177	Heat
C-103	271,44	Net
EX-103	308,96	Heat
SPL-101	0	-
MHX1	-1742,94	Heat
V-101	0	-
V-102	0	-
COL-101 reboiler	171,51	Heat
COL-101 condenser	-643,37	Heat
MHX2	98,394	Heat
V-103	0	-
V-104	0	-
COL-102 reboiler	615,823	Heat
COL-102 condenser	-157,17	Heat
P-101	0,127	Net
C-104	328,97	Net
EX-104	-368,68	Heat
EX-105	-316,62	Heat
C-105	298,598	Net
EX-106	-301,16	Heat
MIX-101	0	-
MIX-102	0	-
C-106	1011,27	Net
EX-107	-1009,46	Heat
C-107	1016,52	Net
EX-108	-1017,84	Heat
C-108	1025,56	Net
EX-109	-1027,15	Heat
C-109	1044,17	Net
EX-110	-1043,57	Heat
C-110	1333,29	Net
EX-111	1196,83	Heat

Table 11.6: Energy requirements for every equipment in the final case simulated: part 2

Equipment	Energy requirement (kW)	Heat or Net duty
MIX-103	0	-
MIX-104	0	-
MIX-105	0	-
MIX-106	0	-
SPL-102	0	-
R-101	0	-
R-102	0	-
R-103	0	-
EX-112	2555,36	Heat
EX-113	9726,85	Heat
EX-114	-13653,82	Heat
F-101	0	-
SPL-103	0	-
C-111	1,54	Net
E-110	0	Heat
Sum (of the absolute values)	144883,143^a	-

^a Considering heat integration

Table 11.7: Energy requirements for each process unit for the final case

Process unit	Energy required (kW)	% of the total energy required
Electrolyser	116809,13	80,62
ASU	2078,965	1,43
Haber-Bosch	12341,228	8,52
Recovery	13653,82	9,42

Table 11.8: Energy requirements for the sum of all equal equipments in the final case simulated

Equipments	Energy Requirement (kW)
Electrolyser	115334,33
Compressors	6927,49
Heat Exchangers	21905,13
Distillation columns	356,23

From Tables 11.2 and 11.6, the difference in the total energy requirements between both

cases can be calculated through equation (11.1)

$$E_{req,base} - E_{req,full} = 1252,959 \text{ kW} \quad (11.1)$$

Value which shows that the energy requirements for the base case are higher than the requirements for the final case. Although the difference in energy requirements does not seem too much, if we take into account that the amount of ammonia produced in the final case is 4,58 times the amount of ammonia produced in the base case, as calculated in section 11.2, having less energy requirements producing the same amount of ammonia is considerably important.

The heat requirements of MHX1, MHX2, EX-112 and EX-113 must not be considered, since it only uses process streams to cold/heat other process streams and not external utilities. Furthermore, the heat requirements of the reactors are not considered, since they are adiabatic.

Figures 11.6, 11.7, 11.8 and 11.9 compares the energy requirements between both cases for two different categories and two different scenarios.

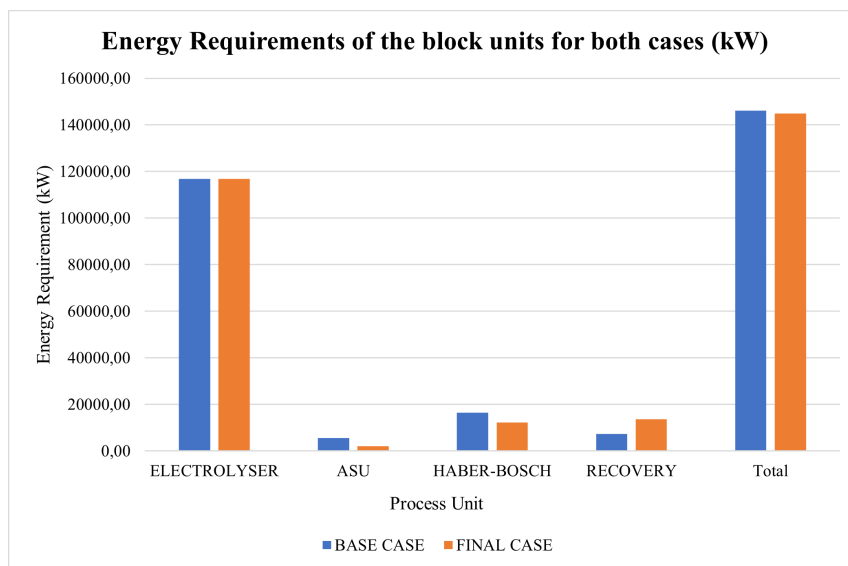


Figure 11.6: Comparison of the energy requirements of the block units between both cases

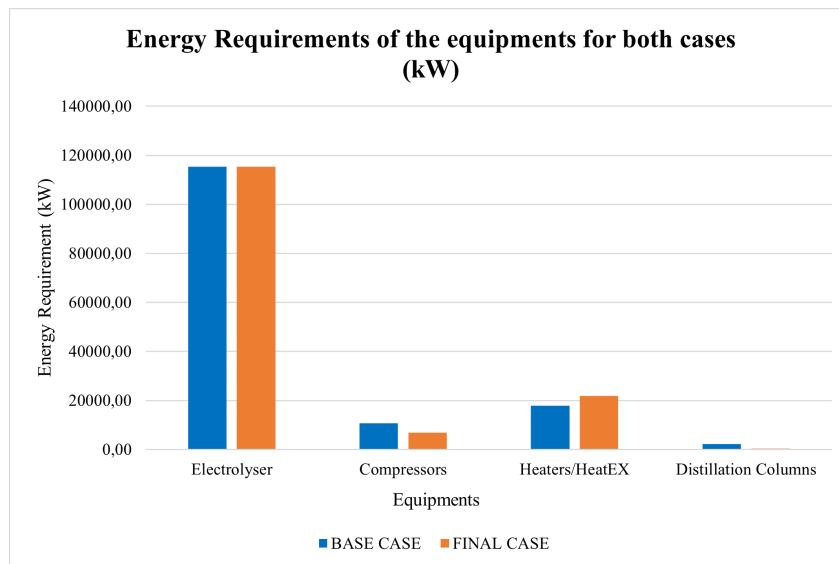


Figure 11.7: Comparison of the energy requirements of the equipment between both cases

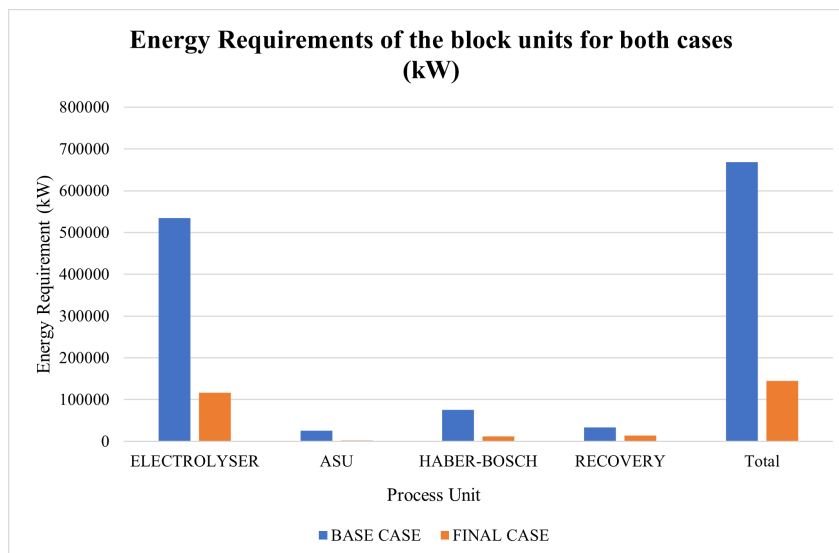


Figure 11.8: Comparison of the energy requirements of the block units between the final case and the modified case

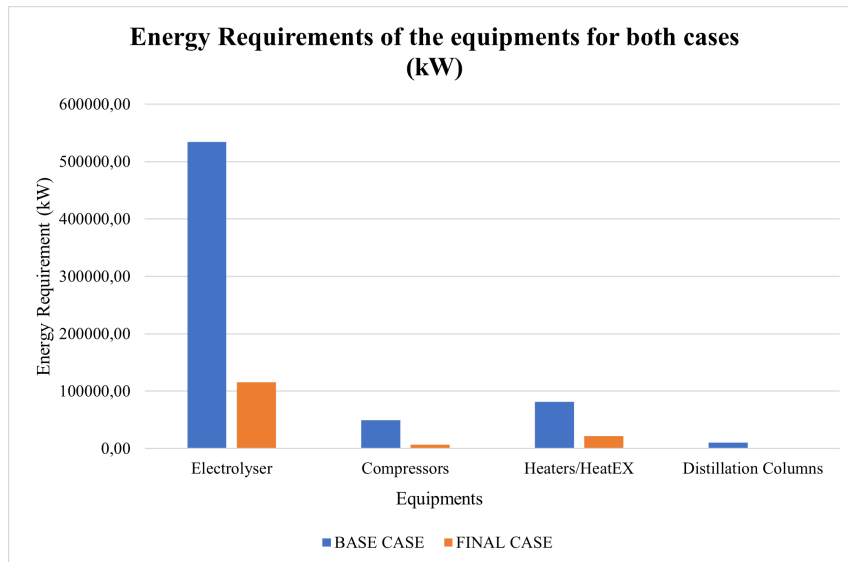


Figure 11.9: Comparison of the energy requirements of the equipment between the final case and the modified case

In Figure 11.6, a comparison between the energy requirements of both cases is shown. It can be observed that the amount of energy that the ASU and Haber-Bosch process need in the base case is higher compared to the amount of energy needed in the final case. This can be explained since the highest energy integrations were done in these units. Coupling both distillation columns, using two different heat exchangers in the Haber-Bosch process to reduce the energy requirements, using multi-compression with inter-cooling before the ASU and before the Haber-Bosch process, are all factors that reduce the energy requirements, making this possible. However, the heat requirements in the recovery unit are higher for the final case, which can be explained since by having a recycle loop the amount of ammonia that must be condensed is higher, which inquires in higher energy requirements.

From Figure 11.7 it can be seen that the amount of energy required from all the compressors in the base case is higher respect to the final case. This can be explained due to the multi-compression with inter-cooling system used, that instead of having one compressors it uses three compressors with intercooling between them, therefore needing less energy requirements. Regarding the distillation columns, the final case requires less energy since both columns are heat integrated. Furthermore, the multi heat exchangers also reduce the energy requirements in the distillation columns by bringing the streams at the desired temperatures before entering both distillation columns. However, the amount of utilities needed for the heat exchangers is higher in the final case, probably due to the fact that the streams have higher flows, which makes necessary the use of higher amounts of utilities.

In Figures 11.8 and 11.9, a comparison between the final case and a modified base is shown. The modified base case is identical to the base, except that electrolyser electricity input and the fresh feed amounts are modified in order to achieve the same amount of ammonia produced in the final case. It can be observed that the amount of energy required in every single block and in all the equipments is higher in the base case respect to the final case, which means that the improvements conducted accomplished their objective.

11.4. Economic Analysis of the Green Ammonia Plant

In this section, the economic analysis of the final case is described. An analysis regarding the capital and operational costs of the simulated plant will be done in order to determine which are the most significant costs nowadays for producing green ammonia. The plant is assumed to work 330 days a year, due to uncertainties in the renewable energy resources, maintenance, etc.

11.4.1. Capital Costs

In this subsection, the installations costs for every single equipment will be calculated. The pump P-101 cost will be neglected, as the amount of nitrogen and the energy input necessary to run it are very low respect to the other equipments. A location factor 2,25 from USA to Latin America [77] will be used as installation factor for each equipment, and a dollar to euro conversion of 0,84.

First, regarding the electrolyser, in [73], the costs for AWE and PEM electrolysers for years 2020 and 2030 are estimated. An analysis is conducted regarding the electrolyser costs if funding on R&D increases and higher scale-up is done.

The economic analysis will be conducted for the AWE and the PEM electrolyser, where the electricity requirement calculated in subsections 9.2.5 and 10.1.5 were of 115,33 and 107,52 MW respectively.

In Tables 11.9 and 11.10, the minimum and maximum value for an electrolyser unit at 2020 and a prediction (90 % of confidence) for years 2030 is done, considering or not scale-up.

Table 11.9: Electrolyser costs without scale-up, adapted from [73]

Type of electrolyser	Without Scale-up			
	Year reference 2020		Year reference 2030	
	Minimum Cost €/kW	Maximum Cost €/kW	Minimum Cost €/kW	Maximum Cost €/kW
AEW	700	1400	700	1000
PEM	800	2200	700	1980

Table 11.10: Electrolyser costs with scale-up, adapted from [73]

Type of electrolyser	With scale-up			
	Year reference 2020		Year reference 2030	
	Minimum Cost €/kW	Maximum Cost €/kW	Minimum Cost €/kW	Maximum Cost €/kW
AEW	574	1148	511	730
PEM	664	1826	539	1524,6

Consequently, by using the values in Tables 11.9 and 11.10 and the electricity requirements for each electrolyser, in Tables 11.11 and 11.12 the costs of the AWE and PEM are reported.

Table 11.11: Costs of the electrolyser simulated without scale-up for years 2020 and 2030

Type of electrolyser	Without scale-up			
	Year reference 2020		Year reference 2030	
	Cost (€)	Cost (€)	Cost (€)	Cost (€)
AEW	59.497.224	118.994.448	59.497.224	84.996.034
PEM	63.392.169	174.328.465	55.468.148	160.065.227

Table 11.12: Costs of the electrolyzers simulated with scale-up for years 2020 and 2030

Type of electrolyser	With scale-up			
	Year reference 2020		Year reference 2030	
	Cost (€)	Cost (€)	Cost (€)	Cost (€)
AEW	48.787.723	97.575.447	43.432.973	62.047.105
PEM	52.615.500	144.692.626	42.710.474	120.809.626

Second, regarding the installation costs of the compressors, heat exchangers, distillation columns, reactors and flash unit, they were calculated using the Guthrie method [74] [75]. In this subsection, the cost of all the equipments previously mentioned simulated in the final case will be calculated. All the equations used for the calculation of the costs are reported in annexes 15 for each equipment. In Tables 11.13, 11.14, 11.15, 11.16, 11.17 and 11.18 the characteristics for each equipment are reported. The use of stainless steel as material was based in [82], since the compatibility of ammonia production with carbon steel and the other materials was not reported as good in comparison with stainless steel.

Table 11.13: Type of compressor used in the final case simulated in Aspen Plus

Compressor	Type
C-101	Reciprocating (volumetric)
C-102	Reciprocating (volumetric)
C-103	Reciprocating (volumetric)
C-104	Reciprocating (volumetric)
C-105	Reciprocating (volumetric)
C-106	Reciprocating (volumetric)
C-107	Reciprocating (volumetric)
C-108	Reciprocating (volumetric)
C-109	Reciprocating (volumetric)
C-110	Reciprocating (volumetric)
C-111	Reciprocating (volumetric)

Table 11.14: Type of heat exchanger used in the final case simulated in Aspen Plus

Heat Exchanger	Type	Design type	Pressure (bar)	Material
EX-101	Shell-and-tube	Floating head	<10,34	SS/SS
EX-102	Shell-and-tube	Floating head	<10,34	SS/SS
EX-103	Shell-and-tube	Floating head	<10,34	SS/SS
EX-104	Shell-and-tube	Floating head	>70	SS/SS
EX-105	Shell-and-tube	Floating head	>70	SS/SS
EX-106	Shell-and-tube	Floating head	>70	SS/SS
EX-107	Shell-and-tube	Floating head	>70	SS/SS
EX-108	Shell-and-tube	Floating head	>70	SS/SS
EX-109	Shell-and-tube	Floating head	>70	SS/SS
EX-110	Shell-and-tube	Floating head	>70	SS/SS
EX-111	Shell-and-tube	Floating head	>70	SS/SS
EX-112	Shell-and-tube	Floating head	>70	SS/SS
EX-113	Shell-and-tube	Floating head	>70	SS/SS
EX-114	Shell-and-tube	Floating head	>70	SS/SS
MULTI1-1	Shell-and-tube	Floating head	>70	SS/SS
MULTI1-2	Shell-and-tube	Floating head	>70	SS/SS
MULTI2	Shell-and-tube	Floating head	>70	SS/SS

Table 11.15: Type of distillation column used in the final case simulated in Aspen Plus

Distillation Column	Material	Pressure (bar)
C-101	SS	<3,45
C-102	SS	<3,45

Table 11.16: Type of distillation column tray used in the final case simulated in Aspen Plus

Distillation Column	Tray spacing (in)	Tray type	Tray material
C-101	24	Sieve	SS
C-102	24	Sieve	SS

Table 11.17: Type of reactor used in the final case simulated in Aspen Plus

Reactors	Material	Pressure (bar)
R-101	SS	>70
R-102	SS	>70
R-103	SS	>70

Table 11.18: Type of flash used in the final case simulated in Aspen Plus

Flash	Material	Pressure (bar)
F-101	SS	>70

The selection of shell and tube as heat exchanger was based in the large flows that must be cooled/heated entering each heat exchanger. For both multi-stream heat exchangers, the first one was divided in two heat exchangers as there were 4 different streams, while the second one was treated as one shell-and-tube heat exchanger.

The flash unit was sized designing an L/D ratio of 5 for economical design and a residence time of 30 seconds to ensure that there is a 99 % of probability that the operator can determine the cause of failure [83]. In Table 11.19 the heat transfer coefficients for the shell-and-tube heat exchangers are reported in function of the cold and hot fluid used. This value was calculated based in the use of Aspen plus with the calculation of Shell-and-Tube heat exchanger, and [76], which details the typical heat transfer coefficients in function of the hot and cold fluid used.

Table 11.19: Heat coefficients of the heat exchangers simulated in the final case

Hot fluid	Cold fluid	U (W/(m ² K))
Gas	Cooling water	135
Steam	Gas	110
Gas	Gas	70
Gas	Refrigerant R-404A	1200

The required parameters for estimating each equipment cost and the installation cost of each one are reported in Tables 11.20, 11.21, 11.22, 11.23, 11.24 and 11.25 based on the materials, design and pressure conditions of each equipment using the Guthire method.

Table 11.20: Installation costs of each heat exchanger in the final simulation

Heat Exchanger	Area (ft ²)	F _d	F _p	F _m	F _c	Installation Costs (€)
EX-101	608,89	1	0	3,75	3,75	439.301
EX-102	629,67	1	0	3,75	3,75	448.993
EX-103	1.019,80	1	0	3,75	3,75	614.257
EX-104	130,27	1	0,55	3,75	5,8125	216.291
EX-105	126,82	1	0,55	3,75	5,8125	212.558
EX-106	421,89	1	0,55	3,75	5,8125	464.276
EX-107	1.291,78	1	0,55	3,75	5,8125	960.878
EX-108	1315,16	1	0,55	3,75	5,8125	972.146
EX-109	1.356,20	1	0,55	3,75	5,8125	991.761
EX-110	1.432,50	1	0,55	3,75	5,8125	1.027.678
EX-111	3.129,02	1	0,55	3,75	5,8125	1.707.701
EX-112	4.535,73	1	0,55	3,75	5,8125	2.173.784
EX-113	7.230,49	1	0,55	3,75	5,8125	2.943.439
EX-114	1.198,02	1	0,55	3,75	5,8125	914.951
MEX1-1	14.950,2	1	0,55	3,75	5,8125	4.719.724
MEX1-2	14.950,2	1	0,55	3,75	5,8125	4.719.724
MEX2	1.521,94	1	0,55	3,75	5,8125	1.068.944
					Total	24.596.404

Table 11.21: Installation costs of each compressor in the final simulation

Compressor	Net duty (bhp)	F_c	Installation Costs (€)
C-101	414,69	1,29	1.567.887
C-102	384,74	1,29	1.474.410
C-103	364,01	1,29	1.408.938
C-104	441,16	1,29	1.649.481
C-105	400,43	1,29	1.523.528
C-106	1.356,13	1,29	4.142.574
C-107	1.363,17	1,29	4.160.201
C-108	1.375,30	1,29	4.190.514
C-109	1.400,25	1,29	4.252.767
C-110	1.787,97	1,29	5.196.578
C-111	2,07	1,29	20.279
TOTAL			29.587.156

Table 11.22: Installation costs of each distillation column in the final simulation

Distillation column	COL-101	COL-102	
Diameter (ft)	1,74	2,4	
Column height (ft)	116	86	
Tray Height (ft)	2	2	
Column F_m	3,75	3,75	
Column F_p	1	1	
Column F_c	3,75	3,75	
Tray F_s	1	1	
Tray F_t	0	0	
Tray F_m	2,25	2,25	
F_c	3,25	3,25	TOTAL
Installation Costs (€)	598.143	661.667	1.259.810

Table 11.23: Installation costs of each reactor in the final simulation

Reactor	Diameter (ft)	Height (ft)	F_m	F_p	F_c	Installation Costs (€)
R-101	2,15	4,29	3,75	2,5	9,375	97.647
R-102	3,34	6,67	3,75	2,5	9,375	224.148
R-103	4,33	8,66	3,75	2,5	9,375	366.688
TOTAL						688.483

Table 11.24: Installation cost of the flash unit in the final simulation

Flash	F-101
Vapor Stream feed (m^2/s)	0,24
Residence time (s)	1.800
Volume (ft^3)	15.549,55
L/D Ratio	5
Diameter (ft)	9,38
Height (ft)	63,28
F_m	3,75
F_p	2,5
F_c	9,375
Installation Costs (€)	7.456.388

Table 11.25: Installation costs of the sum of all equipment units in the final simulation

Equipments	Total Installation Costs (€)	% of the total costs
AWE Electrolyser (maximum cost, 2020, no scale-up, considering location factor)	305.163.180	83,141
Compressors	29.587.156	8,06
Heat Exchangers	22.888.704	6,24
Distillation Columns	1.259.810	0,34
Reactors	688.483	0,19
Flash	7.456.388	2,03
TOTAL	367043721,8	

The operating costs are the ongoing costs necessary to run a business, system, plant, etc. For this case, the main operating costs are:

1. Electricity necessary to run the equipments
2. Utilities costs
3. Amount of catalyst for the Haber-Bosch reactors
4. Labour costs (operators salary)
5. Fresh water feed

The costs related to the amount of KOH necessary for the electrolyser will be neglected.

In the case of the utilities, the refrigerant used for cooling the inlet stream that enters the heat exchanger EX-114 is R-404A [58]. The utility used for cooling the outlet streams of the compressors is cooling water, which enters at 25 °C in each case. For heating the

stream entering the Haber-Bosch process, steam vapor at 45 bar was used.

In order to determine the amount of refrigerant and water vapor necessary formula (11.2) will be used,

$$Q = m\lambda_v \quad (11.2)$$

Where Q is the heat exchanged, m is the mass flow of the stream and λ_v corresponds to the latent heat of vaporization.

The latent heat of vaporization for the steam vapor at 45 bar is $\lambda_{v,vapor} = 1668,42$ kJ/kg [80] and the latent heat of vaporization for the refrigerant R-404A is $\lambda_{v,R404A} = 200$ kJ/kg [85].

In order to determine the amount of cooling water, using Aspen Plus, the amount of heat one must supply to increase the temperature of a flow of 1kg/h of water from 25 °C to 50 °C is 0,0314 kWh/kg. The amount of heat exchanged will be obtained from Tables 11.5 and 11.6. Therefore, by knowing the heat exchanged and the necessary amount of heat that one must supply per kg, one can calculate the amount of utilities needed.

In Table 11.26 the amount of utilities needed in each heat exchanger is shown with the total price that one must spend each year for them. The price was determined by an estimation of how much one spend in order to maintain the required utilities at the desired T and P.

Table 11.26: Price for the utilities required in the green ammonia plant

Heat Exchanger	Utility	Amount needed (t/year)	Price (€/t)	Total Price (€/year)
Feed process water to eletrolyser	Cooling water	764710,47	0,40 [7]	305504,89
EX-101	Cooling water	71913,83	0,40	28729,86
Ex-102	Cooling water	80357,22	0,40	32103,03
Ex-103	Cooling water	86151,59	0,40	34417,91
EX-104	Cooling water	102804,15	0,40	41070,67
EX-105	Cooling water	88287,54	0,40	35271,22
EX-106	Cooling water	83976,61	0,40	33548,99
EX-107	Cooling water	281481,70	0,40	112453,07
EX-108	Cooling water	283818,41	0,40	113386,59
EX-109	Cooling water	286414,45	0,40	114423,72
EX-110	Cooling water	290993,07	0,40	116252,89
EX-111	Vapor Steam	22622,14	0,77 [78]	17458,83
EX-114	R-404A	2152934,34	0,64 [78]	1376169,41

Afterwards, the amount of people that work in the plant must be calculated in order to determine the labour costs. Reference [7] was mainly used to determine the number of operators.

The amount of people working at the plant can be determined by using equation (11.3),

$$N_{OL} = (6,29 + 0,23N_{np})^{0,5} \quad (11.3)$$

Where N_{OL} is the minimum number of operators per shift and N_{np} is the total number of equipments. Subsequently, through equation (11.4) one can determine the total number of operators working in the plant,

$$N_{OP} = 4,5 \cdot N_{OL} \quad (11.4)$$

Where N_{OP} is the total number of operators per shift. Considering three different shifts, in Table 11.27 the labour costs (salaries) for each year is determined.

Table 11.27: Total salaries paid each year

Number of equipment	Number of operators	Number of shifts	Salary (eur/operator/year)	Total salary paid/year
35	18	3	44.436 [7]	2.399.544

Regarding the catalyst required for the Haber-Bosch reactor, the amount needed must also be calculated. For a lifetime of 14 years [7], it will be assumed that for the first year it will be bought a certain amount just once.

In [2] the amount of iron catalyst needed can be obtained using equation (11.5),

$$m_{cat} = 0,334 \frac{g}{cm^3/s} H_2 \quad (11.5)$$

Based on the amount of hydrogen needed calculated in section 9.2, the amount of catalyst needed is 9,611 kg. Considering the cost of the catalyst as 19,32 €/kg [7], the amount one must spend in the catalyst the first year is 185,48 €.

Afterwards, the electricity requirement to run the plant must be calculated. Three cases will be compared: electricity produced from a solar plant, minimum cost of electricity produced from a solar plant and electricity produced from a wind plant.

The main equipments that require electricity are the electrolyser and the compressors, therefore, their net duty will be used for the calculation of the total electricity requirement. In Table 11.28 the cost that one must run each year to run the plant is shown.

Table 11.28: Electricity paid each year to run out the plant

Electricity requirement (MWh)	Solar electricity price (€/MWh)	Minimum solar electricity price (€/MWh)	Wind electricity price (€/MWh)	Total paid (€/year) (solar)	Total paid (€/year) (minimum solar)	Total paid (€/year) (wind)
122,27	27,3	18,04	35,87	26.437.223	34.734.444	17.472.971

Finally, some extra operational costs must be considered. The maintenance, operating supplies, waste treatment, etc are taken as operational costs related to the capital investment. Generally, these costs account for 15% of the plant's installation cost [78]. Labour related costs account for health insurance, retirement, vacations, etc. They are generally considered as 60% of the operating labour costs (salaries paid). Finally, a 20% of the income of the sales is taken as operational cost, regarding patents, packaging, distribution, administrative costs, etc [7]. In Table 11.29, the amount of operational costs regarding these three factors is accounted. For first instance, the ammonia sales price will be calculated as 1295,6 €/t.

Table 11.29: Sales Revenue and additional operational costs to conduct the plant

Sales (€/year)	OPEX for capital investment	Opex for labour costs	OPEX for sales related
97.950.135	55.056.558	1.439.726	19.590.027

Finally, the following four cases will be considered:

1. Maximum cost electrolyser at year 2020 (case just considered).
2. Minimum cost electrolyser at year 2020.
3. Minimum cost electrolyser at year 2030 with scale-up.
4. Minimum cost electrolyser at year 2030 with scale-up with minimum solar electricity price.

Using the Add-in solver from Excel, the ammonia price at which the operational expenditures are equal to the sales revenue for each case is calculated and shown in Figure 11.10.

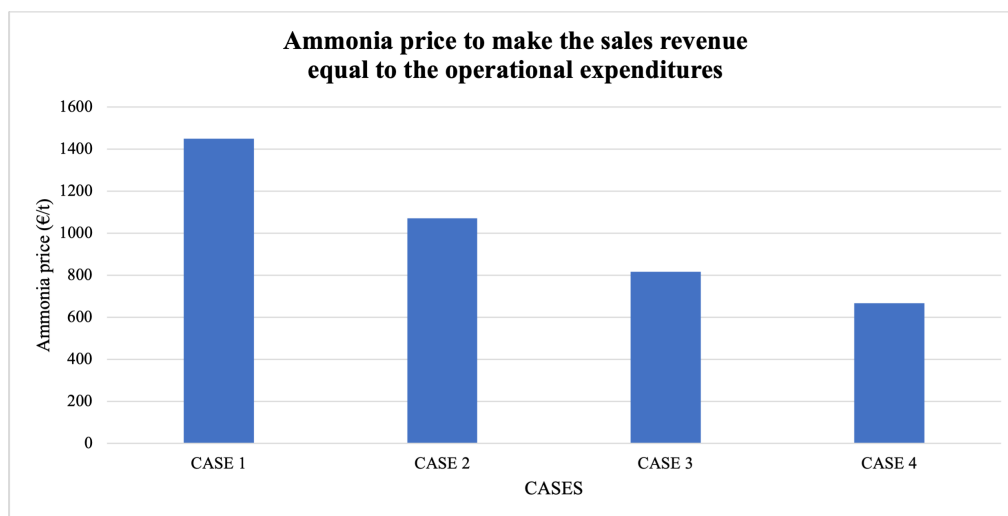


Figure 11.10: Price of ammonia where the operational expenditures are equal to the sales revenue: Cases comparison

As it can be seen, the price of ammonia greatly decreases when the electrolyser and the electricity prices get lower. These can be further explained by Figures 11.11 and 11.12.

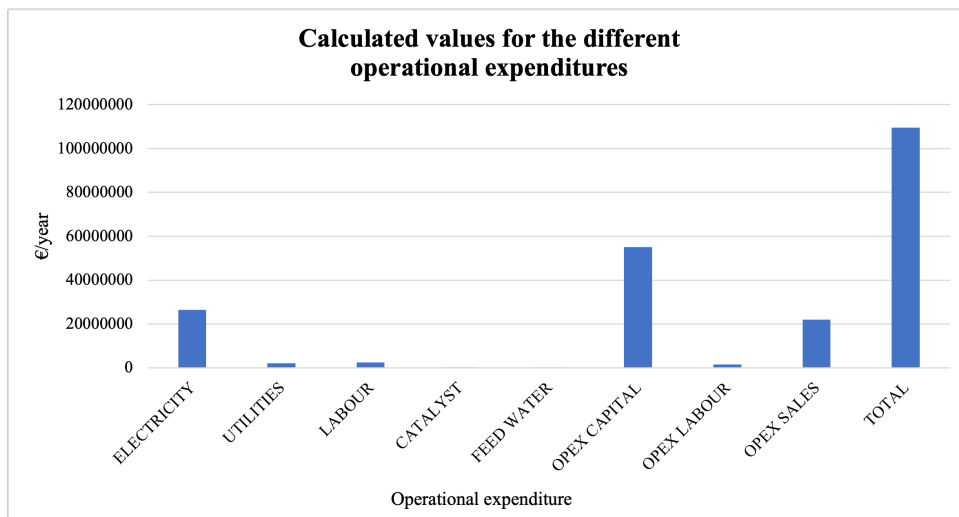


Figure 11.11: Calculated values for the different operational expenditures

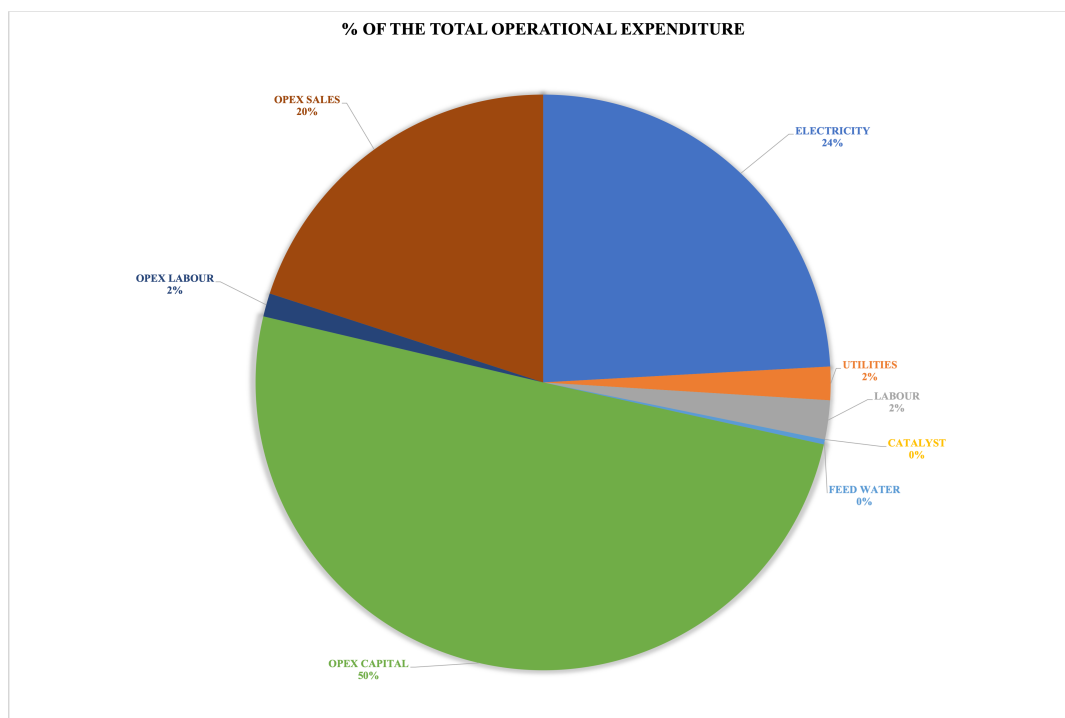


Figure 11.12: Calculated values for the different operational expenditures, % of the total

In Figures 11.11 and 11.12, it can be seen that the main costs regarding the operational expenditures are the electricity and the operational expenditures considering the installation costs (the sales revenue will not be considered, as it increases when the revenue increases). Furthermore in Figure 11.13, it can be seen that the most relevant and incident cost is the electrolyser, which has a very high cost, which explains why the operational expenditures regarding the installation costs are so high.

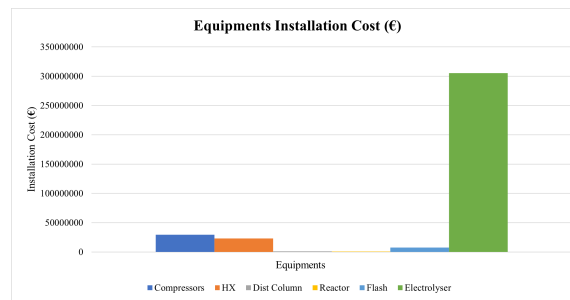


Figure 11.13: CAPEX values for each equipment in the final case

Consequently, the most deterministic and relevant costs regarding the green ammonia plant are the electrolyser installation cost and the cost of electricity. For case 4, the most optimistic, the ammonia price is 667,49 €/t, which is far from the regular ammonia price ~ 440 €/t [7]. Therefore, it is important that the electricity prices get lower and to develop scale-up of electrolyser of more funding on R&D.

12. Conclusions and Recommendations

A green ammonia plant simulation in Aspen Plus was done comparing two cases. A very simple case without heat integration, with only one distillation column and reactor, and a final case with heat integration, two distillation columns, multi-compression with inter-cooling and multi-reactor in series with inter-cooling by quenching and a heat exchanger. All the constraints, typical values and decision making were fulfilled regarding the literature.

From the energy analysis, the final case required less energy requirement from utilities compared to the base case, despite it produced 4,58 times more ammonia respect to the base case. Apart, a better control of the outlet temperature of each compressor and reactor was achieved, which is crucial for not damaging the equipment parts, in addition to the safety of the personal. It is always important to conduct an energy integration in order to decrease the amount of utilities necessary, although it should always be done regarding the control system, not making it too complicated.

Regarding the economic analysis, the most decisive and important costs were the installation of the electrolyser and the electricity price. By switching to an optimistic case with a lower electrolyser price and a lower electricity price from solar energy, the ammonia price did not reach the regular price in the market. Therefore, it is mandatory to start raising the fundings in R&D and scale-up of electrolysers, in addition to lowering the electricity prices. A better study case could be done by running the system when the electricity prices are lower or near 0, and when the electricity prices are high use the hydrogen in storage to produce ammonia. Another important factor is the CO₂ taxes that could be applied. By applying these, the green ammonia production could become more attractive for R&D compared to conventional production using SMR, which is potentially cheaper. It is important to consider that always the first estimation costs have a high percentage of error, as they are generally used to know wheter to construct or not the plant.

A further study case could be implemented by evaluating the PEM electrolyser, adding a storage of hydrogen and nitrogen, adding a distillation column to separate oxygen and argon to make profit by selling them, cooling the outlet of the Haber-Bosch reactor with cooling water and later with refrigerant R-404A to lower the costs, among others. More optimizations and improvements for a green ammonia plant can always be carried out. PEM consider, storage of hydrogen and ammonia and prices.

13. Nomenclature

13.1. Abbreviations

EU: European Union

GHG: Greenhouse gases

GHS: Globally Harmonized System of Classification and Labelling of Chemicals

SMR: Steam Methane Reforming

LFL: Lower Flammability Limit

UFL: Upper Flammability Limit

NFPA: National Fire Protection Association

TNT: Trinitrotoluene

ICE: Internal Combustion Engines

LHV: Lower Heating Value

HHV: Higher heating Value

STP: Standard Temperature and Pressure

CNG: Compressed Natural Gas

CMS: Carbon Molecular Sieves

ASU: Air Separation Unit

PSA: Pressure Swing Adsorption

TSA: Thermal Swing Adsorption

CR: Conventional Reformer

WGSR: Water Gas Shift Reactor

P2G: Power to Gas

P2A: Power to Ammonia

SPE: Solid Polymer Electrolyte

PEM: Proton Electron Membrane

DC: Direct Current

AC: Alternating Current

AWE: Alkaline Water Electrolysis

H-B: Haber Bosch

CSP: Concentrated Solar Power

PV: Photovoltaics

CCS: Carbon Capture and Storage

VPSA: Vacuum Pressure Swing Adsorption

mtpd: metric tons per day

P2A: Power-to-ammonia

HPC: High pressure column

LPC: Low pressure column

R&D: Research and development

13.2. List of main Symbols

T = Temperature

P = Pressure

R = Universal gas constant

G = Gibbs free energy

z = number of electrons transferred

F = Faraday's constant

V = Voltage

i = current density

$I = J$ = current

n_{H_2} = mass/molar flow of hydrogen

n_{N_2} = mass/molar flow of nitrogen

n_{H_2O} = mass/molar flow of water

n_{NH_3} = mass/molar flow of ammonia

W = Electricity requirement

N = Number of cells

A = Area

E = Activation energy

tonnes = t = metric tons (1000 kg)

13.3. Greek Symbols

λ = water content in the membrane

σ = ionic conductivity of the membrane

ρ = density

μ = viscosity

14. Bibliography

References

- [1] Ikäheimo, Jussi & Kiviluoma, Juha & Weiss, Robert & Holttinen, Hannele. (2018). Power-to-ammonia in future North European 100 % renewable power and heat system. *International Journal of Hydrogen Energy*. **43**. [DOI: [10.1016/j.ijhydene.2018.06.121](https://doi.org/10.1016/j.ijhydene.2018.06.121)]
 - [2] Siddiqui, Osamah & Ishaq, Haris & Chehade, G. & Dincer, Ibrahim. (2020). Experimental investigation of an integrated solar powered clean hydrogen to ammonia synthesis system. *Applied Thermal Engineering*. **176**, 115443. [DOI: [10.1016/j.applthermaleng.2020.115443](https://doi.org/10.1016/j.applthermaleng.2020.115443)]
 - [3] Alhassan Salami Tijani, Nur Afiqah Binti Yusup, A.H. Abdol Rahim. (2014). Mathematical Modelling and Simulation Analysis of Advanced Alkaline Electrolyzer System for Hydrogen Production. *Procedia Technology*. **15**, 2014, Pages 798-806, ISSN 2212-0173. [DOI: [10.1016/j.protcy.2014.09.053](https://doi.org/10.1016/j.protcy.2014.09.053)]
 - [4] Rivera-Tinoco R, et al. (2016). Investigation of power-to-methanol processes coupling of electrolytic hydrogen production and catalytic CO₂ reduction. *International Journal of Hydrogen Energy*. Retrieved from <http://dx.doi.org/10.1016/j.ijhydene.2016.01.059>
 - [5] Matzen M, Alhaji M, Demirel Y. (2015). Technoeconomics and Sustainability of Renewable Methanol and Ammonia Productions Using Wind Power-based Hydrogen. *Journal of Advanced Chemical Engineering*. **5**. [DOI: [10.4172/2090-4568.1000182](https://doi.org/10.4172/2090-4568.1000182)]
 - [6] Baltrusaitis J. (2017). Sustainable Ammonia Production. *ACS Sustainable Chemistry & Engineering* **2017** **5**, (11), 9527-9527. [DOI: [10.1021/acssuschemeng.7b03719](https://doi.org/10.1021/acssuschemeng.7b03719)]
 - [7] Zhang, Hanfei & Wang, Ligang & Van Herle, Jan & Maréchal, François & Desideri, Umberto. (2019). Techno-economic comparison of green ammonia production processes. *Applied Energy*. **259**. [DOI: [10.1016/j.apenergy.2019.114135](https://doi.org/10.1016/j.apenergy.2019.114135)]
 - [8] Rebolledo, M. (2008). Estudio De Prefactibilidad Tecnico Y Economica De Una Planta De Amoniaco. Ingeniero Civil Químico. Pontificia Universidad Católica de Valparaíso.
 - [9] U.S. Geological Survey. (2020). Mineral commodity summaries 2020. *U.S. Geological Survey*, **200**, 116-117. Retrieved from <https://doi.org/10.3133/mcs2020>.
 - [10] Kim, S., Chen, J., Cheng, T., Gindulyte, A., He, J., He, S., Li, Q., Shoemaker, B. A., Thiessen, P. A., Yu, B., Zaslavsky, L., Zhang, J., & Bolton, E. E. (2019). PubChem 2019 update: improved access to chemical data. *Nucleic acids research*. **47**. Retrieved from <https://doi.org/10.1093/nar/gky1033>
 - [11] Ghaly AE, Ramakrishnan VV. (2015). Nitrogen Sources and Cycling in the Ecosystem and its Role in the Air, Water and Soil Pollution: A Critical Review. *Journal of Pollution Effects & Control*, **3**, 136. [DOI: [10.4172/2375-4397.1000136](https://doi.org/10.4172/2375-4397.1000136)]
 - [12] Rosen, Marc & Koohi-Fayegh, Seama. (2016). The prospects for hydrogen as an energy carrier: an overview of hydrogen energy and hydrogen energy systems. *Energy, Ecology and Environment*, **1**. [DOI: [10.1007/s40974-016-0005-z](https://doi.org/10.1007/s40974-016-0005-z)]
 - [13] Ram Ramachandran, Raghu K. Menon. (1998). An overview of industrial uses of hydrogen, *International Journal of Hydrogen Energy* **23**, 7, 593-598, ISSN 0360-3199. Retrieved from <http://www.sciencedirect.com/science/article/pii/S0360319997001122>
 - [14] Zamfirescu, C. & Dincer, Ibrahim. (2009). Ammonia as a green fuel and hydrogen source for vehicular applications. *Fuel Processing Technology*, **90**, 729-737. [DOI: [10.1016/j.fuproc.2009.02.004](https://doi.org/10.1016/j.fuproc.2009.02.004)]
 - [15] A. K. Hill, C. Smith & L. Torrente-Murciano. (2020). Current and future role of Haber-Bosch ammonia in a carbon-free energy landscape. *Energy & Environmental Science*. [DOI: [10.1039/C9EE02873K](https://doi.org/10.1039/C9EE02873K)]
 - [16] Basile, A. & Liguori, Simona & Iulianelli, A.. (2015). Membrane reactors for methane steam reforming (MSR). *Membrane Reactors for Energy Applications and Basic Chemical Production*. 31-59. [DOI: [10.1016/B978-1-78242-223-5.00002-9](https://doi.org/10.1016/B978-1-78242-223-5.00002-9)]
-

- [17] P. Millet. Editor(s): Angelo Basile, Suzana Pereira Nunes. 18 - Membrane electrolyzers for hydrogen (H₂) production. *Woodhead Publishing Series in Energy, Advanced Membrane Science and Technology for Sustainable Energy and Environmental Applications*, Woodhead Publishing, 568-609, ISBN 9781845699697. Retrieved from <http://www.sciencedirect.com/science/article/pii/B9781845699697500187>
- [18] Grigoriev SA et al. (2020). Current status, research trends, and challenges in water electrolysis science and technology. *International Journal of Hydrogen Energy*. Retrieved from <https://doi.org/10.1016/j.ijhydene.2020.03.109>
- [19] Sánchez M et al. (2019). Aspen plus model of an alkaline electrolysis system for hydrogen production. *International Journal of Hydrogen Energy*. Retrieved from <https://doi.org/10.1016/j.ijhydene.2019.12.027>
- [20] García-Valverde, Rafael & Espinosa, Nieves & Urbina, Antonio. (2012). Simple PEM water electrolyser model and experimental validation. *International Journal of Hydrogen Energy*, **37**, 1927-1938. [DOI: 10.1016/j.ijhydene.2011.09.027]
- [21] Bartels, Jeffrey Ralph. (2008). A feasibility study of implementing an Ammonia Economy. *Graduate theses and dissertations*, 11132. Retrieved from <https://lib.dr.iastate.edu/etd/11132>
- [22] Dong Xiang, Yunpeng Zhou. (2018). Concept design and techno-economic performance of hydrogen and ammonia co-generation by coke-oven gas-pressure swing adsorption integrated with chemical looping hydrogen process. *Applied Energy*, **229**, 1024-1034, ISSN 0306-2619. Retrieved from <http://www.sciencedirect.com/science/article/pii/S0306261918312200>
- [23] Fernández, B., & Gironás, J. (2021). Water Resources of Chile. *Springer* **8** Retrieved from <https://doi.org/10.1007/978-3-030-56901-3>
- [24] Rossi, G., & Benedini, M. (2020). Water Resources of Italy: Protection, Use and Control. *Springer*, **5**. Retrieved from <https://doi.org/10.1007/978-3-030-36460-1>
- [25] Tesch, Stefanie & Morozjuk, Tatiana. (2019). Comparative Evaluation of Cryogenic Air Separation Units from the Exergetic and Economic Points of View. [DOI: 10.5772/intechopen.85765]
- [26] Colbertaldo, Paolo & Gómez Aláez, Sonia & Campanari, Stefano. (2017). Zero-dimensional dynamic modeling of PEM electrolyzers. *Energy Procedia*, **142**, [DOI: 10.1016/j.egypro.2017.12.594]
- [27] Wilcox J. (2012). Cryogenic Distillation and Air Separation. *Springer*. Retrieved from https://doi.org/10.1007/978-1-4614-2215-0_6
- [28] McEnaney, Joshua & Singh, Aayush & Schwalbe, Jay & Kibsgaard, Jakob & Lin, John & Cargnello, Matteo & Jaramillo, Thomas & Nørskov, Jens. (2017). Ammonia Synthesis from N₂ and H₂O using a Lithium Cycling Electrification Strategy at Atmospheric Pressure. *Energy & Environmental Science*, **10**. [DOI: 10.1039/C7EE01126A]
- [29] Palys, M., McCormick, A., Cussler, E., & Daoutidis, P. (2018). Modeling and Optimal Design of Absorbent Enhanced Ammonia Synthesis. *Processes*, **6**, 91. Retrieved from <http://dx.doi.org/10.3390/pr6070091>
- [30] M. R. Amin, S. Sharear, N. Siddique, Shaidul Islam. (2013). Simulation of Ammonia Synthesis. *American Journal of Chemical Engineering*, **1**, 59-64. Retrieved from <doi:10.11648/j.ajche.20130103.11>
- [31] Orella, M.J., Brown, S.M., Leonard, M.E., Román-Leshkov, Y. and Brushett, F.R. (2020). A General Technoeconomic Model for Evaluating Emerging Electrolytic Processes. *Energy Technol*, **8** Retrieved from <https://doi.org/10.1002/ente.201900994>
- [32] Wentao Wang, José M. Herreros, Athanasios Tsolakis, Andrew P.E. York. (2013). Ammonia as hydrogen carrier for transportation; investigation of the ammonia exhaust gas fuel reforming. *International Journal of Hydrogen Energy*. **38**, 9907-9917, ISSN 0360-3199. Retrieved from: <http://www.sciencedirect.com/science/article/pii/S0360319913013761>
- [33] Graetz, J. (2009). New approaches to hydrogen storage. *Chem. Soc. Rev*, **38**, 73-82. Retrieved from <https://doi.org/10.1039/b718842k>
- [34] Biblioteca Nacional de Chile. La industria del salitre en Chile (1880-1930). *Chilean Memory*. Retrieved

- ved from: <http://www.memoriachilena.gob.cl/602/w3-article-3309.html>
- [35] Servicio Nacional del Patrimonio Cultural. (2019). UNESCO saca a las oficinas salitreras Humberstone y Santa Laura de la Lista de Patrimonio Mundial en Peligro. Retrieved from https://www.patrimoniocultural.gob.cl/614/w3-article-91948.html?_noredirect=1
- [36] Armijo J, Philibert C. (2019). Flexible production of green hydrogen and ammonia from variable solar and wind energy: Case study of Chile and Argentina. *International Journal of Hydrogen Energy*. Retrieved from <https://doi.org/10.1016/j.ijhydene.2019.11.028>
- [37] Shiklomanov, Igor. (2000). Appraisal and Assessment of World Water Resources. *Water International*, **25**, 11-32. [DOI: 10.1080/02508060008686794]
- [38] Andrews JW. (2020). Hydrogen production and carbon sequestration by steam methane reforming and fracking with carbon dioxide. *International Journal of Hydrogen Energy*. Retrieved from <https://doi.org/10.1016/j.ijhydene.2020.01.231>
- [39] Ishan Sharma, Daniel Friedrich, Timothy Golden, & Stefano Brandani. (2020). Monolithic Adsorbent-Based Rapid-Cycle Vacuum Pressure Swing Adsorption Process for Carbon Capture from Small-Scale Steam Methane Reforming. *Industrial & Engineering Chemistry Research*, **59**, 7109-7120. [DOI: 10.1021/acs.iecr.9b05337]
- [40] Soltani R, et al. (2014). Assessment of CO₂ capture options from various points in steam methane reforming for hydrogen production. *International Journal of Hydrogen Energy*. Retrieved from <http://dx.doi.org/10.1016/j.ijhydene.2014.09.161>
- [41] Bihong Lv, Bingsong Guo, Zuoming Zhou, & Guohua Jing. (2015). Mechanisms of CO₂ Capture into Monoethanolamine Solution with Different CO₂ Loading during the Absorption/Desorption Processes. *Environmental Science & Technology* **49**, 10728-10735. [DOI: 10.1021/acs.est.5b02356]
- [42] Trend Economy. (2020). Annual International Trade Statistics by Country, Chile, Imports and Exports, Ammonia. Retrieved from <https://trendeconomy.com/data/h2/Chile/2814>
- [43] Brown, T. (2020, 4 February). Green Ammonia Plants in Chile, Australia, New Zealand. *Ammonia Energy Association*. Retrieved from <https://www.ammoniaenergy.org/articles/green-ammonia-plants-in-chile-australia-new-zealand/>
- [44] Thyssenkrupp. (2019). Small-scale green ammonia plants open up new storage possibilities for wind and solar power. Thyssenkrupp Industrial Solutions AG © 2019. Retrieved from <https://insights.thyssenkrupp-industrial-solutions.com/story/small-scale-green-ammonia-plants-open-up-new-storage-possibilities-for-wind-and-solar-power/>
- [45] Crolius, S. H. (2017). Yara's Solar Ammonia Plant is a Key Step toward Global Trade in Renewable Energy. Ammonia Energy Association. Retrieved from <https://www.ammoniaenergy.org/articles/yaras-solar-ammonia-plant-is-a-key-step-toward-global-trade-in-renewable-energy/>
- [46] Chilean Generators. (2020). Engie y Enaex irrumpen en carrera por el hidrógeno verde: apuntan a operar planta piloto hacia 2024. Retrieved from <http://generadoras.cl/prensa/engie-y-enaex-irrumpen-en-carrera-por-el-hidrogeno-verde-apuntan-a-operar-planta-piloto-hacia-2024>
- [47] Thyssenkrupp. (2021). Ammonia Plants - Fertilizer Plants. Industrial Solutions. Retrieved from <https://www.thyssenkrupp-industrial-solutions.com/en/products-and-services/fertilizer-plants>
- [48] Linde Engineering. (2021). Ammonia. Retrieved from https://www.linde-engineering.com/en/process-plants/hydrogen_and_synthesis_gas_plants/gas_products/ammonia/index.html
- [49] J. lig and Bernd Kaedziora. (1996). Linde Ammonia Concept Linde AG, Wiesbaden, Germany. Retrieved from http://www.iffcokandla.in/data/polopoly_fs/1.2497096.1437770420!/files/514249/filename/Aiche-37-037.pdf
- [50] Rizos et al. (2014). Final Report: For a study on composition and drivers of energy prices and costs in energy intensive industries: The case of the chemical industry - ammonia. Report No.006 Lot 4. Centre for European Policy Studies.
- [51] Irena. (2018). Renewable Power Generation Costs in 2017. *International Renewable Energy Agency*, Abu Dhabi.
-

- [52] Ni, M., Leung, M., & Leung, Y. (2006). Electrochemistry Modeling of Proton Exchange Membrane (PEM) Water Electrolysis for Hydrogen Production.
- [53] Sanchez M, et al. (2018). Semi-empirical model and experimental validation for the performance evaluation of a 15 kW alkaline water electrolyzer. *International Journal of Hydrogen Energy*, Retrieved from <https://doi.org/10.1016/j.ijhydene.2018.09.029>
- [54] Onda, Kazuo & Kyakuno, Takahiro & Hattori, Kikuo & Ito, Kohei. (2004). Prediction of Production Power for High-pressure Hydrogen by High-pressure Water Electrolysis. *Journal of Power Sources*, **132**, 64-70. [DOI: 10.1541/ieejpes.124.605]
- [55] Babu, Dr B V & Angira, Rakesh. (2005). Optimal Design of an Auto-Thermal Ammonia Synthesis Reactor. *Computers & Chemical Engineering*, **29**, 1041-1045. [DOI: 10.1016/j.compchemeng.2004.11.010]
- [56] M. Burhan Kabir Suhan, M. Naimur Rahman Hemal, M. A. A. Shoukat Choudhury et al. (2020). Optimal design of ammonia synthesis reactor for a process industry. *Journal of King Saud University – Engineering Sciences*. Retrieved from <https://doi.org/10.1016/j.jksues.2020.08.004>
- [57] Palys, Matthew J.; McCormick, Alon; Cussler, E. L.; Daoutidis, Prodromos. (2018). Modeling and Optimal Design of Absorbent Enhanced Ammonia Synthesis. *Processes* **6**. Retrieved from <https://doi.org/10.3390/pr6070091>
- [58] Reese, Michael & Marquart, Cory & Malmali, Mahdi & Wagner, Kevin & Buchanan, Eric & McCormick, Alon & Cussler, Edward. (2016). Performance of a Small Scale Haber Process. *Industrial & Engineering Chemistry Research*, **55**. [DOI: 10.1021/acs.iecr.5b04909]
- [59] Atkins, P. W., & De, P. J. (2006). Atkins' Physical chemistry. *Oxford: Oxford University Press*
- [60] Jenkins, H. (2008). Chemical thermodynamics at a glance. Blackwell Pub.
- [61] Einemann, M. & Neumann, F. & Thomé, A.G. & Ghomsi Wabo, Samuel & Rößner, Frank. (2020). Quantitative study of the oxidation state of iron-based catalysts by inverse temperature-programmed reduction and its consequences for catalyst activation and performance in Fischer-Tropsch reaction. *Applied Catalysis* **602**, 117718. [DOI: 10.1016/j.apcata.2020.117718]
- [62] Molburg, John. (2003). Hydrogen from Steam-Methane Reforming with CO2 Capture.
- [63] Malmali, Mahdi & Le, Giang & Hendrickson, Jennifer & Prince, Joshua & McCormick, Alon & Cussler, Edward. (2018). Better Absorbents for Ammonia Separation. *ACS Sustainable Chemistry & Engineering*, **6**. [DOI: 10.1021/acssuschemeng.7b04684]
- [64] Marangio, F. & Santarelli, M. & Calì, Michele. (2009). Theoretical model and experimental analysis of a high pressure PEM water electrolyser for hydrogen production. **International Journal of Hydrogen Energy**, **34**, 1143-1158. [DOI: 10.1016/j.ijhydene.2008.11.083]
- [65] Medina, P. & Santarelli, M. (2010). Analysis of water transport in a high pressure PEM electrolyzer. *International Journal of Hydrogen Energy*, **35**, 5173-5186. [DOI: 10.1016/j.ijhydene.2010.02.130]
- [66] Shimpalee, Sirivatch & Van Zee, J. (2007). Numerical study on rib/channel dimension of flow-field on PEMFC performance. *International Journal of Hydrogen Energy*, **32**. [DOI: 10.1016/j.ijhydene.2006.11.032]
- [67] Woods, Donald. (2007). Rules of Thumb. [DOI: 10.1002/9783527611119.ch1]
- [68] Aneke, Mathew & Wang, Meihong. (2015). Potential for Improving the Energy Efficiency of Cryogenic Air Separation Unit (ASU) using Binary Heat Recovery Cycles. *Applied Thermal Engineering*, **81**. [DOI: 10.1016/j.applthermaleng.2015.02.034]
- [69] Hamayun, M. H., Ramzan, N., Hussain, M., & Faheem, M. (2020). Evaluation of Two-Column Air Separation Processes Based on Exergy Analysis *Energies*, **13**. Retrieved from <http://dx.doi.org/10.3390/en13236361>
- [70] Cheema, I. I., & Krewer, U. (2019). Optimisation of the Autothermal NH3 Production Process for Power-to-Ammonia. *Processes*, **8**. Retrieved from <http://dx.doi.org/10.3390/pr8010038>
- [71] Cheema, Izzat Iqbal & Krewer, Ulrike. (2018). Operating envelope of Haber-Bosch process design for power-to-ammonia *RSC Advances*, **8**, 34926-34936. [DOI: 10.1039/c8ra06821f]

-
- [72] Cheema, Izzat Iqbal & Krewer, Ulrike. (2020). Supplementary Material: Optimisation of the Autothermal NH₃ Production Process for Power-to-Ammonia
- [73] Schmidt, O. & Gambhir, A. & Staffell, Iain & Hawkes, A. & Nelson, J. & Few, Sheridan. (2017). Future cost and performance of water electrolysis: An expert elicitation study. *International Journal of Hydrogen Energy*, **42**, 30470-30492. [DOI: 10.1016/j.ijhydene.2017.10.045]
- [74] Douglas J. M. (1988). Conceptual design of chemical processes, McGraw-Hill Book Company, New York.
- [75] Guthrie K. M., Grace W. R. et al. (1969). Data and techniques for preliminary Capital Cost Estimating. *Chemical Engineering*, **3**, 114-142.
- [76] Cao E. (2010). Heat Transfer in Process Engineering, TYPICAL HEAT TRANSFER COEFFICIENTS. McGraw-Hill Education. Retrieved from <https://www.accessengineeringlibrary.com/content/book/9780071624084/back-matter/appendix7>
- [77] Bridgewater, A.V. (1979). International Construction Cost Location Factors. *Chemical Engineering*, **86**.
- [78] Botermans, Decastilhos, Mclaughlin, Sensenbach. (2020). Modular Ammonia Production Plant. Retrieved from https://events.engineering.oregonstate.edu/sites/expo.engr.oregonstate.edu/files/aiche_report_botermans_decastilhos_mclaughlin_sensenbach_0.pdf
- [79] Djordjevic, Emila & Kabelac, Stephan & Šerbanović, Slobodan. (2008). Heat transfer coefficient and pressure drop during refrigerant R-134a condensation in a plate heat exchanger. *Chemical Papers*, **62**, 78-85. [DOI:10.2478/s11696-007-0082-8]
- [80] Çengel, Yunus A. (2012). Thermodynamics : an engineering approach. Boston :McGraw-Hill Higher Education, **7**.
- [81] New generation of pressurized alkaline electrolysis for large-scale platforms (multi-MW/GW). (2020). McPhy. Retrieved from <https://mcphy.com/en/equipment-services/electrolyzers/large/>
- [82] Chemical Compatibility Database from Cole-Parmer. (2021). Chemical Compatibility Database. Retrieved from <https://www.coleparmer.com/chemical-resistance>
- [83] "3rd Year Design Flash System Design."(2008). Queens University. Retrieved from <https://chemeng.queensu.ca/courses/integratedDesign/Resources/documents/flashsystemdesign.pdf>
- [84] Jenkins, S. (2020). 2019 Chemical Engineering Plant Cost Index Annual Average. *Chemical Engineering*. Retrieved from <https://www.chemengonline.com/2019-chemical-engineering-plant-cost-index-annual-average/>
- [85] Refrigerantes - Gas Servei. (2020). Refrigeración & Climatización. Gas Servei. Retrieved from <https://gas-servei.com/productos/refrigerantes/>
- [86] Boursorama.com. (2021). Boursorama. Retrieved from <https://www.boursorama.com/bourse/devises/convertisseur-devises/dollar-euro>
-

15. Annexes

15.1. Guthrie Method for Estimating Equipment Installation Costs

In the following subsection, the Guthrie formulas [74] for estimating the installation costs of every equipment is described. The CEPCI (Chemical Engineering Plant Cost Index) used for each equipment is reported in Table 15.1

Table 15.1: CEPCI Index for years 1969 and 2019, adapted from [84]

Respective year	1969	2019
Pumps and compressors	119,6	1.060,6
Heat exchangers	115,1	677,3
Distillation columns	115,1	677,3
Reactors	115,1	677,3
Flash	115,1	677,3

15.1.1. Shell-and-Tube Heat Exchangers

$$\text{Installation Cost (€)} = \left(\frac{\text{CEPCI}_{2019}}{\text{CEPCI}_{1969}} \right) \cdot 101,3A^{0,65}(2,29 + F_c) \quad (15.1)$$

Where $A = \text{Area (ft}^2\text{)}$ and $F_c = F_m \cdot (F_d + F_p)$. F_m is a constant corresponding to the shell-and-tube material, F_d is a parameter depending on the design type and F_p is also a constant that depends on the pressure. Each value can be obtained from Tables 15.2, 15.3 and 15.4.

Table 15.2: Factor value in function of the equipment material

Material	F_m
CS/CS	1
CS/Brass	1,3
CS/MO	2,15
CS/SS	2,81
SS/SS	3,75
CS/Monel	3,1
Monel/Monel	4,25
CS/Ti	8,95
Ti/Ti	13,05

Table 15.3: Factor value in function of the heat exchanger design type

Design Type	F_d
Kettle/reboiler	1,35
Floating head	1
U-tube	0,85
Fixed-tube sheet	0,8

Table 15.4: Factor value in function of the heat exchanger design pressure

Design pressure (bar)	F_d
10,3421	0
20,6843	0,1
27,579	0,25
55,1581	0,52
68,9476	0,55

15.1.2. Gas Compressors

$$\text{Installation Cost (€)} = \left(\frac{\text{CEPCI}_{2019}}{\text{CEPCI}_{1969}} \right) 517,5 \cdot \text{bhp}^{0,82} \cdot (2,11 + F_c) \quad (15.2)$$

Where bhp is the net duty requirement of each compressor in bhp and F_c is a factor that depends on the compressor type, as seen in Table 15.5.

Table 15.5: Factor value in function of the compressor type

Compressor type	F_c
Centrifugal	1
Reciprocating	1,29

15.1.3. Distillation Columns, Reactors and Flash Units

$$\text{Installation Cost (€)} = \left(\frac{\text{CEPCI}_{2019}}{\text{CEPCI}_{1969}} \right) (101,9D^{2,066}H^{0,82}(2,18 + F_c)) \quad (15.3)$$

Where D = Diameter (ft), H = Height (ft), and $F_c = F_m F_p$. F_m corresponds to the same values as in Table 15.2 and F_p is a parameter that depends on the pressure, as seen in Table 15.6.

Table 15.6: Factor value in function of the distillation column, reactor or flash unit design pressure

Pressure (bar)	F_d
Up to 3,45	1
6,89	1,05
13,79	1,15
20,68	1,2
27,58	1,35
34,47	1,45
41,37	1,6
48,26	1,8
55,16	1,9
62,05	2,3
68,95	2,5

In the case of the distillation columns, the column trays and tower internals must be consider:

$$\text{Installation Cost (€)} = \left(\frac{\text{CEPCI}_{2019}}{\text{CEPCI}_{1969}} \right) 4,7D^{1,55}HF_c \quad (15.4)$$

Where D = diameter (ft), H = tray stack height (ft), and $F_c = F_s + F_t + F_m$. F_s is a parameter that depends on the tray spacing, F_t is a parameter that depends on tray type and F_m is a parameter that depends on tray material, as seen in Table 15.7.

Table 15.7: Values of the different factors in function of the tray spacing, type and material of the distillation column

Tray spacing (in)	F_s
24	1
18	1,4
12	2,2
Tray type	F_t
Grid	0
Plate	0
Sieve	0
Trough or valve	0,4
Bubble cap	1,8
Koch Cascade	3,9
Tray Material	F_m
CS	0
SS	1,7
Monel	8,9

15.2. Aspen Plus diagram of the final case process simulated

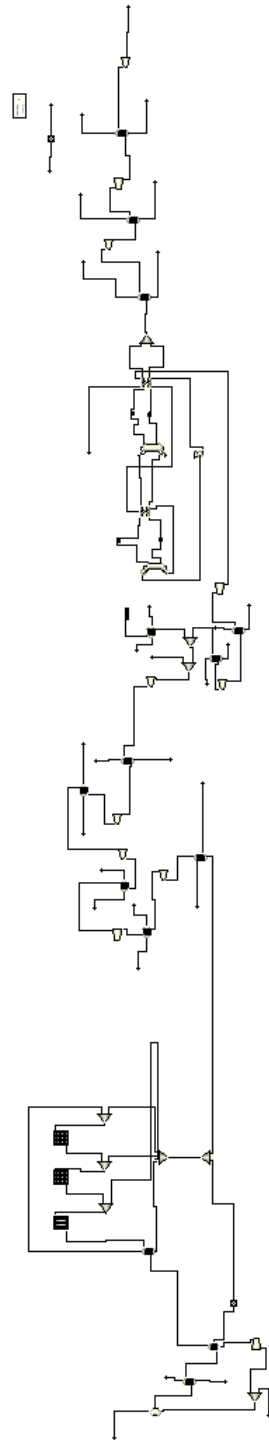


Figure 15.1: Final case simulated in Aspen Plus

16. Acknowledgments

I would like to thank my family for always supporting throughout my entire life. I would also like to thanks my girlfriend, Paula, who has been always there for me, helping me and giving me love every moment. To my friends, who have always been there for me, making me happy even in the most stressful moments. To all the people that helped me all over my university career, prompting me to always be a better person, student and professional. Finally, an honorific mention to the groovy, who always entertained me with the best music.
